Massey University Library. Thesis Copyright Form

Title of thesis: Rotating Frame Relaxation of Polymer Melts

(1) (a) I give permission for my thesis to be made available to readers in the Massey University Library under conditions determined by the Librarian.

~~(b) I do not wish my thesis to be made available to readers without my written consent for _____ months.~~

(2) (a) I agree that my thesis, or a copy, may be sent to another institution under conditions determined by the Librarian.

~~(b) I do not wish my thesis, or a copy, to be sent to another institution without my written consent for _____ months.~~

(3) (a) I agree that my thesis may be copied for Library use.

~~(b) I do not wish my thesis to be copied for Library use for _____ months.~~

Huiras

Signed Paul Callaghan (for T.M. Huiras)

Date 16/3/89

The copyright of this thesis belongs to the author. Readers must sign their name in the space below to show that they recognise this. They are asked to add their permanent address.

NAME AND ADDRESS	DATE

Rotating Frame Relaxation in Polymer Melts

A thesis presented in partial fulfilment of
the requirements for the degree of
Master of Science
in Physics at
Massey University

by

Te Whitinga Mark Huirua

1988

Maori Proverb

Ehara ta te tangata kai, he kai titongi kau;
engari mahi ai ia ki te wherna; tino kai, tino makona.

(Food provided by someone else is only food to be nibbled;
food produced by one's own labour on the land is good, satisfying food).

" Writing a book is an adventure. To begin with, it is a toy
and an amusement. Then it becomes a mistress, then it
becomes a master, then it becomes a tyrant. The last phase
is that just as you are about to be reconciled to your servitude,
you kill the monster and fling him about to the public ".

... Sir Winston Churchill

Abstract

Entangled high polymers in the melt or semidilute solution exhibit motion dependent on the timescale. This motion may be characterised in terms of the " tube model " in which the random coil polymer under investigation is enclosed in a tube formed by its neighbours. At the shortest timescale, motion consists principally of segment reorientation. The topology of the tube implies that some residual anisotropy will exist in this motion[3]. On the next higher timescale reptative displacements around tube bends occur, thus causing a fluctuation in the direction of residual orientation. On the longest timescale, final correlation loss occurs by tube renewal.

$T_{1\rho}$ is the relaxation time for a spin system to come to thermal equilibrium in a transverse RF field. It is sensitive to components of the motion at the RF Larmor frequency. This frequency is low and adjustable (10^2 to 10^5 Hz) and extends the regime accessible to Field cycling T_1 experiments[4]. $T_{1\rho}$ therefore provides access to the intermediate and long timescale fluctuations in entangled polymers. It is a major conclusion of this work that reptation and tube renewal effects can be directly observed.

The BPP theory of relaxation[25] has been extended to $T_{1\rho}$ for three proton spins in a methyl group. Results of a relaxation study in two polymer melt systems, namely polydimethylsiloxane and polyethylene oxide are presented. In the latter case the results are compared with $T_{1\rho}$ dispersions made on Polyethylene melts[13]. The experimental data is seen to follow the theoretical predictions made by Kimmich[3,4].

Acknowledgements

I wish to express my sincere gratitude to the following people for their involvement in this work:

My supervisor Prof. Paul Callaghan for providing both theoretical and technical knowledge when most needed as well as an " extra hand " at experiment (" harvest ") time. His great insight and unlimited enthusiasm for Physics gave encouragement enabling me to complete this task.

Dr Craig Eccles for his interest and assistance in the probe development.

The Mechanical Workshop Staff for the construction of the probe body.

The Electronic Workshop Staff for their practical suggestions and tips throughout the development of the hardware.

Fellow post-graduate students Yang Xia, Peter Daivis, Peter Saunders, James Conway, and Andrew Coy for both their educated and uneducated opinions and discussions throughout the course of this work. " Pawn to King four !! ".

Dr Rosie Wang who shared in the long hours necessary, at " harvest " time, to gather experimental data. Your empathy is greatly appreciated.

Dr Ted Garver whose keen interest was shown to me through constructive comments, good questions, and all round support during the writing of this thesis.

The Education Department for providing financial support through the award of a Maori and Polynesian Scholarship for Higher Education.

The Department of Scientific and Industrial Research for providing financial support through the award of a Post-graduate Scholarship.

The Maori Education Foundation, the Taranaki Trust Board, and the Wanganui Trust Board for providing financial assistance enabling me to continue.

Massey University for providing financial assistance and the opportunity to carry out this research.

And of course To'aiga Su'a, my fiancee at the present time of writing, whose unfailing love and support provides an all-win situation in everything I do.

Contents

List of Figures

Tables and Photographic Plates

List of Symbols

Symbol

a	Anisotropy constant
a	Radius of sphere
a_{mj}	Complex admixture amplitudes
$\mathbf{B}_0$	Main magnetic field directed along the z axis
$\mathbf{B}_1$	Applied RF field
c	The Curie constant
c.c	Complex conjugate
C	Capacitance
d	Diameter of wire
D	Diffusion coefficient
E	Energy
f_0	Larmor frequency
f_1	Frequency of applied field
$F_i(t)$	Spatial operator where i = 0,1,2
$\mathbf{F}$	Fourier transform operator
G	Correlation function
$\hbar$	Plancks constant divided by 2π
$\mathcal{H}$	Energy Hamiltonian
i	$(-1)^{1/2}$
I	Electrical current
I	Nuclear spin quantum number
j	Total angular momentum quantum number
$J_i(\omega)$	Spectral density for a two spin system where i = 0,1,2
J	Spin magnetisation
k	Boltzmanns' constant
$K_{ij}(\omega)$	Spectral density for an N spin system
l	Length of the RF coil
l	Mean path length
L	Inductance
L_0	Extended tube length
m	Azimuthal or magnetic quantum number
M_c	Critical entanglement molar mass
M_N	Number average molar mass
M_W	Weight average molar mass
$\mathbf{M}$	Macroscopic magnetisation vector
n	Number of turns on the RF coil
N	Number of spins per unit volume
$p_{\pm 1/2}$	Relative probability of finding a spin in the state $m_j = \pm 1/2$
p_n	Population of the nth energy level
$P(\Omega, \Omega_0, t)$	Conditional probability of finding the system at Ω at time t if it is at Ω_0 at time zero
Q	Quality factor of RF coil
r	Diameter of RF coil
r	Internuclear separation
r	Radius of coaxial cylinder

r'	Matching impedance
R	Resistance
s	Scaling factor
S	Resultant NMR signal
t	Time parameter
t_{90}	$\pi / 2$ pulse time
T	General temperature
T_L	Lattice temperature
T_s	Spin temperature
T_1	Spin-lattice relaxation time
T_2	Spin-spin relaxation time
$T_{1\rho}$	Rotating frame spin-lattice relaxation time
Tr	Trace of a matrix
$U_E(t)$	Evolution operator
$U_{RZ}(\theta)$	Rotation operator
W_{nm}	Transition probability between quantum levels $\|n>$ and $\|m>$
x	Distance parameter
Y_n	Spherical harmonic of order n
$2Z_0$	Width of RF probe (Spacing between the shim coils)

α	Angle between main magnetic field and the methyl group
β	Rotation about the methyl bond
$\hat{\beta}$	Equal to $1 / kT$
γ	Gyromagnetic ratio
γ	Rotation of the methyl group about the magnetic field
δ	Skin depth
Δ_s	Laplacian operator on the surface of a sphere
Δ_0	Mean tube length per fold
ε	Dielectric constant
ε_0	Permittivity of free space
η	Parameter of shim coil
θ	Polar angle
λ	Wavelength
μ_z	z magnetisation
μ_0	Permeability of free space
ρ	Resistivity
ρ	Density matrix
σ	Proximity factor
τ	Correlation time
ϕ	Azimuthal angle
$\Psi(\theta,\phi)$	Probability of finding the internuclear vector at (θ,ϕ) at time t
ω_0	Larmor precession frequency due to B_0
ω_1	Larmor precession frequency due to B_1

$< A >$	Observable
$\mid jm_j >$	Basis set of eigenstates
$\mid \Psi >$	General state of a nuclei
*	Complex conjugate

Chapter 1 Introduction

Pawn to King four

1.1 Polymer Melt Dynamics

Molecular motion in polymer melts can be studied using NMR relaxation time measurements to probe the spectral densities which are based on fluctuating dipolar interactions between nuclear spins.

It has been shown[1] that there are two types of viscoelastic behaviour. Low molecular mass polymers behave similar to isolated polymers and follow the predictions made by Rouse[2]. The high molecular mass spectrum, however, can be separated into a high frequency component and a low frequency component. The high frequency component is similar to that observed in the low molecular mass polymers. The low frequency component exists due to the effects of entanglements in polymer melts. The molecular mass at which the characteristics of the melt change is designated the critical molecular mass, M_c . It is the topic of this thesis to study the behaviour of polymer chains of masses higher than M_c, since this is the regime where entanglements occur, and it is the effect of these entanglements which govern the overall motion.

The motion can be separated into three components[3]. In the shortest timescale, that of the "local" (and therefore molecular weight independent processes) the motion is largely due to segment re-orientation by diffusing local " defects " (rotational isomers of neighbouring segments). This motion can be considered to correspond to the diffusion of a particle between two reflecting barriers[4,5] with correlation time τ_s.

Since the polymer chains are not able to pass through each other they are effectively confined inside a tight-tube region (see Fig.1-1).This tube which surrounds the chain is not fixed in space but is constantly renewed as the chain diffuses throughout the tube[6]. This curvilinear chain diffusion, known as a a " semi-local " process, occurs in the intermediate timescale with correlation time τ_l . The dynamics of such a process has been studied by de Gennes[7] who shows that local defect diffusion is the elementary process which finally causes the " reptation " phenomenon; the motion is due to further segment re-orientation by reptative displacements around bends of the tight-tube.

The centre line of the tube, called the primitive chain by Doi & Edwards[6], moves randomly forwards or backwards only along itself. The chain ends are free, therefore, to orient themselves randomly. It is the reptative process which finally leads to the transportation of material to and from the chain ends causing the surrounding tube to thread itself into a new configuration. This tube renewal, a " global " process, occurs in the largest timescale with correlation time τ_r .

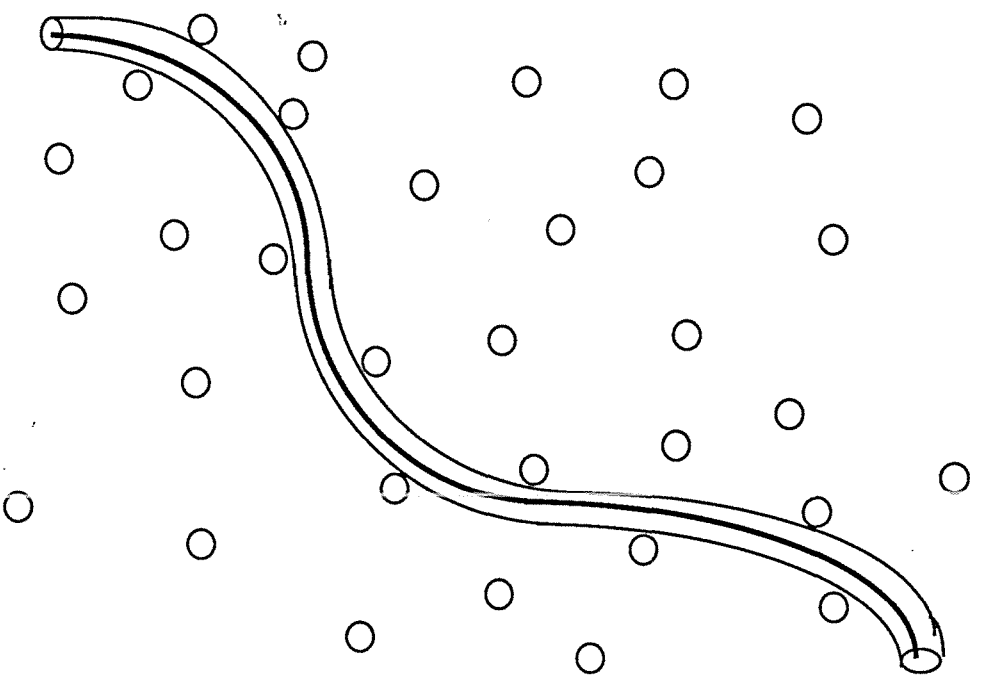

Fig.1-1

Schematic illustration of a chain in polymer melts. The chain is confined to a tight tube formed by the matrix of neighbouring chains (circles).

1.2 The Relationship Between NMR Relaxation Times and the Spectral Densities

The relaxation phenomenon is caused by the fluctuating dipolar interactions arising from the tumbling of the molecule. Although this tumbling motion is a random process it can be characterised by a correlation time, τ_c. By taking the Fourier transform of the correlation functions the spectral densities can be obtained. If the conditions of BPP[8] apply then by measuring T_1, the spin-lattice relaxation time, and T_2, the spin-spin relaxation time, information can be gained relating to the spectral densities at the characteristic frequencies of zero, ω_0 and $2\omega_0$ where ω_0 is the Larmor precession frequency about the main field B_0.

When $T_{1\rho}$ is measured, the spin-lattice relaxation time in the rotating frame, it is possible to probe the low frequency regime, while maintaining the high field sensitivity, and extract information at the characteristic frequency $2\omega_1$, where ω_1 is the Larmor precession frequency about the RF field; hence, because ω_1 is variable, and much less than ω_0, this allows us to study slow semi-local and global processes, i.e motion sensitive to τ_l and τ_r (see Fig.1-2).

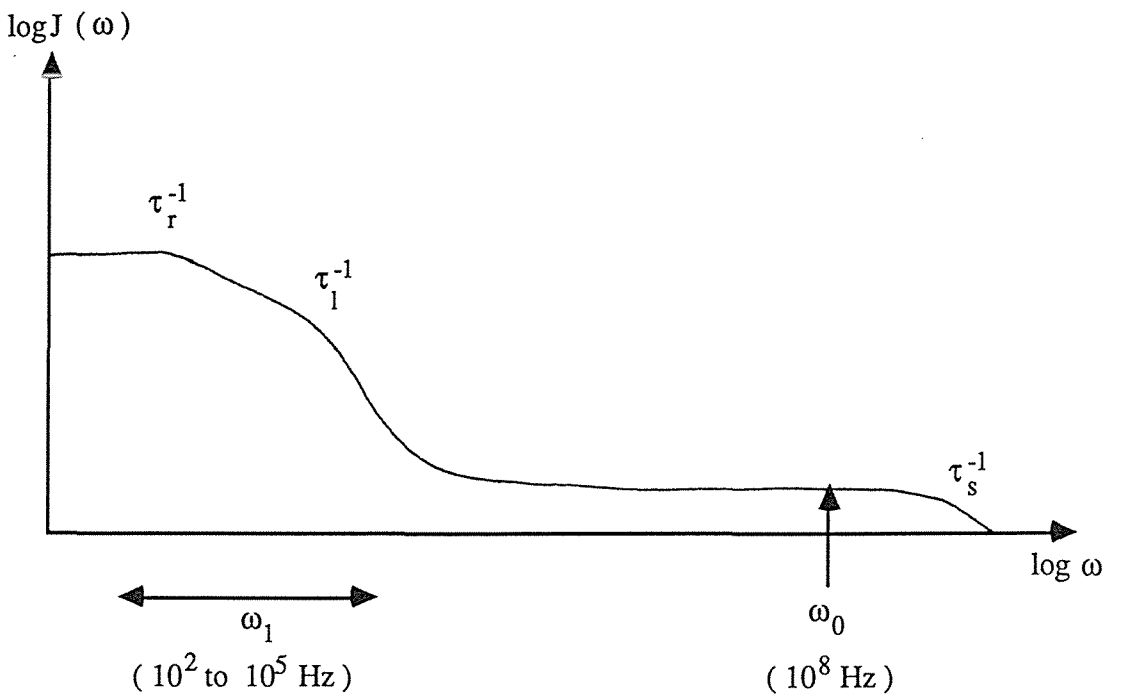

Fig.1-2

Schematic log J_0 (ω) dispersion predicted by the reptation model of Kimmich.

1.3 The " Tight Tube " Condition and the Polymer Melts

The motion of the internuclear vector causes the dipolar interaction to fluctuate. In a polymer there is a hierarchy of motion with the local segmental reorientation being most rapid and the overall molecular reorientation and centre of mass motion the slowest. If the most rapid motion involves a total correlation loss then the slow motion cannot be observed in the dipole relaxation process. The " tight tube " condition arises when the rapid processes leaves a residual correlation which remains to be modulated by slow motion. Such a residual correlation is akin to a fast local motion residual anisotropy and is characteristic of polymers in the melt. By contrast, in the solution phase the local motion is isotropic and no long range processes can be observed.

1.4 T_1 Dispersions - The Experiments of Kimmich et al

In a series of papers Kimmich and co-workers[3,4,9 - 12] have examined the dependence of the NMR longitudinal relaxation time T_1 on polarising field strengths, a technique known as field-cycling spectroscopy. Their experiments yield spectral densities at 10^4 to 10^8 Hz. In this thesis we extend this frequency range down to 10^2 Hz using $T_{1\rho}$ measurements. Two polymer systems are employed, namely, polydimethylsiloxane and polyethylene oxide. In the latter case the results are compared with $T_{1\rho}$ dispersions made on polyethylene melts[13].

It is a major conclusion of this work that $T_{1\rho}$ measurements (unlike T_1 dispersions) probe a sufficiently low frequency regime that reptation and tube renewal effects can be directly observed.

Chapter 2 Basic NMR Theory

He who would learn to fly one day must first learn to stand and walk and run and climb and dance: one cannot fly into flying ... Nietzsche

2.1 Historical

In 1924 W.Pauli[14] suggested that the hyperfine structure of optical spectral lines is due to a special property of the atomic nuclei; certain nuclei possess angular momentum and thus, a magnetic moment.

As early as 1921 and 1924 Stern[15] and Gerlach[16], directing a beam of molecules through an inhomogeneous magnetic field, showed that various states of *atomic* magnetic moments existed. These molecular beam experiments were later refined to permit the detection of *nuclear* magnetic moments.

It was not until late 1945 that the first successful nuclear magnetic resonance signal was detected at Harvard University in which a team, headed by E. Purcell[17], used a single coil probe to detect the proton magnetic absorption signal of a piece of paraffin wax at 30 MHz. At the same time work was independently being carried out at Stanford University in which a team, headed by F. Bloch[18], detected the magnetic induction signal from the protons in water at 7.765 MHz using a crossed coil probe. The simplest description of the phenomena (Purcell et al) is that of an absorption by the nuclear spin system of electromagnetic energy provided by an RF generator. Because the power is transmitted continuously the phenomenon is aptly named *continuous wave* nuclear magnetic resonant absorption. This absorption can be described and detected as a change in the quality factor Q of the resonant circuit of the ' driving system '.

Another way of looking at the nuclear resonance phenomenon, proposed by F. Bloch, is to describe it as a forced precession of the nuclear magnetisation in the applied RF field; the effect of the precession being to induce a detectable emf in a receiving coil. In 1952 Bloch and Purcell were jointly awarded the Nobel prize for their discovery.

Continuous wave NMR is simple and inexpensive. It is used to obtain a multi-line spectrum characterised by chemical shifts and coupling constants. These spectra are widely used in Chemistry and, in particular, Organic Chemistry where they have revolutionised techniques in determining structure.

A totally different approach originated at the same time as continuous wave NMR but this method was more efficient and had greater sensitivity. In 1946 Bloch et al[19] had already proposed *pulsed* NMR. The RF field exciting the nuclear sample is no longer continuous but now a short pulse. This technique was pioneered theoretically by Torrey[20] and practically by Hahn[21] as well as Ernst and Anderson[22]. In the pulse technique data is acquired in the time domain rather than the frequency domain and hence the method is useful for studying time dependent processes such as chemical exchange, molecular diffusion and, as is the work of this thesis, molecular motion.

Thus, having briefly traced the history of NMR and its application to molecular motion, the next section of this chapter considers basic NMR theory from a quantum mechanical point of view.

2.2 NMR Theory

2.2.1 Nuclear Magnetism

We start by simply considering a system of N nuclei in a magnetic field B_0, applied traditionally along the z axis, and define a general state for each nuclei to be

$$|\Psi> = \sum_{m_j} a_{m_j} | j\ m_j > \qquad (2.1)$$

where j = Total angular momentum quantum number (can be any half integral value)
m_j = Azimuthal or magnetic quantum number whose values range from -j to j
a_{mj} = Complex admixture amplitudes
$| j\ m_j >$ = Basis set of eigenvectors

The result of making a measurement on the system is to place each nuclei into a specific state denoted by $a_{m_j} | j\ m_j >$. One such measurement that could be made is the energy of each state that develops after applying the magnetic field B_0. This is called the Zeeman energy and is given by

$$E(m_j) = -m_j \gamma \hbar B_0 \qquad (2.2)$$

where γ is the gyromagnetic ratio and depends on the specific nuclei and $\hbar$ is Plancks constant divided by 2π .

It is of particular interest to concentrate on spin 1/2 nuclei since all measurements in this work were carried out using proton NMR. Hence for $\gamma > 0$ the $m_j = 1/2$ state has the higher energy and the energy difference between the two states, as illustrated in Fig.2-1, is

$$\Delta E = 1/2\gamma\hbar B_0 - (-1/2)\gamma\hbar B_0$$

$$= \gamma\hbar B_0 \qquad (2.3)$$

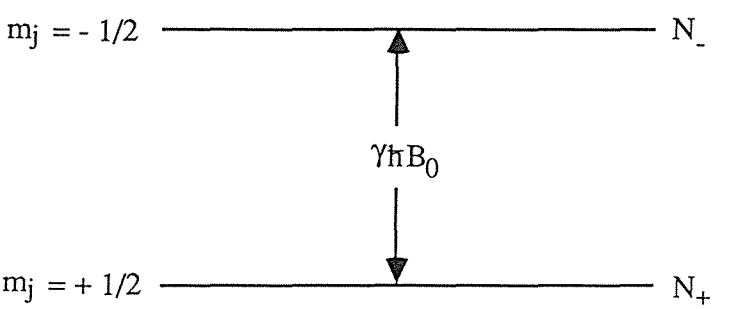

Fig.2-1
The energy level separation in a spin 1/2 system.

Note that the population difference $N_+ - N_-$ is given by Boltzmann as

$$N_+ - N_- = \exp(\Delta E / kT) \qquad (2.4)$$

where k is the Boltzmann constant and T is the temperature. (The density of our system is assumed to be low enough for the particles to be non-interacting and so Fermi-Dirac and Bose-Einstein statistics need not apply).

The energy Hamiltonian for the B_0 field is defined to be

$$\mathcal{H} = -\gamma B_0 J_z \qquad (2.5)$$

where J_z is the spin magnetisation along the z axis. Comparing Eq.(2.5) with the semi-classical energy

$$E = -\mu.\mathbf{B} \qquad (2.6a)$$

$$= -\mu_z.B_0 \qquad (2.6b)$$

identifies γJ_z with the z magnetisation μ_z. Hence

$$\mu_z = \gamma J_z \qquad (2.7)$$

Now,

$$\mathcal{H} | \psi > = E(m_j) | \psi > \qquad (2.8)$$

Thus the result of measuring the energy of the system is to place each nuclei into an energy eigenstate $| j\ m_j >$ with its corresponding energy eigenvalue $E(m_j)$.

2.2.2 Precession

The question naturally arises " how is the state $| \Psi >$ affected by time ? ". For example if we begin at time t = 0 with $| \Psi(0) >$ what will $| \Psi(t) >$, the final state, be after a time t ? The evolution operator $U_E(t)$ is defined such that

$$| \Psi(t) > = U_E(t) | \Psi(t) > \qquad (2.9)$$

where

$$U_E(t) = \exp -(i/\hbar) \mathcal{H}t. \qquad (2.10)$$

$U_E(t)$ obeys the Schrodinger equation

$$i \partial U_E(t) / \partial t = \mathcal{H} U_E(t). \qquad (2.11)$$

Inserting the energy Hamiltonian of Eq.(2.5) into Eq.(2.10) gives for the evolution operator

$$U_E(t) = \exp -(i/\hbar) \mathcal{H} t$$

$$= \exp -(i/\hbar) \gamma B_0 J_z t. \qquad (2.12)$$

We introduce the rotation operator

$$U_{RZ}(\theta) = \exp i/\hbar \, \theta J_z \qquad (2.13)$$

Eq.(2.13) describes a rotation θ about the z axis. So then comparing Eq.(2.12) with that of Eq.(2.13) it is seen that $U_E(t)$ is equivalent with $U_{RZ}(\theta)$ if

$$\theta = \gamma B_0 t \qquad (2.14)$$

or

$$\omega_0 = \gamma B_0 \qquad (2.15)$$

In other words our initial state $| \Psi(0) >$ will rotate about the z axis at the Larmor frequency given by $\omega_0 = \gamma B_0$ so that at any later time t

$$| \Psi(t) > = U_E(t) | \Psi(0) >$$

$$= U_{RZ}(\theta) | \Psi(0) >. \qquad (2.16)$$

Consider a simple NMR experiment whereby a sample of water, say, has been placed in a magnetic field B_0 along the z axis and a sufficient amount of time has elapsed for the system to be in thermal equilibrium. The ensemble of spins will have developed a magnetisation M_0 directed along z. The next section will consider M_0 in more detail but for now we only need be concerned that M_0 does not appear immediately but takes a finite time to ' grow ' to its thermal equilibrium value. Now apply an RF pulse about the x axis such that M_0 is rotated by 90^o see Fig.2-2. It is important that the 90^o flip-time t_{90}, is very much less than the time for the ensemble of spins to relax to M_0.

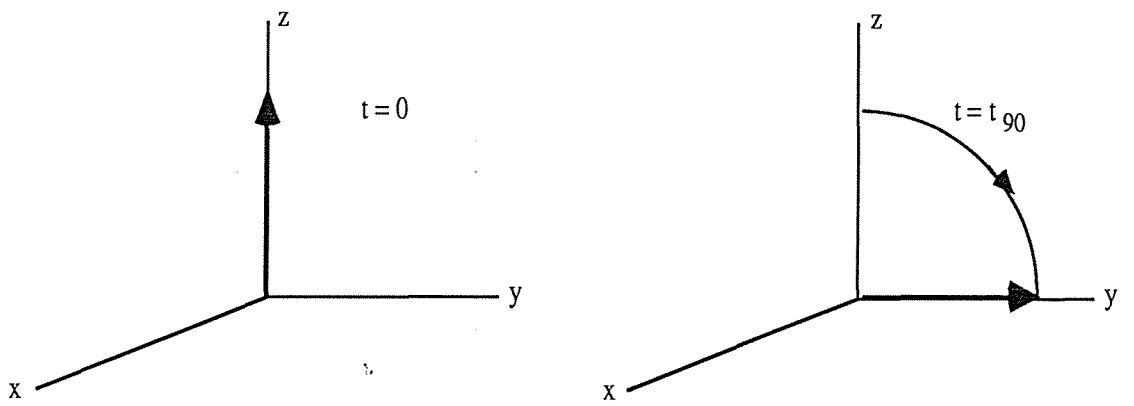

Fig.2-2
The rotation of $M_z = M_0$ into the x-y plane in time t_{90}.

According to our evolution operator M_0 should now rotate about z indefinitely. However, in the presence of T_1 and T_2 processes (e.g magnetic field inhomogeneities, dipolar interactions) the motion, instead of rotating, subsequently precesses about z in a manner such that the magnetisation relaxes to its thermal equilibrium value M_0 along z. This process occurs with a characteristic time aptly named the T_1 relaxation time. Other names include the spin-lattice relaxation time and the longitudinal relaxation time both of for which the names shall become clearer a little later in this chapter.

2.2.3 The Density Matrix

In this section we define the density matrix ρ. The density matrix contains all the information necessary for the description of a statistical ensemble of identical spins. In particular, the predicted value of any observable A of the system is given by the equation

$$< \overline{A} > = Tr(\rho A) \qquad (2.17)$$

We will now use Eq.(2.17) to find the thermal equilibrium magnetisation M_0 of an ensemble of spins with angular momentum quantum number j in a magnetic field B_0 along the z axis (this problem was originally solved by Brillouin). If the spins are widely separated so that no spin-spin interactions are involved then the energy Hamiltonian as given by Eq.(2.5) is

$$\mathcal{H} = -\gamma B_0 J_z$$

The density matrix in thermal equilibrium is

$$\rho = \{ \exp - \mathcal{H}/ kT \}/\{ Tr (\exp - \mathcal{H}/ kT) \} \qquad (2.18)$$

Using Eq.(2.17) ,the ensemble average of the magnetisation $< \mu_z >$ is

$$< \overline{\mu_z} > = Tr (\rho \mu_z) \qquad (2.19)$$

but from Eq.(2.18) then

$$< \overline{\mu_z} > = Tr \{ \gamma J_z [\mathbf{1} + (\gamma B_0 / kT) \mathbf{J_z} + (\gamma B_0 / kT)^2 \mathbf{J_z}^2 + ...] \} / (2j + 1) \qquad (2.20)$$

now

$$Tr (\mathbf{1}) = 2j + 1 \qquad (2.21a)$$
$$Tr (\mathbf{J_z}) = 0 \qquad (2.21b)$$
$$Tr (\mathbf{J_z}^2) = (1/3) j(j + 1) \qquad (2.21c)$$

wherefore it can be seen that in the high temperature approximation (H.T.A) and for N spins per unit volume then

$$M_0 = N < \overline{\mu_z} > = N\gamma^2 j(j + 1)B_0 / 3kT. \qquad (2.22)$$

or

$$M_0 = cB_0 / T_s \qquad (2.23)$$

Eq.(2.23) is Curies law for paramagnetism where c is the Curie constant, and T_s is the spin temperature.

2.2.4 The Bloch Equations and Relaxation Times

Having just described the thermal equilibrium magnetisation M_0 and the idea of precession we are now placed in a position to better (more intuitively) understand the Bloch equations. These are as follows:

$$dM_z / dt = \gamma (\mathbf{M} \times \mathbf{B})_z + (M_0 - M_z) / T_1 \qquad (2.24a)$$

$$dM_{x,y} / dt = \gamma (\mathbf{M} \times \mathbf{B})_{x,y} - M_{x,y} / T_2 \qquad (2.24b)$$

Bloch intended, with these phenomenological equations, to describe the motion of the macroscopic magnetisation M_0. As can be seen the first term describes precession while the second term, relaxation. Bloch assumed that the internal interaction of spins with each other could be expressed by the equation

$$\partial M_{x,y} / \partial t = - M_{x,y} / T_2 \qquad (2.25)$$

Eq.(2.25) defines the parameter T_2. This is the so-called transverse or spin-spin relaxation time. Eq.(2.25) describes an exponential decay to zero of the magnetisation. This exponential decay as shown in Fig.2-3 occurs in the laboratory frame with a time constant of T_2.

$$M_x(t) = M_{x0} \sin \omega_0 t. \exp(-t/T_2) \qquad (2.26)$$

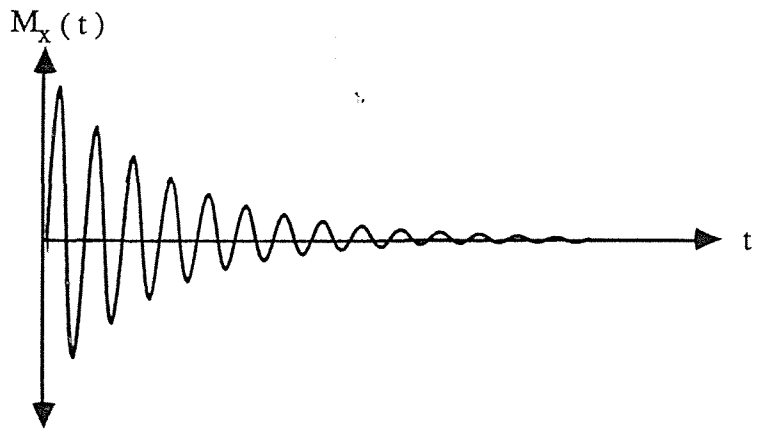

$$M_y(t) = M_{y0} \cos \omega_0 t \exp(-t/T_2)$$

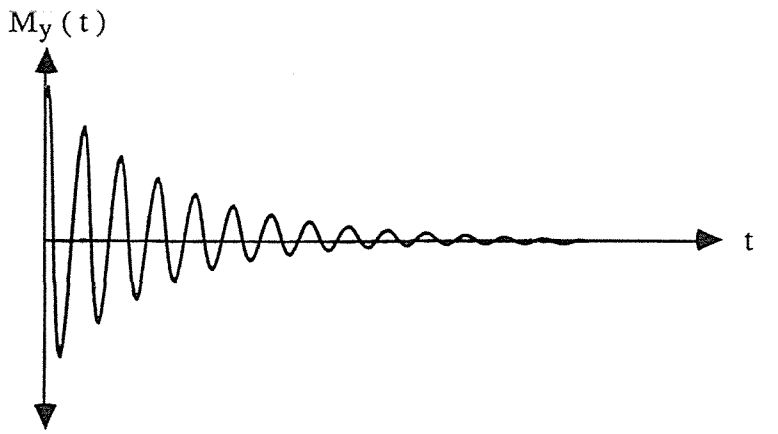

Fig.2-3
Exponential decays of M_x and M_y with time constant T_2.

In the rotating frame where $\omega_0 = \gamma B_0$ the transverse component M_x is created at t = 0. What then causes it to decay ? It is the dipolar interactions between adjacent nuclei which produce a range of resonant frequencies causing a dephasing of the nuclear magnetic moment. This results in a reduction of the transverse magnetisation but note however that no energy is lost; it is simply re-distributed among the spins[23].

Just as Eq.(2.25) defines T_2, in likewise fashion the equation

$$\partial M_z / \partial t = (M_0 - M_z) / T_1 \qquad (2.28)$$

defines the parameter T_1 to be the time constant of the exponential approach of M_z to its thermal equilibrium value M_0. This is the so-called longitudinal or spin-spin relaxation time. In the laboratory frame the magnetisation M_z appears as shown in Fig.2-4.

$$M_z(t) = M_0 \{ 1 - 2\exp (-t / T_1) \} \qquad (2.29)$$

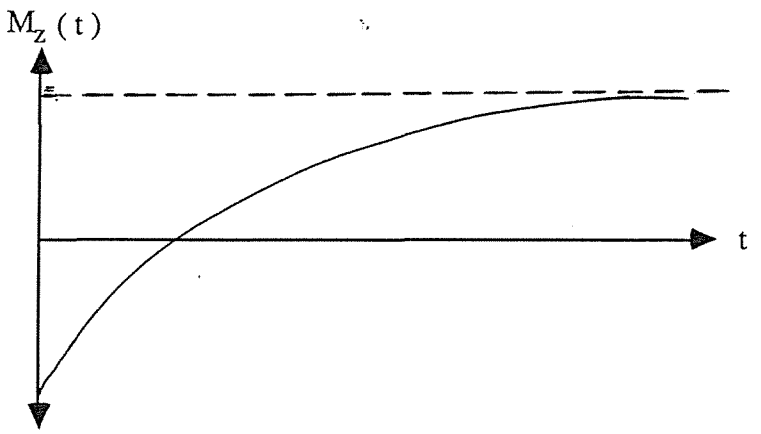

Fig.2-4
Exponential decay of M_z with time constant T_1.

Transvese components of the external field oscillating at the Larmor frequency cause a dephasing of the longitudinal magnetisation. Unlike T_2 processes, this results in a reduction of the net spin energy by energy exchange with the surrounding medium made up of all rotational, vibrational and translational motions - collectively (and for historical reasons) called the lattice. Although a single time constant does not always describe adequately the trend of nuclear spins towards the equilibrium with the lattice, such a constant is usually introduced to give the time scale of the process.

2.2.5 The Density Matrix Description of State Populations

For our spin 1/2 system, at time zero the populations of each state can be given by the density matrix as

$$\rho_0 = \begin{bmatrix} |a_{1/2}|^2 & \overline{a_{1/2}a_{-1/2}^*} \\ \overline{a_{1/2}a_{-1/2}^*} & |a_{-1/2}|^2 \end{bmatrix} \qquad (2.30)$$

$$= \begin{bmatrix} p_{1/2} & 0 \\ 0 & p_{-1/2} \end{bmatrix} \qquad (2.31)$$

The diagonal terms give the population in the corresponding eigenstate and the off-diagonal terms are related to the coherence between the states. $|a_{1/2}|^2$ and $|a_{-1/2}|^2$ are the relative probabilities $p_{1/2}$ and $p_{-1/2}$ of finding each spin in the state + 1/2 or - 1/2 respectively, often called the relative populations. The off-diagonal elements of ρ_0 being zero corresponds to phase incoherence. This is due to the even distribution of the azimuthal phase angle of the precessing nuclei in the transverse plane (see Fig.2-5).

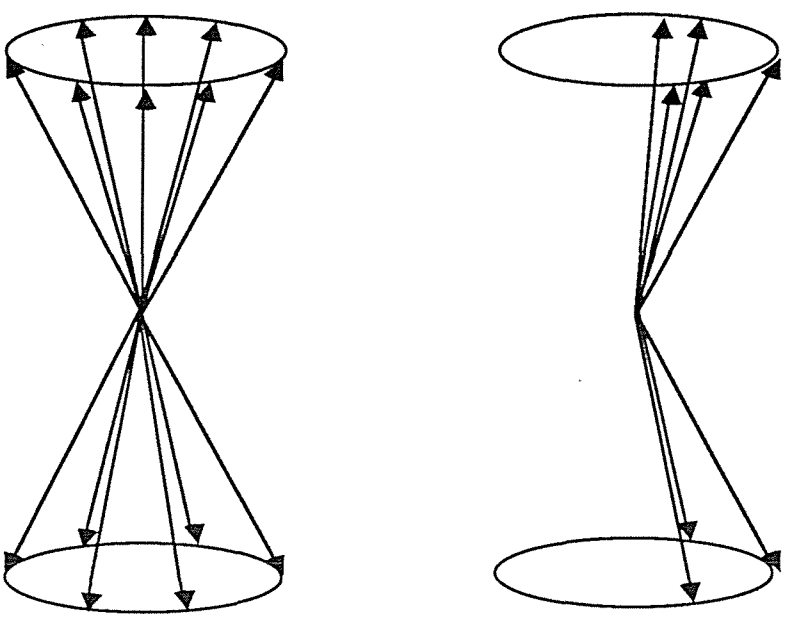

Fig.2-5

Schematic illustrating both phase coherence (leftmost figure) and phase incoherence (rightmost figure) of a two-spin system given by the off-diagonal elements of the density matrix.

At any later time t then

$$\rho(t) = \begin{bmatrix} p_{1/2} - |\overline{a_{1/2}}|^2 e^{-t/T_1} & |\overline{a_{1/2}a_{-1/2}^*}| e^{-t/T_2} \\ |\overline{a_{1/2}^* a_{-1/2}}| e^{-t/T_2} & p_{-1/2} - |\overline{a_{-1/2}}|^2 e^{-t/T_1} \end{bmatrix} \quad (2.32)$$

Hence the diagonal terms show that the spin system relaxes to its thermal equilibrium value at the rate T_1^{-1}. The off-diagonal elements show that the transverse components decay to zero at the rate T_2^{-1}.

2.3 NMR Observables

Throughout this chapter we have illustrated the theory using the macroscopic magnetisation **M**. Because this is our NMR observable we hereby make the definition

$$M_x = N\gamma \langle \overline{J_x} \rangle \quad (2.33a)$$

$$M_y = N\gamma \langle \overline{J_y} \rangle \quad (2.33b)$$

$$M_z = N\gamma \langle \overline{J_z} \rangle \quad (2.33c)$$

and $\mathbf{M} = N\gamma \{ \langle \overline{J_x} \rangle \mathbf{i} + \langle \overline{J_y} \rangle \mathbf{j} + \langle \overline{J_z} \rangle \mathbf{k} \}$ where N is the number of spins per unit volume.

2.4 Description of NMR Pulse Sequences

2.4.1 Single 90° Pulse

It was previously mentioned that a simple NMR experiment consists firstly of turning the magnetisation $M_z = M_0$ through 90° until it comes to lie in the x-y plane. This is achieved by applying a single 90° pulse defined to be a transverse RF pulse of magnitude B_1 in the rotating frame at $\omega_0 = \gamma B_0$ which acts for a time t_{90} such that $\gamma B_1 t_{90} = \pi/2$. If B_1 is stationary in the x' direction (the prime denotes the rotating frame) then $M_z = M_0$ precesses about B_1 at $\omega_1 = \gamma B_1$ until at time $t_{90} = \pi/2\ \gamma B_1$ it is pointing in the y' direction.

The pulsed RF field that produces the 90° rotation of M_0 in the rotating frame must act in the presence of T_1 and T_2 processes, consequently the 90° nutation of M_0 is only an approximate description of what happens. So how good an approximation is it ? If the major torque on the magnetisation is to be from B_1 during $0 < t < t_{90}$, then the relaxation towards B_0 (in time T_1) and the dephasing of the transverse magnetisation (in time T_2) must not be important compared with the precession about B_1 during $t_{90} << T_2 < T_1$. The requirement on B_1 is thus $(\pi / 2\gamma B_1) << T_2$ or

$$\gamma B_1 >> \pi / 2T_2 \quad (2.34)$$

This is the same as saying that we must assume (plausibly) B_1 to be much greater than any internal fields or external field inhomogeneity described by T_2. The 90^0 pulse time for the JEOL FX60 (the spectrometer used in the present work) was $t_{90} \sim 14\mu s$ for low B_1 fields and T_2 was the order of ms.The pulse sequence is given in Fig.2-6.

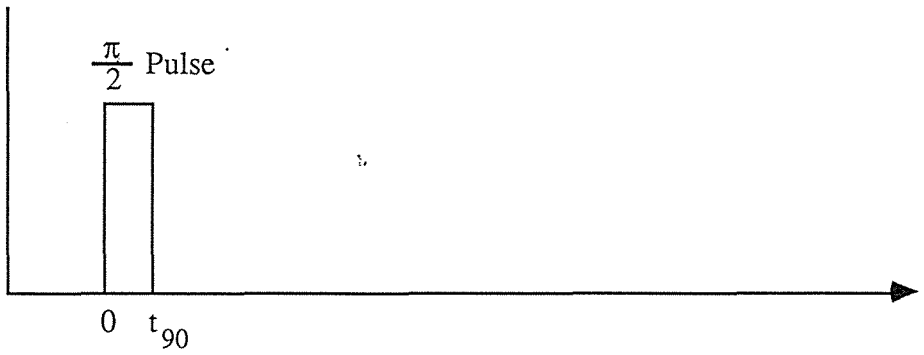

Fig.2-6
π / 2 RF pulse sequence.

2.4.2 Spin-locking

A single 90^0 pulse is applied. However instead of turning off the RF field at t_{90} it is phase shifted by 90^0 in the laboratory frame so that B_1 is brought to lie along M_0 in the rotating frame. When the RF field is applied exactly on resonance the magnetisation M_0 in the rotating frame experiences B_1. The small field B_1 is now analogous to B_0 in the laboratory frame and M_0 is said to be spin-locked to B_1. Hence, M_0 relaxes along B_1 to a much smaller equilibrium value given by $M = cB_1 / T_L$ with an exponential time constant $T_{1\rho}$ (T_1 in the rotating frame; see Fig.2-7).

Note that the temperature is now that of the lattice and so the spin system has cooled. Relaxation back to M_0 along z occurs in the time taken for the system to ' warm up ' again to a spin temperature T_s (the concept of the temperatures T_L and T_s will be looked at again in chapter three).

A measurement is made by turning off the RF field after a suitable spin-locking period and monitoring the height of the resulting F.I.D.Thus, the $T_{1\rho}$ pulse sequence is as shown in Fig.2-8.

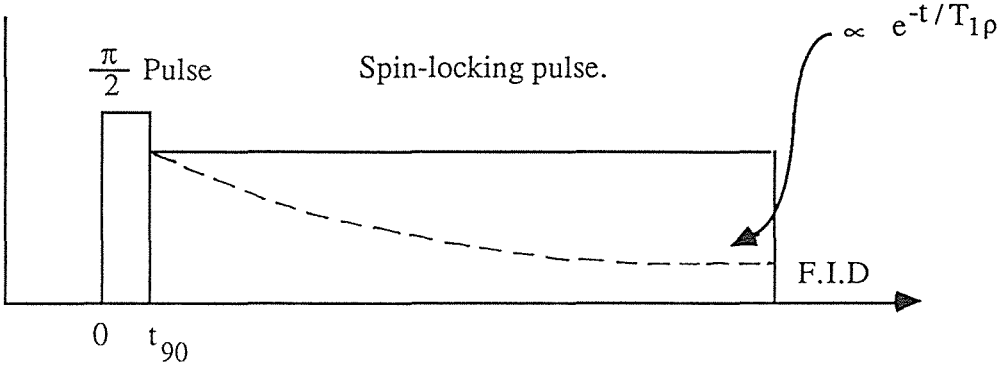

Fig.2-8 Spin-locking RF pulse sequence.

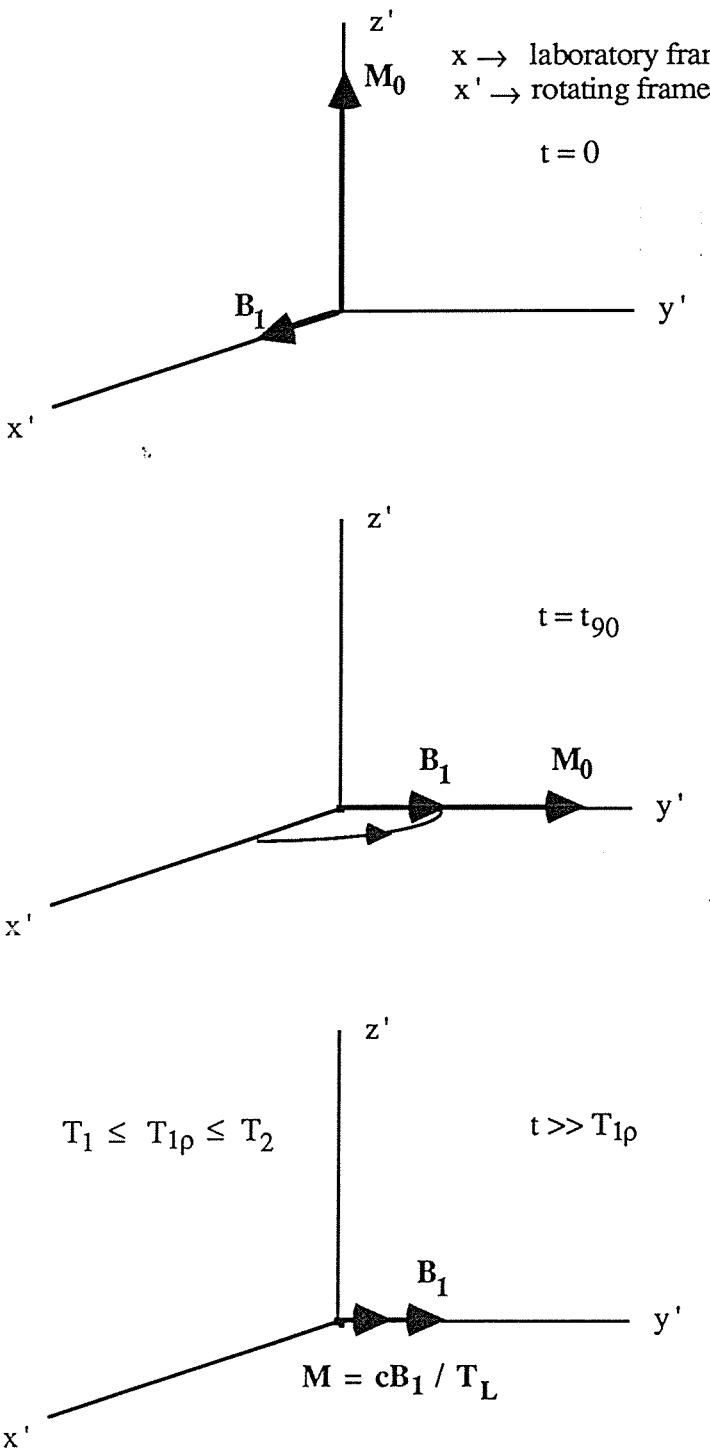

Fig.2-7

In the rotating frame, B_1 becomes analogous to B_0. Consequently M_0 relaxes along B_1 with a time constant $T_{1\rho}$.

It should be noted that $T_{1\rho}$ approaches T_2 as $\omega_1 \rightarrow 0$. However, this can never be achieved in practice because ω_1 must be sufficiently large so as to satisfy the Redfield condition[24] which states that experimentally we are limited to RF field intensities corresponding to ω_1 comparable with or greater than the resonance linewidth.

2.4.3 Spin-echoes

Because of the finite size of the sample each nucleus experiences a slightly different main magnetic field B_0 and therefore precesses either slightly faster or slower than the mean. This results in an unwanted contribution $1/T_2'$ to the natural relaxation rate $1/T_2$ and thus the observed value can be written as

$$1 / T_2^* = 1 / T_2' + 1 / T_2 \qquad (2.35)$$

It is possible to reverse this inhomogeneous dephasing and produce what is known as a spin-echo (devised by Carr-Purcell).After a time τ apply a $180^0|_x$. The echo will therefore form at time 2τ. The Carr-Purcell pulse sequence for a spin echo is shown together with the nuclear signal in Fig.2-9. This sequence is useful for measuring rapid T_2 decays.

The Carr-Purcell Train.

After the first echo, successive refocusing of the signal can be achieved resulting in a Carr-Purcell train. If a chain of pulses is applied at times $(2n + 1)\tau$ then the chain of echoes will be formed at times $(2n + 2)\tau$ with their amplitudes decaying as T_2. This will happen provided:

(a) τ is kept short enough (as must be the case in the Carr-Purcell spin echo pulse sequence) so as to prevent significant diffusion occurring between pulses since this would inhibit echo formation.

(b) The RF pulses are homogeneous.

The problem of RF inhomogeneity can be overcome by using phase shifted pulses. This is the Carr-Purcell-Meiboom-Gill (CPMG) sequence:

$$90^0|_x - \tau - 180^0|_y - 2\tau - 180^0|_y - 2\tau - 180^0|_y.$$

The CPMG pulse sequence thus enables the measurement of much longer T_2 decays. The spin echo will refocus all of the Zeeman interaction. The interested reader is referred to appendix A.

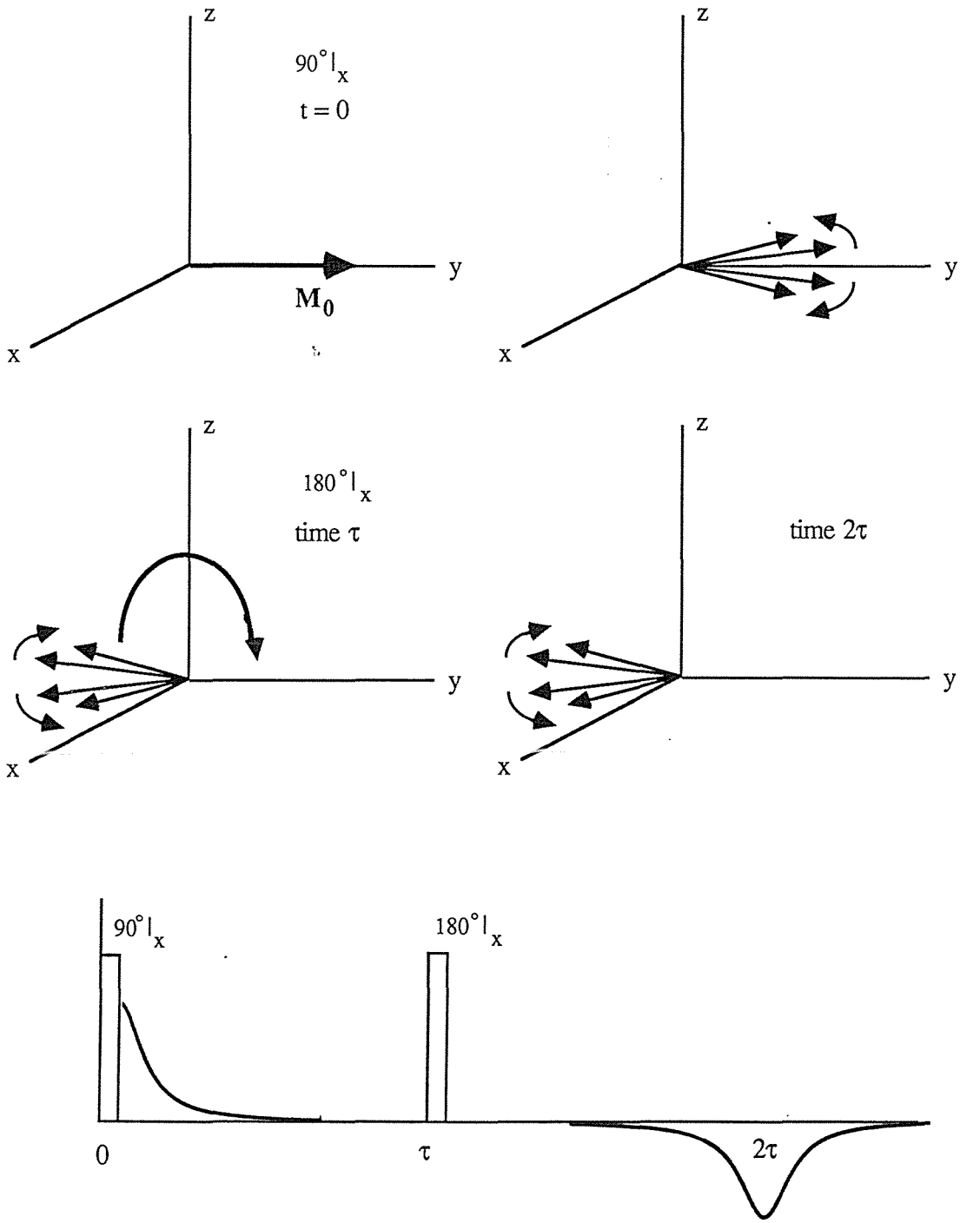

Fig.2-9

The Carr-Purcell spin echo which refocuses M_0 after dephasing occurs due to magnetic field inhomogeneities.

Chapter 3 Theory of Relaxation

When I do count the clock that tells the time
... William Shakespeare

3.1 Introduction

This chapter considers in detail the derivation of formulae for T_1 and $T_{1\rho}$. The procedure follows that of Look and Lowe[25] and the results obtained will be seen to contain an admixture of spectral densities evaluated at the characteristic frequencies $2\omega_1$, ω_0, $2\omega_0$ as pointed out in chapter one.

3.1.1 The Assumption of a Spin Temperature

The starting point is to consider a system of N spins which is able to be described by a spin temperature T_s. For the spin system to be in thermodynamic equilibrium and describable by T_s, it is required that, for any pair of levels separated in energy by ΔE, the ratio of the spin populations be determined by the Boltzmann factor $\exp[- \Delta E / kT_s]$. When dealing with a spin 1/2 system the description by a spin temperature is always valid, however for systems having spins > 1/2 this description can only be used as long as $T_2 << T_1$. As long as this condition exists the system of N spins interacts within itself more strongly than with the lattice and so will come to internal equilibrium more rapidly than it will come to equilibrium with the lattice.

The population p_n of the nth energy level, which is often given by the element ρ_{nn} of the density matrix is

$$p_n = \rho_{nn} = (1/Z) \exp[- E_n / kT]$$

$$= (1/Z) \exp[- \beta E_n] \qquad (3.1)$$

where $\beta = 1 / kT$ and $Z = \sum_n \exp[- \beta E_n]$.

Let W_{nm} be the probability per unit time that a transition is induced between the quantum levels $| n >$ and $| m >$ by interaction with the reservoir. Then the rate of change of the spin population, $\dot{\rho}_{mm}$, of the level $| m >$ is due to all the contributions from the other levels minus the contribution of $| m >$ to the other levels, or more succinctly,

$$\dot{\rho}_{mm} = \sum_{n \neq m} (\text{gain from} | n > - \text{loss from} | m >) \qquad (3.2)$$

Thus the relaxation master equation for the diagonal elements of the density matrix (i.e spin populations) is[26]

$$\dot{\rho}_{mm} = \sum_{n \neq m} (\rho_{nn} W_{nm} - \rho_{mm} W_{mn}) \qquad (3.3)$$

3.1.2 Consideration of the Reservoir from an Energy Viewpoint

In order for the spin system to undergo a transition between energy levels | n > and | m > the reservoir must necessarily undergo the reverse transition between its corresponding levels | N > and | M > respectively. Fig.3-1 illustrates this

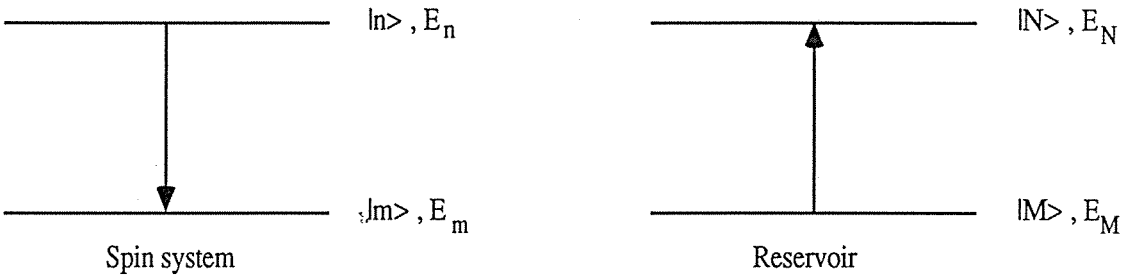

$E_n \rightarrow E_m$ requires a transition $E_M \rightarrow E_N$

Likewise $E_m \rightarrow E_n$ requires a transition $E_N \rightarrow E_M$

Fig.3-1

Schematic showing the energy coupling between the Spin system and the Reservoir.

This can be seen, for example, in a two-spin system whereby the spins in the higher energy state | -1/2 > must give up a certain amount of energy, γB_0, to the lattice in order to align themselves with the magnetic field (Fig.3-2).

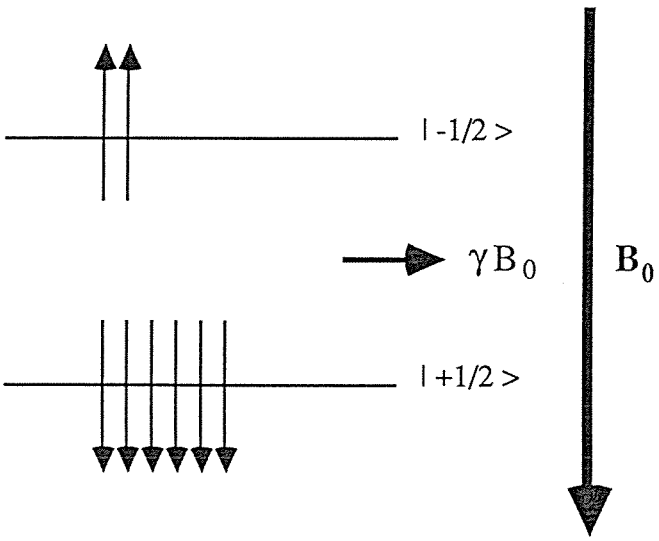

Fig.3-2

The Spin system must exchange energy with the Reservoir in order to align the higher energy spins with the main magnetic field B_0.

Hence, for general levels | n > and | m > then W_{mn} / W_{nm} must have the ratio of the density of states in the reservoir (as required by the fact that the system left to itself will come to thermal equilibrium and the principle of detailed balancing); that is

$$W_{mn} / W_{nm} = \exp[-\beta_L(E_N - E_M)]$$

$$= \exp[-\beta_L(E_n - E_m)] \qquad (3.4)$$

where $\beta_L = 1 / kT_L$, and T_L is the reservoir (lattice) temperature. Combining Eq.(3.3) with Eq.(3.4) yields

$$\dot{\rho}_{mm} = \sum_{n \neq m} \{ \rho_{nn} - \rho_{mm} \exp[-\beta(E_n - E_m)] \} W_{nm} \qquad (3.5)$$

3.1.3 Derivation of Hebel-Slichter Expression for T_1

The groundwork just covered will prove useful in obtaining the general relation of Hebel and Slichter[27] giving the spin-lattice relaxation time T_1 for systems maintaining a spin temperature, which is derived as follows:
We find $d\beta / dt$ using

$$d < \overline{E} > / dt = (d < \overline{E} > / d\beta)(d\beta / dt) \qquad (3.6)$$

Now

$$d < \overline{E} > / dt = d / dt [\sum_m \rho_{mm} E_m]$$

$$= \sum_m \dot{\rho}_{mm} E_m$$

$$= \sum_m [\sum_{n \neq m} \rho_{nn} W_{nm} - \rho_{mm} W_{mn}] E_m$$

$$= \sum_{m,n} [\rho_{nn} W_{nm} - \rho_{mm} W_{mn}] E_m \qquad (3.7)$$

Note that a more symmetrical form can be defined as follows since also

$$d < E > / dt = \sum_{m,n} [\rho_{mm} W_{mn} - \rho_{nn} W_{nm}] E_n$$

$$= - \sum_{m,n} [\rho_{nn} W_{nm} - \rho_{mm} W_{mn}] E_n \qquad (3.8)$$

$$\Rightarrow \quad d\langle \overline{E} \rangle / dt = 1/2 \sum_{m,n} [\ \rho_{nn} W_{nm} - \rho_{mm} W_{mn}\ ]\ [\ E_m - E_n\ ] \qquad (3.9)$$

$$= 1/2 \sum_{m,n} W_{nm}\ \rho_{nn}\ [\ 1 - \exp(\ \beta - \beta_L\ )(\ E_n - E_m\ )\ ]\ [\ E_m - E_n\ ] \qquad (3.10)$$

using $\rho_{mm} / \rho_{nn} = \exp\ \beta(\ E_n - E_m\ )$. Now

$$\langle \overline{E} \rangle = 1/Z \sum_m E_m \exp(\ -\beta E_m\ ) \quad \ldots \quad (= \sum_m \rho_{mm} E_m) \qquad (3.11)$$

and $Z = \sum_m [\ 1 - \beta E_m + (\ \beta E_m / 2!\ )^2 + \ldots\ ]$. If we restrict ourselves to high temperatures

then Z can be approximated by

$$Z = Z_\infty = \sum_m (\ 1 - \beta E_m\ ) \qquad (3.12)$$

and $Tr\ (\ Z\ ) = Tr\ (\ Z_\infty\ ) = 2I + 1$. Thus differentiating Eq.(3.11) with respect to β gives

$$d\langle \overline{E} \rangle / d\beta = - 1/Z_\infty \sum_m E_m^2 \exp(\ - \beta E_m\ )$$

$$\approx - 1/Z_\infty \sum_m E_m^2 \qquad (3.13)$$

So under the high temperature approximation (H.T.A)

$$d\langle \overline{E} \rangle / dt = 1/2 \sum_{m,n} W_{nm}\ \rho_{nn} [\ (\ \beta_L - \beta\ )(\ E_n - E_m\ )(\ E_m - E_n\ )\ ]$$

$$= - 1/2 \sum_{m,n} W_{mn}\ \rho_{nn}\ (\ \beta_L - \beta\ )(\ E_n - E_m\ )^2$$

$$\approx - 1/2 \sum_{m,n} W_{mn}\ (\ E_n - E_m\ )^2\ (\ \beta_L - \beta\ ) / Z_\infty \qquad (3.14)$$

Therefore $d\beta / dt = \beta_L - \beta / T_1$ where

$$1 / T_1 = [\ 1/2 \sum_{m,n} W_{nm} (\ E_n - E_m\ )^2\ ] / \sum_m E_m^2 \qquad (3.15)$$

It should be noted that β relaxes exponentially to β_L. Also the assumption of a spin temperature forces the system to relax with a single exponential. Eq.(3.15) is the Hebel-Slichter[27] expression for T_1 and provides for us the stepping stone to attaining general formulae for T_1 and $T_{1\rho}$ to which the next section is hereby devoted to in detail.

3.2 Derivation of the Spin-lattice Relaxation Times

3.2.1 Relaxation along the Static Field

Fig.3-3 shows two spins i and j subject to a main magnetic field B_0. Let the direction of B_0 define the z-axis of a spherical polar co-ordinate system with θ_{ij} and ϕ_{ij} denoting the usual polar and azimuthal angles respectively of the internuclear vector r_{ij} between the two spins.

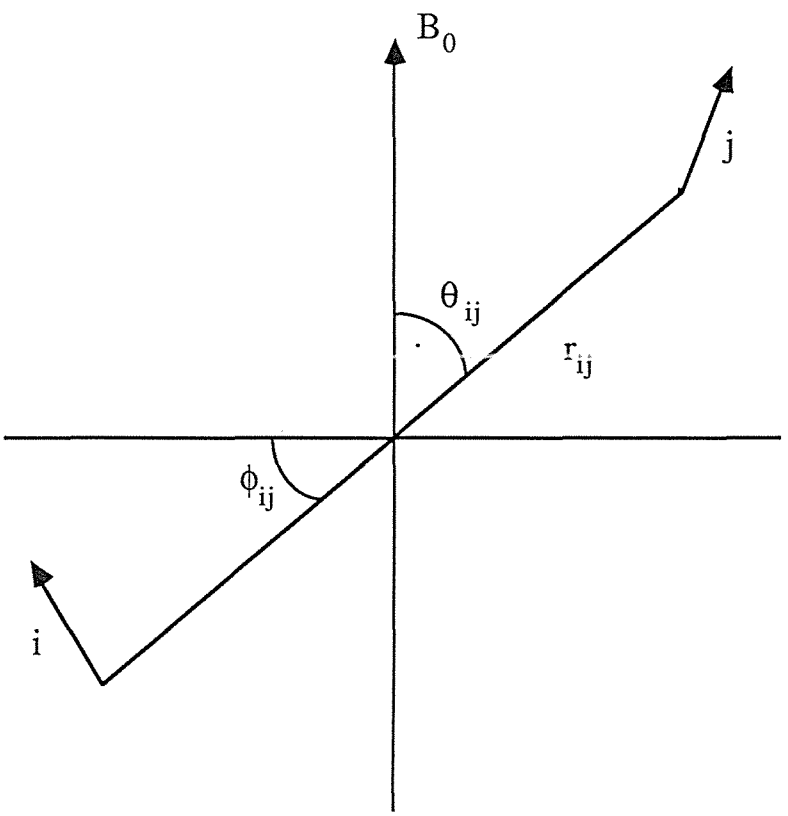

Fig.3-3

The geometry for two spins i and j subject to a main magnetic field B_0.

In computing the spin-lattice relaxation time T_1 along the static magnetic field B_0, the zeroth order Hamiltonian is assumed to be

$$\mathcal{H}_0 = -\gamma\hbar B_0 \sum_i I_z^i \qquad (3.16)$$

The perturbing Hamiltonian is made up from the sum of the dipole-dipole interactions between pairs of spins and is given in Cartesian co-ordinates by[28]

$$\mathcal{H}_1 = (\gamma\hbar)^2 \{ [3(\mathbf{I}^1.\mathbf{r})(\mathbf{I}^2.\mathbf{r}) / r^5] - [\mathbf{I}^1.\mathbf{I}^2 / r^3] \} \qquad (3.17)$$

with $< | \overline{\mathcal{H}_0} | >$ much greater than $< | \overline{\mathcal{H}_1} | >$. Expressing $\mathcal{H}_1$ into spherical-polar co-ordinates gives[29]

$$\mathcal{H}_1 = (\gamma\hbar)^2 \sum_{i<j} (A_{ij} + B_{ij} + C_{ij} + D_{ij} + E_{ij} + F_{ij}) \qquad (3.18)$$

where

$$A_{ij} = r_{ij}^{-3} (1 - 3\cos^2\theta_{ij}) I_3^i I_3^j \qquad (\Delta m = 0) \qquad (3.19)$$

$$B_{ij} = -1/4\ r_{ij}^{-3} (1 - 3\cos^2\theta_{ij}) (I_+^i I_-^j + I_-^i I_+^j) \qquad (\Delta m = 0)$$

$$C_{ij} = -3/2\ r_{ij}^{-3} \sin\theta_{ij}\cos\theta_{ij} \exp(-i\phi_{ij}) (I_z^i I_+^j + I_+^i I_z^j) \qquad (\Delta m = 1)$$

$$D_{ij} = C_{ij}^+ \qquad (\Delta m = -1)$$

$$E_{ij} = -3/4\ r_{ij}^{-3} \sin^2\theta_{ij} \exp(-i2\phi_{ij}) I_+^i I_+^j \qquad (\Delta m = 2)$$

$$F_{ij} = E_{ij}^+ \qquad (\Delta m = -2)$$

where the dagger denotes the Hermitian conjugate and I_+^j and I_-^j are the usual raising and lowering operators, respectively, for eigenfunctions of I_z^j. The reader should note that each of the terms above is the product of a spatial operator and a spin operator. Also because of the relative motion of the nuclei the r_{ij}, θ_{ij} and ϕ_{ij} are all time dependent and thus $\mathcal{H}_1$ has the form[25]

$$\mathcal{H}_1(t) = \sum_{\alpha} \mathcal{H}_{1r}^{\alpha}(t)\ \mathcal{H}_{1s}^{\alpha} \qquad (3.20)$$

where the subscripts r and s refer to the spatial and spin operators respectively and $\alpha = A_{ij}, B_{ij}, C_{ij}, D_{ij}, E_{ij}$ and F_{ij} is summed over all i and j. It should also be pointed out that only terms where off-diagonal elements appear in the product of the spin operators are involved in causing transitions (i.e. those with $\Delta m \neq 0$). Thus the terms C_{ij}, D_{ij}, E_{ij} and F_{ij} are important and in this regard form the selection rules for transitions. The terms with $\Delta m = 0$ are time independent and leave the energy unchanged.

In chapter two, Eq.(2.1) defined a general state $| \Psi >$ to be $| \Psi > = \sum a_m | m >$. If the complex admixture amplitudes are now considered to be time dependent then

$$| \Psi > = \sum_m a_m(t) \exp(-iE_m t) | m > \qquad (3.21)$$

By writing down the Schrodinger equation

$$(1/i\hbar) \partial | \Psi > / \partial t = (\mathcal{H}_0 + \mathcal{H}_1) | \Psi > \qquad (3.22)$$

then from first order perturbation theory it can easily be shown that

$$\dot{a}_m = (1/i\hbar) \sum_{n \neq m} < m | \mathcal{H}_1(t) | n > a_n \exp[i(\omega_m - \omega_n)t] \qquad (3.23)$$

$$\approx (1/i\hbar) \sum_{n \neq m} < m | \mathcal{H}_1(t) | n > \exp[i(\omega_m - \omega_n)t] \qquad (3.24)$$

if $a_n \approx 1$ and $a_m \approx 0$ for all time. This approximation, as Bloembergen, Purcell and Pound point out, is only valid for slow relaxation; i.e.,

$$1 / T_1 << (\gamma\hbar)^2 / r^3 \qquad (3.25)$$

which is approximately 200 kHz for this work. Upon integrating Eq.(3.24) we get

$$a_m = (1/i\hbar) \int_0^t < m | \mathcal{H}_1(t') | n > \exp[i \omega_{mn} t'] dt' \qquad (3.26)$$

where $\omega_{mn} = \omega_m - \omega_n$. Assuming that the time dependence of $\mathcal{H}_{1r}^{\alpha}(t)$ is random, we can now proceed to obtain W_{mn}; hence[30]

$$W_{mn} = dP_m / dt = d/dt (a_m a_m^*)$$

$$= a_m (da_m^* / dt) + \text{complex conjugate (c.c)} \qquad (3.27)$$

Therefore

$$W_{mn} = (1/\hbar^2) \int_0^t < n | \mathcal{H}_1(t) | m > < m | \mathcal{H}_1(t') | n > \exp[i \omega_{mn}(t' - t)] dt' + \text{c.c} \qquad (3.28)$$

Let $t' - t = \tau$. Then $dt' = d\tau$. Thus

$$W_{mn} = (1/\hbar^2) \int_{-t}^0 \overline{< n | \mathcal{H}_1(t) | m > < m | \mathcal{H}_1(t + \tau) | n >} \exp[i \omega_{mn}(\tau)] d\tau + \text{c.c} \qquad (3.29)$$

The limits on the integral of the complex conjugate will range from 0 to t and so the total range integrated over will be -t to t. Letting the limits then tend to infinity and allowing that $\mathcal{H}_1(t)$ is stationary, gives

$$W_{mn} = (1/\hbar^2) \int_{-\infty}^{\infty} \overline{< n | \mathcal{H}_1(t) | m > < m | \mathcal{H}_1(t + \tau) | n >} \exp[i \omega_{mn} \tau] d\tau_{AV} \qquad (3.30)$$

Inserting the $\mathcal{H}_1(t)$ of Eq.(3.20) into Eq.(3.30) yields

$$W_{mn} = (1/\hbar^2) \sum_{\alpha,\alpha'} \int_{-\infty}^{\infty} \overline{[\mathcal{H}_{1r}^{\alpha}(t)\ \mathcal{H}_{1r}^{\alpha'}(t+\tau)]} \exp[i\omega_{mn}\tau]\, d\tau_{AV} \times \langle n|\mathcal{H}_{1s}^{\alpha}|m\rangle\langle m|\mathcal{H}_{1s}^{\alpha'}|n\rangle \qquad (3.31)$$

Therefore[25]

$$W_{mn} = (1/\hbar^2) \sum_{\alpha,\alpha'} \{ \int_{-\infty}^{\infty} G_{1r}^{\alpha\alpha'}(t,\tau) \exp[-i\omega_{mn}\tau]\, d\tau \} \times \langle n|\mathcal{H}_{1s}^{\alpha}|m\rangle\langle m|\mathcal{H}_{1s}^{\alpha'}|n\rangle \qquad (3.32)$$

where $G_{1r}^{\alpha\alpha'}(t,\tau)$, a correlation function is defined by

$$G_{1r}^{\alpha\alpha'}(t,\tau) \equiv \overline{\langle \mathcal{H}_{1r}^{\alpha}(t)\ \mathcal{H}_{1r}^{\alpha'}(t+\tau)\rangle} \qquad (3.33)$$

For stationary random processes $G_{1r}^{\alpha\alpha'}(t,\tau)$ is independent of t and so becomes $G_{1r}^{\alpha\alpha'}(\tau)$. Since we are assuming that $\langle|\overline{\mathcal{H}_0}|\rangle$ is much greater than $\langle|\overline{\mathcal{H}_1}|\rangle$ then the energy difference $E_n - E_m$ depends only upon $\mathcal{H}_{1s}^{\alpha}$ and not upon the spin states $|n\rangle$ and $|m\rangle$. Then letting the energy difference $E_n - E_m = \hbar\omega^{\alpha}$, we can define our spectral density by

$$J_{1r}^{\alpha\alpha'}(\omega^{\alpha}) \equiv \int_{-\infty}^{\infty} G_{1r}^{\alpha\alpha'}(\tau) \exp[-i\omega^{\alpha}\tau]\, d\tau \qquad (3.34)$$

and so W_{nm} then becomes[25]

$$W_{nm} = 1/\hbar^2 \sum_{\alpha,\alpha'} J_{1r}^{\alpha\alpha'}(\omega^{\alpha}) \langle n|\mathcal{H}_{1s}^{\alpha}|m\rangle\langle m|\mathcal{H}_{1s}^{\alpha'}|n\rangle \qquad (3.35)$$

Thus inserting the W_{nm} of Eq.(3.35) into the Hebel-Slichter formula of Eq.(3.15) and using $E_m = \langle m|\mathcal{H}_0|m\rangle$ we find,

$$1/T_1 = (1/2\hbar^2) \sum_{\alpha,\alpha'} J_{1r}^{\alpha\alpha'}(\omega^{\alpha}) \{ \sum_{m,n} \langle n|\mathcal{H}_{1s}^{\alpha}|m\rangle\langle m|\mathcal{H}_{1s}^{\alpha'}|n\rangle \times [\langle n|\mathcal{H}_0|n\rangle^2 - 2\langle n|\mathcal{H}_0|n\rangle\langle m|\mathcal{H}_0|m\rangle + \langle m|\mathcal{H}_0|m\rangle^2] \} / \sum_{m} \langle m|\mathcal{H}_0|m\rangle^2 \qquad (3.36)$$

$$= (1/2\hbar^2) \sum J_{1r}^{\alpha\alpha'}(\omega^\alpha) \sum \{ \sum ($$

$$\langle n | \mathcal{H}_{1s}^{\alpha} | m \rangle \langle m | \mathcal{H}_0 | m \rangle \langle m | \mathcal{H}_0 | m \rangle \langle m | \mathcal{H}_{1s}^{\alpha'} | n \rangle$$

$$+ \langle n | \mathcal{H}_0 | n \rangle \langle n | \mathcal{H}_{1s}^{\alpha} | m \rangle \langle m | \mathcal{H}_{1s}^{\alpha'} | n \rangle \langle n | \mathcal{H}_0 | n \rangle$$

$$- \langle n | \mathcal{H}_0 | n \rangle \langle n | \mathcal{H}_{1s}^{\alpha} | m \rangle \langle m | \mathcal{H}_0 | m \rangle \langle m | \mathcal{H}_{1s}^{\alpha'} | n \rangle \qquad (3.37)$$

$$- \langle n | \mathcal{H}_{1s}^{\alpha} | m \rangle \langle m | \mathcal{H}_0 | m \rangle \langle m | \mathcal{H}_{1s}^{\alpha'} | n \rangle \langle n | \mathcal{H}_0 | n \rangle) \} /$$

$$\sum_m \langle m | \mathcal{H}_0 | m \rangle^2$$

By arranging the terms in the above order one can easily see that the relaxation rate can now be written more succinctly as[25]

$$1 / T_1 = (1/2\hbar^2) \{ - \sum_{\alpha,\alpha'} J_{1r}^{\alpha\alpha'}(\omega^\alpha) \, \mathrm{Tr} ([\mathcal{H}_0 , \mathcal{H}_{1s}^{\alpha}] [\mathcal{H}_0 , \mathcal{H}_{1s}^{\alpha}]) \} / \mathrm{Tr}\ \mathcal{H}_0^2 \qquad (3.38)$$

where Tr means trace or sum over the diagonal matrix elements. At this stage it is important to realise that the identity matrix $\mathcal{I}$ is present since, for example, the Zeeman Hamiltonian can be written as

$$\mathcal{H}_0 = - \gamma\hbar B_0 I_z^i \, \mathcal{I} \qquad (3.39)$$

and as seen in chapter two the $\mathrm{Tr}(\mathcal{I}) = 2I + 1$ and so

$$\mathrm{Tr}(\mathcal{H}_0^2) = (\gamma\hbar B_0)^2 \, \mathrm{Tr}[(I_z^i)^2] \, \mathrm{Tr}(\mathcal{I})$$

$$= (\gamma\hbar B_0)^2 (1/3) I (I + 1) (2I + 1)^2 \qquad (3.40)$$

The evaluation of the traces is straightforward and is shown below for α corresponding to C_{ij}. (Refer to Eq.(3.19)).

$$C_{ij} = - (3/2) c_{ij} (I_z^i I_+^j + I_+^i I_z^j) \qquad (3.41)$$

where $c_{ij} = r_{ij}^{-3} \sin\theta_{ij}\cos\theta_{ij} \exp(-i\phi_{ij})$. Then

$$[\mathcal{H}_0 , \mathcal{H}_{1s}^{\alpha}] = (\gamma\hbar B_0) [I_z^i , I_z^i I_+^j + I_+^i I_z^j]$$

$$= (\gamma\hbar B_0) \{ I_z^i [I_z^i , I_+^j] + [I_z^i , I_+^i] I_z^j \}$$

$$= (\gamma\hbar B_0) (I_z^i I_+^j + I_+^i I_z^j) \qquad (3.42)$$

where we have made use of the relationships

$$I_+ = I_x + i\, I_y \qquad (3.43a)$$

$$[\, I_z , I_x \,] = i\, I_y \qquad (3.43b)$$

$$[\, I_z , I_y \,] = -i\, I_x \qquad (3.43c)$$

Then $[\, \mathcal{H}_0 , \mathcal{H}_{1s}^{\alpha'} \,]$ can be written down directly as

$$[\, \mathcal{H}_0 , \mathcal{H}_{1s}^{\alpha'} \,] = (\gamma\hbar B_0) (I_z^i I_-^j + I_-^i I_z^j) \qquad (3.44)$$

since this must be the case so as to bring Eq.(4.42) back to a diagonal matrix. This gives for our trace then,

$$\mathrm{Tr} ([\, \mathcal{H}_0 , \mathcal{H}_{1s}^{\alpha} \,] [\, \mathcal{H}_0 , \mathcal{H}_{1s}^{\alpha'} \,]) = 2\, \mathrm{Tr} \{ (I_z^i)^2 I_+^j I_-^j \}$$

$$= 2 (1/3) I (I + 1) (2I + 1) \times (2/3) I (I + 1) (2I + 1) \qquad (3.45)$$

Finally then, when all the factors have been brought together, the spin-lattice relaxation rate for N spins becomes

$$1 / T_1 = \gamma^4 \hbar^2 \{ 3I (I + 1) / 2N \} \sum_{i \neq j} [\, K_{ij}^{(1)} (\omega_0) + K_{ij}^{(2)} (2\omega_0) \,] \qquad (3.46)$$

where we make the definitions

$$K_{ij}^{(1)} (\omega) \equiv 1/2 \int_{-\infty}^{\infty} \exp (- i \omega\tau) [\, \overline{< c_{ij} (\tau) c_{ij}^* (0) >} + \mathrm{c.c} \,] \qquad (3.47a)$$

$$K_{ij}^{(2)} (\omega) \equiv 1/2 \int_{-\infty}^{\infty} \exp (- i \omega\tau) [\, \overline{< e_{ij} (\tau) e_{ij}^* (0) >} + \mathrm{c.c} \,] \qquad (3.47b)$$

For a pair of spins where N = 2 then[31]

$$1 / T_1 = 3/2\ \gamma^4 \hbar^2 I (I + 1) [\, J^{(1)} (\omega_0) + J^{(2)} (2\omega_0) \,] \qquad (3.48)$$

This shows the dependence of T_1 upon the spectral densities evaluated at the characteristic frequencies ω_0 and $2\omega_0$.

3.2.2 Relaxation along the Rotating Field

In order to calculate the relaxation time along the rotating field $T_{1\rho}$ it is necessary to assume that the interactions within the spin system are strong enough so that a temperature is maintained within the spin system at all times (in the rotating frame) and that the effect of the spin-lattice interaction is to change this temperature slowly until an equilibrium value is reached.(The reason why the system behaves as if it were proceeding toward equilibrium in the rotating frame is because the Hamiltonian is less time dependent in such a frame[24]). The spins and the lattice in the laboratory frame are two ordinary thermodynamic systems and that clearly when their temperatures are equal then an equilibrium between them will exist; however, as pointed out by Abragam[32], no such simple predictions can now be made because the spin and lattice temperatures in the present problem are now defined in two different frames of reference. The transformation to the rotating frame involves the use of the operator

$$S = \exp (i\omega_0 t \sum_i I_z^i) \qquad (3.49)$$

and

$$\mathcal{H}^r = S \mathcal{H} S^{-1} + i\hbar S^{-1} (\partial S / \partial t) \qquad (3.50)$$

where $\mathcal{H}^r$ is the Hamiltonian in the rotating frame. By inserting the $\mathcal{H}_0$ and $\mathcal{H}_1$ of the Eq.(3.16) and Eq.(3.18) respectively we get

$$\mathcal{H}_0^r = - \gamma\hbar B_1 \sum_i I_x^i \qquad (3.51)$$

$$\mathcal{H}_1^r = \gamma^2\hbar^2 \sum_{i<j} [A_{ij} + B_{ij} + \exp (i\omega_0 t) C_{ij} + \exp (-i\omega_0 t) D_{ij} + \exp (2i\omega_0 t) E_{ij} + \exp (-2i\omega_0 t) F_{ij}] \qquad (3.52)$$

The result of the dipolar interaction terms of Eq.(3.52) being multiplied by coherent time dependent interaction terms is simply a shift of their frequency spectrums. Their general stochastic nature is left unchanged and can be inserted into Eq.(3.46) as our perturbative terms yielding,

$$1 / T_{1\rho} = \gamma^4\hbar^2 \{ 3I (I + 1) / 2N \} \times \sum_{i \neq j} [5/2 K_{ij}^{(1)} (\omega_0) + 1/4 K_{ij}^{(2)} (2\omega_0) + 1/4 K_{ij}^{(0)} (2\omega_1)] \qquad (3.53)$$

where the $K_{ij}^{(1)} (\omega)$ and $K_{ij}^{(2)} (\omega)$ are defined in Eq.(3.47) and

$$K_{ij}^{(0)} (\omega) \equiv 1/2 \int_{-\infty}^{\infty} \exp (-i\omega\tau) [\overline{< b_{ij} (\tau) b_{ij}^* (0) >} + c.c] \qquad (3.54)$$

$T_{1\rho}$ then has the further dependence on the low frequency ω_1.

For N = 2 then

$$1 / T_{1\rho} = 3/2\, \gamma^4\hbar^2\, I(I+1)\, [\, 1/4\, J_0(2\omega_1) + 5/2\, J_1(\omega_0) + 1/4\, J_2(2\omega_0)\,] \qquad (3.55)$$

The relaxation times T_1 and $T_{1\rho}$ have been calculated for N = 2 spin systems. The next section deals with the problem of the 3-spin methyl group CH_3 present in the PDMS chain,

$$[\, Si(CH_3)_2 \text{ --- } O\,]_n$$

3.3 The Problem of the Rotating Methyl Group

3.3.1 General

As mentioned in the previous section the formula for $T_{1\rho}$ is valid for a two-spin system. This section will show how the three-spin methyl group CH_3 present in the PDMS chain can in fact behave as a two-spin system comprised of two protons coupled together. This problem has been treated by Stejskal and Gutowsky[33] for T_1 and T_2 relaxation involving the J_1 and J_2 spectral densities. It is extended here for $T_{1\rho}$ by obtaining the J_0 term.

The expressions for both T_1 and $T_{1\rho}$ are based on the spatial operators

$$F_0(t) = (1 - 3\cos^2\theta) / r^3 \qquad (3.56a)$$

$$F_1(t) = \sin\theta\cos\theta \exp(i\phi) / r^3 \qquad (3.56b)$$

$$F_2(t) = \sin^2\theta \exp(2i\phi) / r^3 \qquad (3.56c)$$

where θ and ϕ denote the usual polar and azimuthal angles respectively of the internuclear vector **r** between the two spins, (see Fig.3-3), and

$$J_0(\omega) = \int_{-\infty}^{\infty} \exp(-i\omega\tau)\, \overline{F_0(t).F_0^*(t+\tau)}\, d\tau \qquad (3.57a)$$

$$J_1(\omega) = \int_{-\infty}^{\infty} \exp(-i\omega\tau)\, \overline{F_1(t).F_1^*(t+\tau)}\, d\tau \qquad (3.57b)$$

$$J_2(\omega) = \int_{-\infty}^{\infty} \exp(-i\omega\tau)\, \overline{F_2(t).F_2^*(t+\tau)}\, d\tau \qquad (3.57c)$$

The geometry for the CH_3 methyl group is as follows in Fig.3-4.

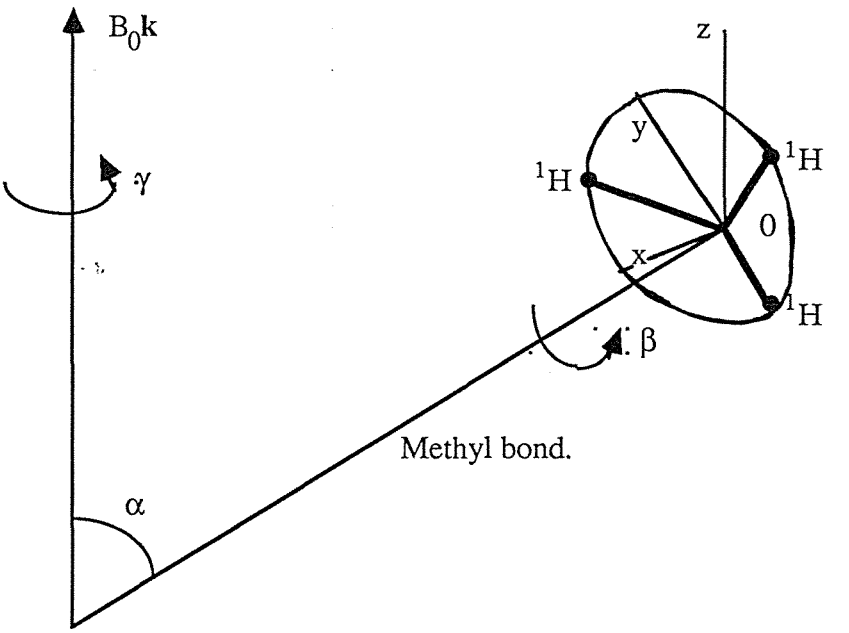

Fig.3-4
The geometry for the CH_3 methyl group subject to a main magnetic field B_0.

This group rapidly rotates due to quantum tunnelling as pointed out by Stejskal and Gutowsky[33]. Adding the relaxation effects of each proton separately is unwarranted. Instead, each proton must be assumed to interact with the other two protons in a manner that the motion of these protons is correlated .

A new axis system has been defined in which two azimuthal angles are now involved. The angle β for rotation about the methyl bond and the angle γ for rotation about the magnetic field. The H^1 - H^1 internuclear vectors lie in the plane of the equilateral triangle shown in Fig.3-4. At some arbitrary angle β, the orientation of one of the internuclear vectors can be represented by a radius r from the point where **r** makes an angle β with OX where XYZ form an orthogonal axis set and α is given in the YZ plane (see Fig.3-5).

Consider then the picture in the YZ plane. Note that **r** makes an angle θ with the vertical and so has a vertical component r cosθ; then referring to Fig.3-6,

$$r\cos\theta = r\sin\beta\cos(\pi/2 - \alpha)$$

$$= r\sin\beta\sin\alpha \qquad (3.58)$$

Therefore,

$$\cos\theta = \sin\beta\sin\alpha. \qquad (3.59)$$

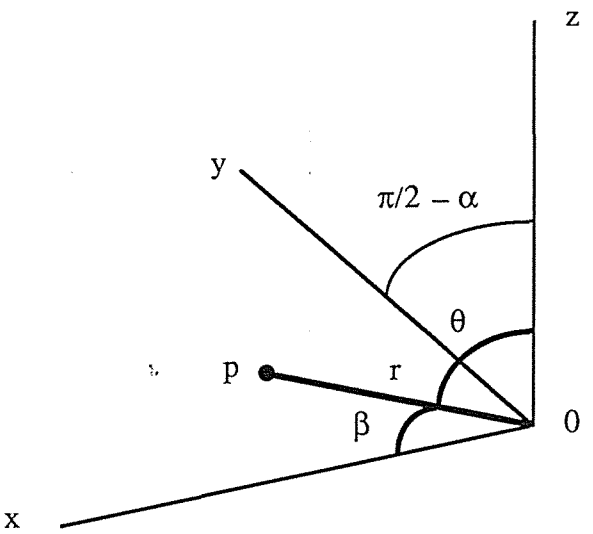

Fig.3-5
Schematic illustrating the new axis system for the CH_3 methyl group.

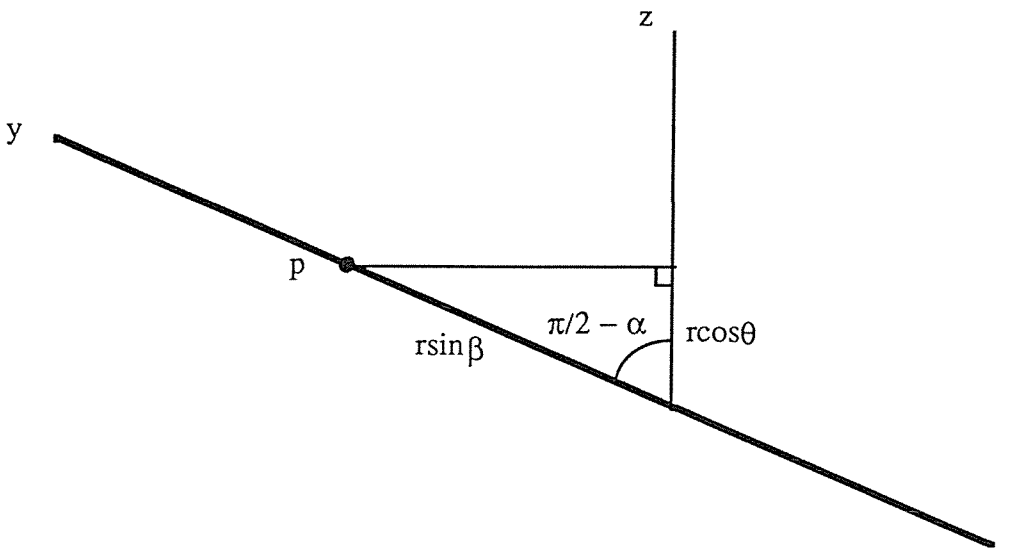

Fig.3-6
The geometry for the CH_3 methyl group shown in the y-z plane.

Consider the picture in the plane normal to z (see Fig.3-7),

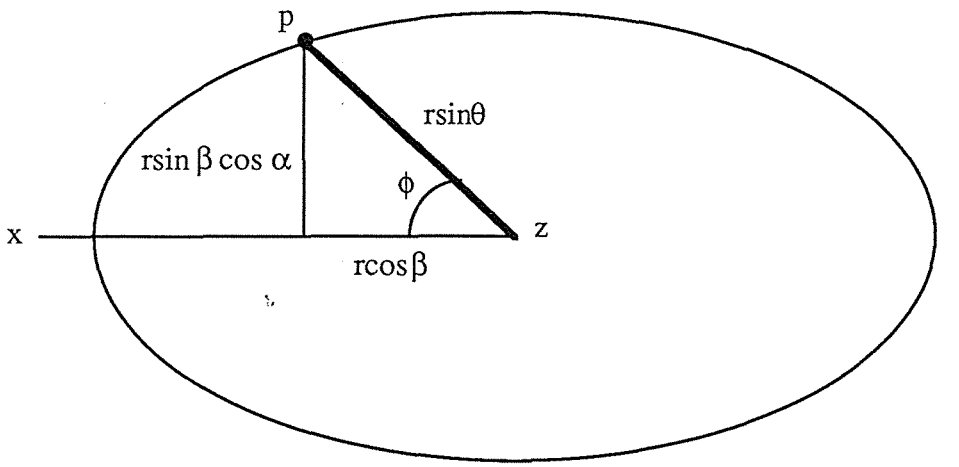

Fig.3-7

The geometry for the CH_3 methyl group shown in the plane normal to z.

then,

$$\cos\phi = \cos\beta / \sin\theta \qquad (3.60)$$

and

$$\sin\phi = \cos\alpha\sin\beta / \sin\theta \qquad (3.61)$$

In fact the additional azimuthal angle γ must be added to ϕ. Following Stejskal and Gutowsky[33] we may write down the spatial operators $F_0(t)$, $F_1(t)$ and $F_2(t)$ for two spins in the XY plane as

$$F_0(t) = 1/r^3 (1 - 3\cos^2\theta)$$

$$= 1/r^3 (1 - 3\sin^2\beta.\sin^2\alpha) \qquad (3.62a)$$

$$F_1(t) = 1/r^3 [\exp(i\phi_{tot})] \sin\theta\cos\theta$$

$$= 1/r^3 [\exp i(\gamma + \phi)] \sin\theta\sin\beta\sin\alpha \qquad (3.62b)$$

$$F_2(t) = 1/r^3 [\exp(2i\phi_{tot})] \sin^2\theta \qquad (3.62c)$$

Making use of the identities

$$\exp i\phi = (\cos\beta / \sin\theta) + i (\cos\alpha\sin\beta / \sin\theta) \qquad (3.63a)$$

$$\exp 2i\phi = [(\cos\beta / \sin\theta) + i (\cos\alpha\sin\beta / \sin\theta)]^2 \qquad (3.63b)$$

yields

$$F_0 (t) = 1/r^3 (1 - 3\sin^2\beta\sin^2\alpha) \qquad (3.64a)$$

$$F_1 (t) = 1/4r^3 [\exp(i\gamma)] (2\sin\alpha\sin2\beta - 2i\sin2\alpha\cos^2\beta + 2i\sin2\alpha) \qquad (3.64b)$$

$$F_2 (t) = 1/2r^3 [\exp(2i\gamma)] [2i\cos\alpha\sin2\beta + (1 + \cos^2\alpha)\cos2\beta + \sin^2\alpha] \qquad (3.64c)$$

To take into account the interaction from the third nucleus we must add to the above equations another similar set in which β is replaced by $\beta + \pi/3$ since the additional nucleus has its internuclear vector rotated by $\pi/3$ with respect to the original. Doing this yields

$$F_0 (t) = 1/4r^3 [8 - 6\sin^2\beta\sin^2\alpha - 9\sin^2\alpha - 3\ 3\sin2\beta\sin2\alpha] \qquad (3.65a)$$

$$F_1 (t) = 1/4r^3 [\exp(i\gamma)] [\sin\alpha\sin2\beta + 3\sin\alpha\cos2\beta - (i/2)\sin2\alpha\cos2\beta + (i\ 3/2)\sin2\alpha\sin2\beta + 2i\sin\alpha] \qquad (3.65b)$$

$$F_2 (t) = 1/2r^3 [\exp(2i\gamma)] [i\cos\alpha\sin2\beta + i\ 3\cos\alpha\cos2\beta - (1/2) (1 + \cos^2\alpha)\cos2\beta - (3/2)(1 + \cos^2\alpha)\sin2\beta + 2\sin^2\alpha] \qquad (3.65c)$$

3.3.2 Rapid Rotation

Finally if we consider the averages of $F_0 (t)$, $F_1 (t)$ and $F_2 (t)$, which can be taken for rapid changes in β (i.e. as long as β is much greater than $2\omega_0$), then the above equations simplify to yield

$$\overline{F_0 (t)} = 1/r^3 (3\cos^2\alpha - 1) \qquad (3.66a)$$

$$\overline{F_1 (t)} = i/r^3 [\exp(i\gamma)] \sin\alpha\cos\alpha \qquad (3.66b)$$

$$\overline{F_2 (t)} = 1/r^3 [\exp(2i\gamma)] \sin^2\alpha \qquad (3.66c)$$

On comparing Eq.'s (3.66) with Eq.'s (3.56) one finds that on replacing θ and ϕ with α and γ respectively, they are identical apart from altering their phase. However these phase changes do not affect the spectral densities $J_0(\omega)$, $J_1(\omega)$ and $J_2(\omega)$. By this analysis then the relaxation of protons in methyl groups under rapid rotation, due to the effect of the other two protons, is the same as that of protons in a pair whereby the orientation of the internuclear vector (θ , ϕ) is changed to that of the C-axis vector in the CH_3 group (α , γ).

Chapter 4 Derivation of the Spectral Densities

Therefore let us leave the elementary teachings of Christ
and go on to maturity ... The letter to the Hebrews 6:1

This chapter continues the discussion of spectral densities in chapter three. The three terms $J_0(2\omega_1)$, $J_1(\omega_0)$ and $J_2(2\omega_0)$ involved in the relaxation rate $1/T_{1\rho}$ are derived for the CH_3 group. The problem of the polymer chain in the melt is considered in more detail with particular emphasis being towards developing correlation functions which adequately describe the three components. Finally a spectral density for the molten polymer chain is outlined and briefly summarised.

4.1 Rotational Diffusion Outlined

4.1.1 Autocorrelation of $F_k(t)$ with Spherical Freedom

For a single pair of nuclei the spatial operators $F_k(t)$ where $k = 0, 1, 2$ can be related to the spherical harmonics Y_2^k respectively. This idea will be used in accordance with the rotational model of Abragam[34] where rotational diffusion takes place on the surface of a sphere and can be described by a diffusion equation

$$\partial\Psi / \partial t = (D_s / a^2)\,\Delta_s \Psi \qquad (4.1)$$

where Δ_s is the Laplacian operator on the surface of a sphere and Ψ is the probability of finding the internuclear vector at (θ, ϕ) at time t. Then expressing Ψ as an expansion of spherical harmonics,

$$\Psi(\theta, \phi, t) = \sum_{l,m} c_l^m(t) Y_l^m(\theta, \phi) \qquad (4.2)$$

$$= \sum_{l,m} c_l^m(t) Y_l^m(\Omega) \qquad (4.3)$$

Inserting Eq.(4.3) into Eq.(4.1) and taking into account the relation $\Delta_s Y_l^m(\Omega) = -l(l+1) Y_l^m(\Omega)$ as well as the orthogonality of the spherical harmonics it is seen that

$$\partial c_l^m(t) / \partial t = (-D_s / a^2)\, l(l+1)\, c_l^m(t) \qquad (4.4)$$

$$\Rightarrow c_l^m(t) = c_l^m(0) \exp(-t/\tau_l) \qquad (4.5)$$

where Abragam introduces τ_l such that

$$\tau_l = (D_s / a^2)\, l(l+1) \qquad (4.6)$$

$P(\Omega, \Omega_0, t)$ is the conditional probability of finding the system at Ω at time t if it is at Ω_0 at time zero. This means that $P(\Omega, \Omega_0, t)$ is the solution Ψ which obeys the initial condition

$$\Psi(\Omega, 0) = \delta(\Omega - \Omega_0) = \sum_{l,m} Y_l^{m*}(\Omega_0)\, Y_l^m(\Omega) \qquad (4.7)$$

Whence,

$$c_l^m(0) = Y_l^{m*}(\Omega_0) \qquad (4.8)$$

and

$$P(\Omega, \Omega_0, t) = \sum_{l,m} Y_l^{m*}(\Omega_0)\, Y_l^m(\Omega) \exp(-t/\tau_l) \qquad (4.9)$$

Now the a priori probability $p(\Omega_0)$ is $1/4\pi$ so that

$$G_{kk'}(t) = \iint F_k^*(\Omega)\, F_{k'}(\Omega_0)\, P(\Omega, \Omega_0, t)\, p(\Omega_0)\, d\Omega\, d\Omega_0 \qquad (4.10)$$

$$= \iint F_k^*(\Omega)\, F_{k'}(\Omega_0) \left[\sum_{l,m} Y_l^{m*}(\Omega_0)\, Y_l^m(\Omega) \exp(-t/\tau_l) \right] 1/4\pi\, d\Omega d\Omega_0 \qquad (4.11)$$

It is often convenient to express the F_k in a basis of Y_l^m because of the orthogonality of the spherical harmonics

$$F_k(\Omega) = \sum_{l',m'} a^k_{l'm'}\, Y_{l'}^{m'}(\Omega) \qquad (4.12)$$

Therefore

$$G_{kk'}(t) = 1/4\pi \sum_{l,m} a^k_{lm}\, a^{k'}_{lm} \exp(-|t|/\tau_l) \qquad (4.13)$$

4.1.2 Autocorrelation of $F_k(t)$ with Azimuthal Freedom only

Consider the rotational diffusion taking place around one axis only so that now

$$\partial\Psi/\partial t = (D_s/a^2)\, \partial^2\Psi/\partial\phi^2 \qquad (4.14)$$

If Ψ is expanded in a Fourier series $\Psi(\phi) = \sum_m c_m \exp(im\phi)$ then

$$(dc_m/dt) \exp(im\phi) = (-D_s/a^2)\, m^2 \exp(im\phi)\, c_m \qquad (4.15)$$

$$\Rightarrow c_m(t) = c_m(0) \exp(-|t|/\tau_m) \qquad (4.16)$$

where

$$1/\tau_m = (D_s/a^2)\ m^2 \qquad (4.17)$$

By similar reasoning to 4.1.1 $P(\phi, \phi_0, t)$ is $\Psi(\phi, t)$ where

$$\Psi(\phi, 0) = \delta(\phi - \phi_0) \qquad (4.18)$$

$$= N \sum_m \exp(-im\phi_0) \exp(im\phi) \qquad (4.19)$$

and N is some normalisation factor. Thus

$$P(\phi, \phi_0, t) = N \sum_m \exp(-im\phi_0) \exp(im\phi) \exp(-t/\tau_m) \qquad (4.20)$$

and so

$$G_{kk'}(t) = 1/2\pi \iint F_k^*(\phi) F_{k'}(\phi_0) N \sum_m \exp(-im\phi_0) \exp(im\phi) \exp(-t/\tau_m)\, d\phi\, d\phi_0 \qquad (4.21)$$

Because of the orthogonality of the $\exp(im\phi)$, it is convenient to expand the azimuthal parts of F_k in the following Fourier basis

$$F_k(\phi) = \sum_{m'} b^k_{m'} \exp(im\phi) \qquad (4.22)$$

This gives for the autocorrelation function

$$G_{kk'}(t) = N/2\pi \sum_m b^k_m\ b^{k'}_m \exp(-|t|/\tau_m) \qquad (4.23)$$

4.2 Application to the Methyl Group

4.2.1 First Steps

The preceding theory can now be applied to the CH_3 group to determine the spectral densities involved. By comparing with Eq.(3.65) the $F_k(t)$ can be decomposed into

$$F_k(t) = \phi_k^1(t) + \phi_k^2(t) \sin 2\beta + \phi_k^3(t) \cos 2\beta. \qquad (4.24)$$

where β is the angle for methyl group azimuthal rotations.Since (γ, α) and β are uncorrelated then

$$\langle F_k^*(t+\tau) F_k(t) \rangle = \langle \phi_k^{1*}(t+\tau) \phi_k^1(t) \rangle + \langle \phi_k^{2*}(t+\tau) \phi_k^2(t) \rangle \langle \sin 2\beta(t+\tau) \sin 2\beta(t) \rangle \qquad (4.25)$$

$$+ < \phi_k^{3*}(t + \tau)\, \phi_k^{3} (t) > < \cos 2\beta(t + \tau) \cos 2\beta(t) >$$

since cross-terms have zero correlation because of the orthogonality of 1, sin2β and cos2β. This makes, then

$$< F_k^*(t + \tau)\, F_k (t) > = < \phi_k^{1*}(t + \tau)\, \phi_k^{1} (t) > \qquad (4.26)$$

$$+ < \phi_k^{2*}(t + \tau)\, \phi_k^{2} (t) > \times 1/2 \exp(-| \tau | / \tau_c)$$

$$+ < \phi_k^{3*}(t + \tau)\, \phi_k^{3} (t) > \times 1/2 \exp(-| \tau | / \tau_c)$$

where

$$1 / \tau_c = 4D_s / a^2. \qquad (4.27)$$

4.2.2 Identification of the ϕ_k and the Derivation of $J_0 (\omega)$

Each of the ϕ_k can be readily identified by examining their corresponding $F_k (t)$. If we consider $F_0 (t)$, then

$$F_0 (t) = 1/r^3 [3\cos^2\alpha - 1 + (3\ \ 3/4)\cos 2\beta \sin^2\alpha + (3\ \ 3/4)\sin 2\beta \sin^2\alpha] \qquad (4.28)$$

From this we see

$$\phi_0^1 = 1/r^3 [3\cos^2\alpha - 1] \qquad (4.29a)$$

$$\phi_0^2 = 1/r^3\ \ 3/4 [2 + (1 - 3\cos^2\alpha)] \qquad (4.29b)$$

$$\phi_0^3 = 1/r^3\ 1/4 [2 + (1 - 3\cos^2\alpha)] \qquad (4.29c)$$

Writing the ϕ_k in the form given above, one can easily make the change to spherical harmonics. Doing this yields

$$\phi_0^1 = 1/r^3\ 2(4\pi/5)^{1/2}\, Y_2^0 \qquad (4.30a)$$

$$\phi_0^2 = 1/r^3\ \ 3/4\ \ 2(4\pi)^{1/2} [Y_0^0 - (1/5)^{1/2}\, Y_2^0] \qquad (4.30b)$$

$$\phi_0^3 = 1/r^3\ 1/4\ \ 2(4\pi)^{1/2} [Y_0^0 - (1/5)^{1/2}\, Y_2^0] \qquad (4.30c)$$

Moreover

$$< \phi_0^{1*}(t + \tau)\, \phi_0^{1} (t) > = (4/5r^6) \exp(-t/\tau_2) \qquad (4.31a)$$

$$< \phi_0^{2*}(t + \tau)\, \phi_0^{2} (t) > = (3/4r^6) [1 + 1/5 \exp(-t/\tau_2)] \qquad (4.31b)$$

$$< \phi_0^{3*}(t + \tau)\, \phi_0^{3} (t) > = (1/4r^6) [1 + 1/5 \exp(-t/\tau_2)] \qquad (4.31c)$$

The autocorrelation of $F_0(t)$ can now be written directly as

$$< F_0^*(t+\tau) F_0(t) > = < \phi_0^{1*}(t+\tau) \phi_0^1(t) >$$

$$+ < \phi_0^{2*}(t+\tau) \phi_0^2(t) > < \sin 2\beta(t+\tau) \sin 2\beta(t) >$$

$$+ < \phi_0^{3*}(t+\tau) \phi_0^3(t) > < \cos 2\beta(t+\tau) \cos 2\beta(t) > \quad (4.32)$$

$$= 1/10r^6 \{ 8\exp(-t/\tau_2) + 5\exp(-t/\tau_c) + \exp(-t/\tau_{2'}) \} \quad (4.33)$$

where $1/\tau_{2'} = 1/\tau_2 + 1/\tau_c$. The Fourier transform of Eq.(4.33) is straightforward and so the spectral density $J_0(\omega)$ is therefore

$$J_0(\omega) = 1/5r^6 \{ (8\tau_2 / 1 + \omega^2\tau_2^2) + (5\tau_c / 1 + \omega^2\tau_c^2) + (\tau_{2'} / 1 + \omega^2\tau_{2'}^2) \} \quad (4.34)$$

The remaining two spectral densities $J_1(\omega)$ and $J_2(\omega)$ follow the same procedure and the results are stated as

$$J_1(\omega) = 1/30r^6 \{ (8\tau_2 / 1 + \omega^2\tau_2^2) + (5\tau_{1'} / 1 + \omega^2\tau_{1'}^2) + (\tau_{2'} / 1 + \omega^2\tau_{2'}^2) \} \quad (4.35)$$

$$J_2(\omega) = 1/30r^6 \{ (32\tau_2 / 1 + \omega^2\tau_2^2) + (9\tau_{2'} / 1 + \omega^2\tau_{2'}^2)$$

$$+ (7\tau_{3'} / 1 + \omega^2\tau_{3'}^2) + (3\tau_{4'} / 1 + \omega^2\tau_{4'}^2) + (11/7)(\tau_{5'} / 1 + \omega^2\tau_{5'}^2) \} \quad (4.36)$$

The details of the derivation of $J_1(\omega)$ and $J_2(\omega)$ for this model are presented in appendix B. The numerical subscripts of the correlation times τ_i are related to the corresponding spherical harmonics Y_i^k for k = 0, 1, 2. Spherical harmonics of higher order than those presently tabulated were calculated using the formula

$$Y_n^m(\theta, \phi) \equiv (-1)^m \{ [(2n+1)/4\pi] [(n-m)!/(n+m)!] \}^{1/2}$$

$$\times P_n^m(\cos\theta) \exp(im\phi) \quad (4.37)$$

where $P_n^m(\cos\theta)$ is the associated Legendre function

$$P_n^m(\cos\theta) = (1/2^n n!)(1 - x^2)^{m/2} d^{m+n}/dx^{m+n}(x^2 - 1), -n \le m \le n. \quad (4.38)$$

4.3 T_1 and $T_{1\rho}$ for Rapid Rotation

Rapid β rotation can be considered if we take the limit as $\tau_c \rightarrow 0$. In the spectral densities this means that $\tau_{k'} \rightarrow 0$ for all k. Hence

$$1 / T_1 = (9/8) \gamma^4 \hbar^2 [J_1 (\omega_0) + J_2 (2\omega_0)] \qquad (4.39)$$

$$\rightarrow 3\gamma^4 \hbar^2 / 40 r^6 \times \{ (4\tau_2 / 1 + \omega_0^2 \tau_2^2) + (16\tau_2 / 1 + 4\omega_0^2 \tau_2^2) \} \qquad (4.40)$$

This is in agreement with that of Stejskal and Gutowsky[33] for rapid rotation of the CH_3 in a crystal powder. For relaxation in the rotating frame,

$$1 / T_{1\rho} = (9/8) \gamma^4 \hbar^2 \{ 1/4 J_0 (2\omega_1) + 5/2 J_1 (\omega_0) + 1/4 J_2 (2\omega_0) \} \qquad (4.41)$$

This is identical to the equation of Look and Lowe[25] for rotating frame relaxation for a pair of spins. In the methyl group therefore the equivalent relaxation behaviour is that of two spins with internuclear vector of length equal to the methyl bond separation but oriented along the rotation axis of the methyl group. Where the correlation time for the motion of the spins is such that $\tau_c^{-1} << \omega_0$,the spectral density term $J_0 (2\omega_1)$ sensitive to the lower RF Larmor frequency will dominate. In this regime, applicable to high polymer motion in the melt,

$$1 / T_{1\rho} \approx 9\gamma^4 \hbar^2 / 32 r^6 \times \{ \tau_c / (1 + 4\omega_1^2 \tau_c^2) \}. \qquad (4.42)$$

4.4 Polymer Motion

4.4.1 The Kimmich Model

Having dealt with the methyl group problem it is appropriate here to review polymer reptation and in particular the spectral density function derived by Kimmich for the purpose of elucidating T_1 dispersions[3,4]. This model is aptly illustrated in Fig.4-1 below.

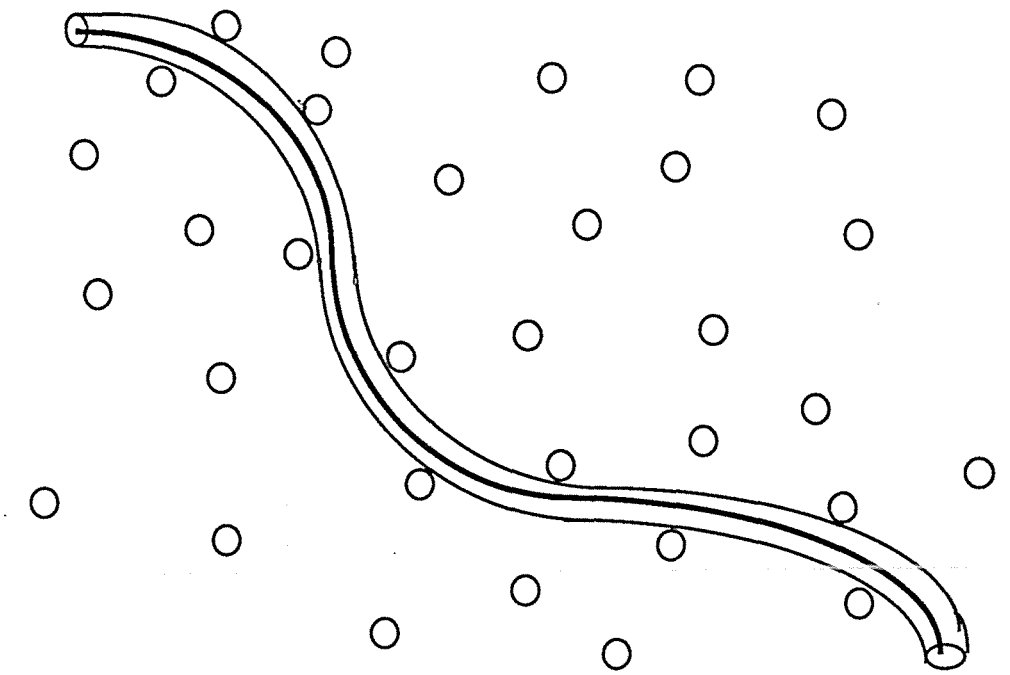

Fig.4-1
Schematic illustration of a chain in polymer melts. The circles represent the matrix of neighbouring chains that confine the polymer chain into a tight tube.

The chain is confined to a tight tube formed by the matrix of neighbouring chains according to the model of Edwards[35]. The diameter of the tight tube is given by the mean fluctuation amplitude of the local processes. These processes are designated Component A and consist of anisotropic reorientations of the spin dipole-dipole interaction. This is the most rapid of the processes and the existence of residual anisotropy is essential if any other motions occurring on timescales much larger than that for segment rotation are to be observed. In the Kimmich model these other motions form the reptation within the tight tube and tube renewal designated Components B and C respectively. The correlation functions describing each component will now be discussed.

4.4.2 Component A: Local Processes

These are local motions such as defect diffusion over short distances. Component A is not connected with translational segment displacements but reorientations about the chain axis caused by, for example, diffusing defects as illustrated in Fig.4-2.

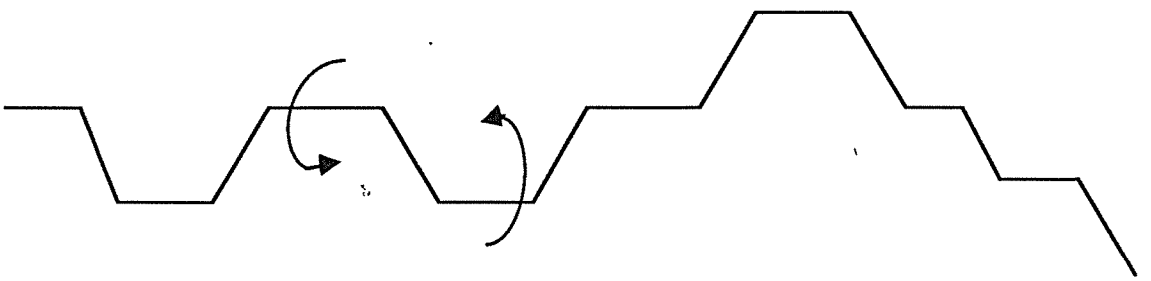

Fig.4-2

Schematic representation showing the component A process of the molecular motion in a chain entangled by neighbouring chains. Segmental rotation about the bonds.

These segments reorient themselves due to dipolar fluctuations and this causes the effect of what is aptly named " crank-shaft rotation ", so called since the twisting of one part of the chain affects another part of that same chain. In the short time limit Kimmich et al has shown[3,4] that defect diffusion approximately corresponds to the diffusion of a particle between two reflecting barriers. (The reflecting barriers here represent the quasi-static ensemble of neighbouring defects). This results in a relaxation process, the width of which is determined by the mean diffusion time over the distance of the reflecting barriers. As the time constants of the other components must be longer than this diffusion time the long-time behaviour of component A can be described by a single exponential function with an anisotropy constant.

$$G_A(t) = a_1 \exp(-t/\tau_s) + a_2 \qquad (4.43)$$

where τ_s is the effective time constant characterising long time behaviour, and a_1 and a_2 are determined by the degree of anisotropy of component A. It is important to note that only a non-vanishing a_2 allows observation of further non-local processes.

4.4.3 Component B: Semi-local Processes

Component B is a semi-local process and is associated with reptation around tube bends. We assume the validity of a one-dimensional diffusion equation for chains reptating along a curvilinear path; i.e. $\tau_l = l^2 / 2D_l$ where D_l is the curvilinear diffusion coefficient and l is the mean path length (see Fig.4-3).

The correlation function of Kimmich is given by the ensemble averaged probability that a reference segment with a given initial orientation has the same orientation after time τ. This can be written symbolically as

$$G_B(t) = \int_0^{\infty} \rho(\bar{x})\, 2 \int_0^{\bar{x}} \eta(x, \tau)\, dx\, d\bar{x} \qquad (4.44)$$

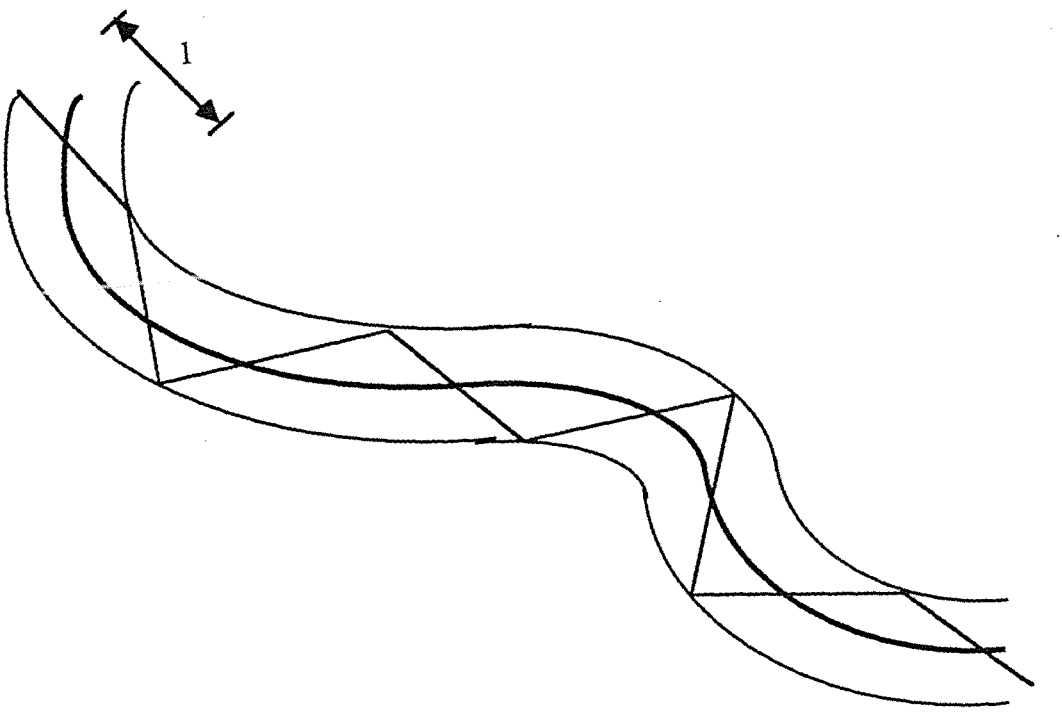

Fig.4-3
Curvilinear diffusion

where $\rho(\bar{x})$ is the probability that the nearest bend of the surrounding tube is at a distance $\bar{x}$ from the reference segment. The factor of 2 shown appears since there are two final positions with the same orientations on both sides of the reference segment. The term $\eta(x, \tau)$ is the probability that the reference segment diffuses a distance x within a period τ. Therefore,

$$\int_0^{\bar{x}} \eta(x, \tau)\, dx \qquad (4.45)$$

represents the probability that the reference segment is in the range $0 \leq x \leq \bar{x}$. The exterior integral gives the average over all lengths $\bar{x}$.

Chandrasekhar has shown[36] the solution of the diffusion equation yields

$$\eta(x, \tau) = 1 / [\, 2(\pi D_1 \tau)^{1/2} \,] \exp(-x^2 / 4D_1\tau) \qquad (4.46)$$

At times large compared with the correlation times of defect sequences (i.e. $\tau_l >> \tau_s$) then D_1 can be taken as constant. Thus

$$2\int_0^{\bar{x}} \eta(x, \tau)\, dx = \mathrm{erf}\{\, \bar{x} \,/ (4D_1\tau)^{1/2} \} \qquad (4.47)$$

Now $\rho(\bar{x})$ depends on the microstructure. A plausible case is an exponential distance-distribution of the nearest tube bends, which means that there is the same probability at each segment that the surrounding tube changes its orientation.

$$\rho(\bar{x}) = (1/l) \exp(-\bar{x}/l) \qquad (4.48)$$

2l is now the mean distance from one bend to the next. Thus, the correlation function of Kimmich for component B is

$$G_B(t) = \exp(t / 2\tau_l)\, \mathrm{erfc}(t / 2\tau_l)^{1/2} \qquad (4.49)$$

It is assumed the chain diffuses within a stationary tube of infinite length. That the tube be infinitely long is justified since any tube renewal process is attributed to component C which is of a competitive nature to component B. The stationarity of the tight tube is more problematic as it contradicts the growth or shrinkage of folds. Rather the fluctuation of a fold in principle can contribute to component B. However the correlation length of the tight-tube orientation is expected to be so short that reptative displacements around tight-tube bends will be fast compared with fold fluctuations. (Also it is unlikely that a reference segment will be situated in a fold at all).

4.4.4 Component C: Global Processes

Component C is a global processes and involves the alteration of a chain to a new configuration. In the Kimmich model, there are two ways in which this can be brought about. Contour length fluctuation which involves no longitudinal diffusion, and is due to changes in the environmental microstructure of a chain; and tube renewal due to reptation. The correlation function is

$$G_C(t) = p_c \exp(-t / \tau_R{}^c) + p_r \exp(-t / \tau_R{}^r) \qquad (4.50)$$

where τ_R^r and τ_R^c are the tube renewal time constants for reptation and contour length fluctuation weighted by p_r and p_c respectively (and $p_r + p_c = 1$). In the model of Kimmich the mean tube length per fold Δ_0, and the extended tube length L_0, determine the mean contour length fluctuation $2x_r = (L_0\Delta_0)^{1/2}$ and the weighting $p_c = 2x_r / L_0$.

4.5 Summary of the Spectral Density

It is next assumed that all three components are stochastically independent. This is plausible since components A and B are intrachain processes and component C is an interchain process. Now B is a consequence of A; however in the timescale in which reptation influences NMR relaxation each segment has reorientated many times, i.e. Reptation is caused in this limit by the movement of a large ensemble of defects and is thus practically uncorrelated to the diffusion of a single defect.Therefore

$$G(t) = G_A (t) G_B (t) G_C (t) \qquad (4.51)$$

$$= [a_1 \exp(-t / \tau_s) + a_2]$$

$$\times \exp(t / 2\tau_l) \operatorname{erfc}(t / 2\tau_l)^{1/2}$$

$$\times [p_c \exp(-t / \tau_R^c) + p_r \exp(-t / \tau_R^r)] \qquad (4.52)$$

The exact expression for the spectral density arising from Eq.(4.52) is given in Appendix C together with the derivation of various limiting cases applicable to $J_0 (2\omega_1)$ since it is this spectral density which provides the dominant influence on $T_{1\rho}$.These limiting cases are helpful in summarising the spectral regimes covered in spin-locking and are stated below.

(i) Low frequencies ($2\omega_1 << 1 / \tau_R^r$) and long chains ($\Delta_0 << L_0$)

$$J_0 (2\omega_1) \approx 2a_2 (2\tau_l\tau_R^r)^{1/2} \qquad (4.53)$$

(ii) Intermediate frequencies ($1 / \tau_R^r << 2\omega_1 << 1 / \tau_l$)

$$J_0 (2\omega_1) \approx 2a_1\tau_s + 2a_2 (2\omega_1)^{-1/2} \tau_l^{1/2} \qquad (4.54)$$

(iii) High frequencies ($2\omega_1 >> 1 / \tau_l , 1 / \tau_R^r$)

$$J_0 (2\omega_1) \approx 2a_1\tau_s + a_2 (2\omega_1)^{-3/2} \tau_l^{-1/2} \qquad (4.55)$$

These regimes are depicted schematically in Fig.4-4.

An approximate expression which describes the crossovers from one region to another has been given in reference 3.

$$I(\omega) = \sum_{j=1}^{4} \gamma_j [\, 2\tau_c(j) + \tau_c(j)^{3/2} \tau_1^{-1/2} (1 + K(j))^{1/2}]$$
$$\div \{ K(j)^2 + (1/2)\tau_c(j) \tau_1^{-1} K(j) + \tau_c(j)^{1/2} \tau_1^{-1/2}$$
$$\times [(1 + K(j))^{1/2} + \omega\tau_c(j) (K(j) - 1)^{1/2}] \} \qquad (4.56)$$

where $K(j) = (1 + (\omega\tau_c(j))^2)^{1/2}$

$$\tau_c(1) \approx \tau_c(2) \approx \tau_s$$
$$\tau_c(3) \approx \tau_R^c$$
$$\tau_c(4) \approx \tau_R^r$$
$$\gamma_1 = a_1 (\Delta_0 / L_0)^{1/2} \qquad (4.57)$$
$$\gamma_2 = a_1 (1 - (\Delta_0 / L_0)^{1/2})$$
$$\gamma_3 = a_2 (\Delta_0 / L_0)^{1/2}$$
$$\gamma_4 = a_2 (1 - (\Delta_0 / L_0)^{1/2})$$

Note that as $a_2 \rightarrow 0$ Eq.(4.56) yields the isotropic limit. By comparison with the isotropic limit expression for rotational motion given by BPP it can be seen that $J_0(\omega)$ is given by Eq.(4.56) within a numerical factor of (2 / 3) for T_1 theory and (4 / 5) for $T_{1\rho}$ theory.

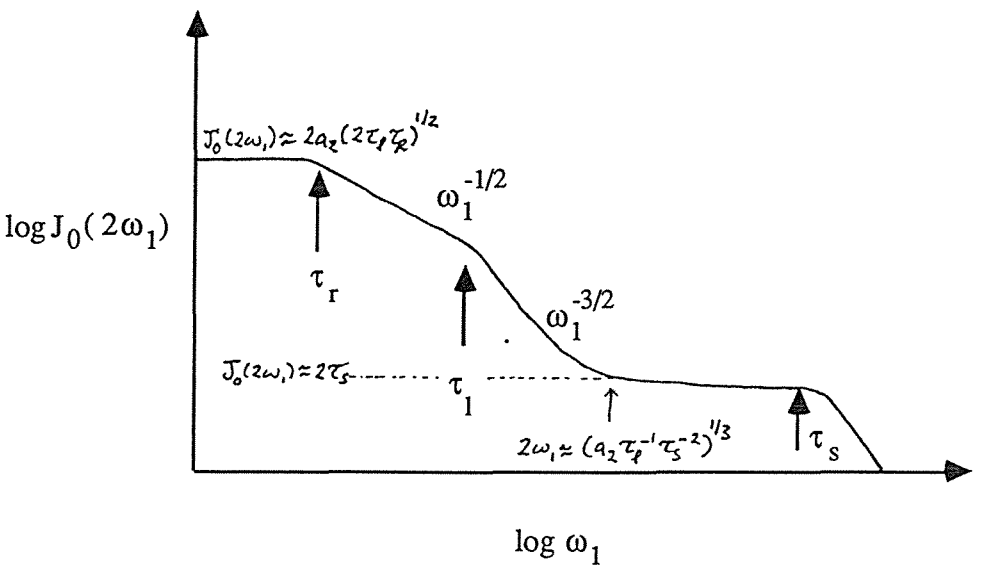

Fig.4-4

Schematic log $J_0(\omega)$ dispersion predicted by the reptation model of Kimmich.

Chapter 5 Hardware and Software

Thou hast made me, and shall thy work decay?

... John Donne

5A Hardware

5A.1 General Outline of the $T_{1\rho}$ System

Having dealt with the theory of NMR relaxation in some detail we now turn our attention to the practical aspect of this work and consider the " nuts and bolts " of measuring $T_{1\rho}$.

The $T_{1\rho}$ system is built around the JEOL FX60 multinuclear NMR spectrometer. The essential components of which are given in the block diagram of Fig.5-1.

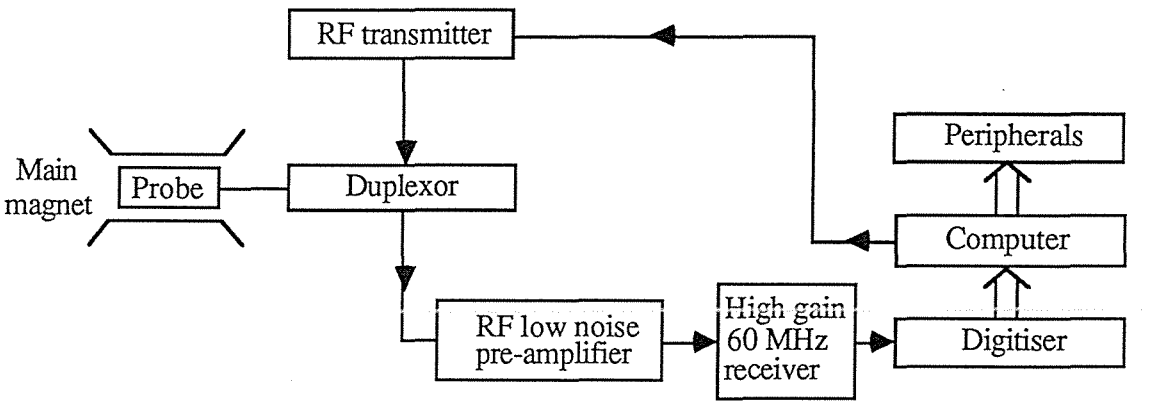

Fig. 5-1
Block diagram of the FX60 spectrometer.

Upon receiving instructions from the computer, the appropriate pulse sequence is sent from the RF transmitter to the probe via the duplexor. The probe then stimulates the nuclei and observes the subsequent response. The small nuclear signal is then channeled to the pre-amp and high-gain receiver once again via the duplexor. The role of the duplexor is thus to switch between these two functions. The voltage generated by the receiver is then digitised and transferred to the computer for spectral analysis.

The RF probe and duplexor were constructed especially to withstand high voltages necessary to attain certain frequency regimes of $T_{1\rho}$ and are important features of this work. Thus a full description of both follows in section 5A.2 and 5A.3 respectively. The powerful Henry Radio 1kW 60MHz amplifier needed to produce the high voltages is discussed in section 5A.4. The remainder of the hardware has already been described in detail elsewhere[37] although a summary is included in sections 5A.5 and 5A.6.

5A.2 RF Probe

The RF probe used in this work incorporates an RF tank circuit housed between two walls made from fibreglass pcb.

A single RF coil included in the tank circuit is the most important part of the probe since it must transmit the RF pulse sequence in an efficient manner to the nuclear sample, which is placed within the coil, and simultaneously detect the response of the nuclei; a small signal whose strength is in the order of microvolts.

The fibreglass pcb is copper plated so as to provide electrical shielding from outside interference and the construction of the probe body is such as to maximise the area shielded. Shim coils are mounted on the outside walls of the probe. These are current coils used to compensate magnetic field inhomogeneities.

All materials used in the construction of the RF probe must be of a non-ferrous type to prevent magnetic field distortions. The important feature in the design of the $T_{1\rho}$ probe is that it must be able to withstand high voltages applied to the RF coil. Thus the distance between the coil and the probe walls must be large enough to prevent arcing (10^4 V cm^{-1} for dry air). This poses a difficulty when it is borne in mind that the distance between the poles of the magnet (which governs the probe width) must be small enough to achieve magnetic field homogeneity. This places an upper limit on the width that the probe can take (approximately 30mm for this work). Another problem faced by this limitation was that most high voltage capacitors were too large in size compared with the amount of space allotted. For this reason special capacitors were constructed.The details of the probe now follow.

5A.2.1 RF Coil

The single RF coil, comprised of three turns of 1.26mm diameter (18 s.w.g.), was wound around a glass dewar into which the NMR sample tubes are placed. The considerations in the design of the coil were:

(i) To choose the number of turns so that, for a given length, the quality factor Q is optimised.

(ii) The distance between each turn needs to be large enough to prevent arcing.

(iii) The length must be small in keeping with the homogeneity of the magnetic field.

To achieve the first consideration (i.e. a high Q) the empirical rule given by Fukushima & Roeder[38] was followed whereby the distance between each turn in the coil is equal to one diameter of the wire used. Thus a large diameter wire was chosen to fulfill the second consideration. Practically, the actual spacing is achieved by winding two wires of the chosen diameter around a former after which one of the wires is simply removed. The coil dimensions are given in Table 5-I according to the parameters shown in Fig.5-2.

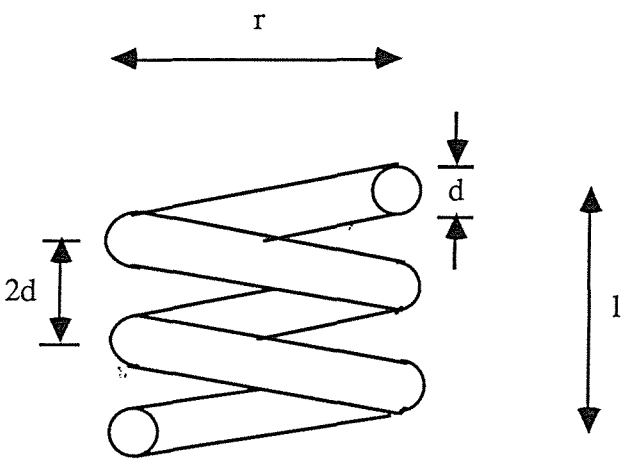

Fig.5-2
The RF coil.

At VHF frequencies , the current exists within a thin skin on the surface; the current density decreasing exponentially as one penetrates the surface. The skin depth is given by Hoult[39] as

$$\delta = (2\rho / \mu_r\mu_0\omega_0)^{1/2} \qquad (5.1)$$

$$= 8.47\ \mu m \text{ for Copper at } f_0 = 60\ MHz$$

where ρ is the resistivity of the wire (in this case $\rho_{Cu} = 1.7 \times 10^{-8}\ \Omega m$), $\mu_r \approx 1$ for Cu and μ_0 is the permeability of free space and has the value $\mu_0 = 4\pi \times 10^{-7}\ Hm^{-1}$. Thus the effective cross-sectional area of the wire A_{wire} is equal to the circumference of the wire $\times$ δ. The resistance of the coil R_{coil} is therefore

$$R_{coil} = \sigma\rho l / A_{wire} \qquad (5.2)$$

and σ is a proximity factor.

The inductance for a solenoid is given by

$$L = \mu_0 n^2 A_{coil} / l \qquad (5.3)$$

and so this allows Q to be calculated by

$$Q \approx \omega_0 L / R_{coil} \qquad (5.4)$$

Experimentally one would measure the bandwidth Δf and find Q by using

$$Q = \Delta f / f_0 \qquad (5.5)$$

Table 5-I lists the values of L and Q measured at 60 MHz for the RF coil used.

RF coil measurements (experimental)	
n	3
r	6 mm
l	8 mm
L	0.27 μH
Q	60

Table 5-I

5A.2.2 High Voltage Capacitors

Special capacitors were needed which could withstand the high voltages that would be applied and also be physically small enough to fit inside the probe. The design and mounting of these capacitors is shown in Fig.5-3a and Fig.5-3b respectively.The capacitance is that for a coaxial cylinder and is given by

$$C = 2\pi \varepsilon\varepsilon_0 l / \ln (r_2 / r_1) \qquad (5.6)$$

where ε is the dielectric constant of the material, ε_0 is the permittivity of free space, r_2 is the inner radius of the outer cylinder of the coaxial and r_1 is the radius of the inner cylinder. The length of the cylindrical tube was determined by the amount of space allotted inside the probe body. Because Teflon (polytetrafluoroethylene) does not give a proton NMR signal it is a suitable material to use as a dielectric; ε for Teflon is 2.1 over 10^3 to 10^8 Hz and the dielectric strength is 480 Vmm^{-1}. The minimum thickness of the dielectric was based on the expected voltages between the inner and outer cylinders. The two capacitors made for this work as measured were tunable between 2.5pf and 13pf.Perspex tuning rods were added to reduce hand capacitance.

5A.2.3 Series-Parallel Tank Circuit

Because the signal induced by the nuclei is small, it is important that the probe be efficiently coupled to the next stage in the system. For maximum power transfer between two stages then the output impedance of one stage should be equal to the input impedance of the next.

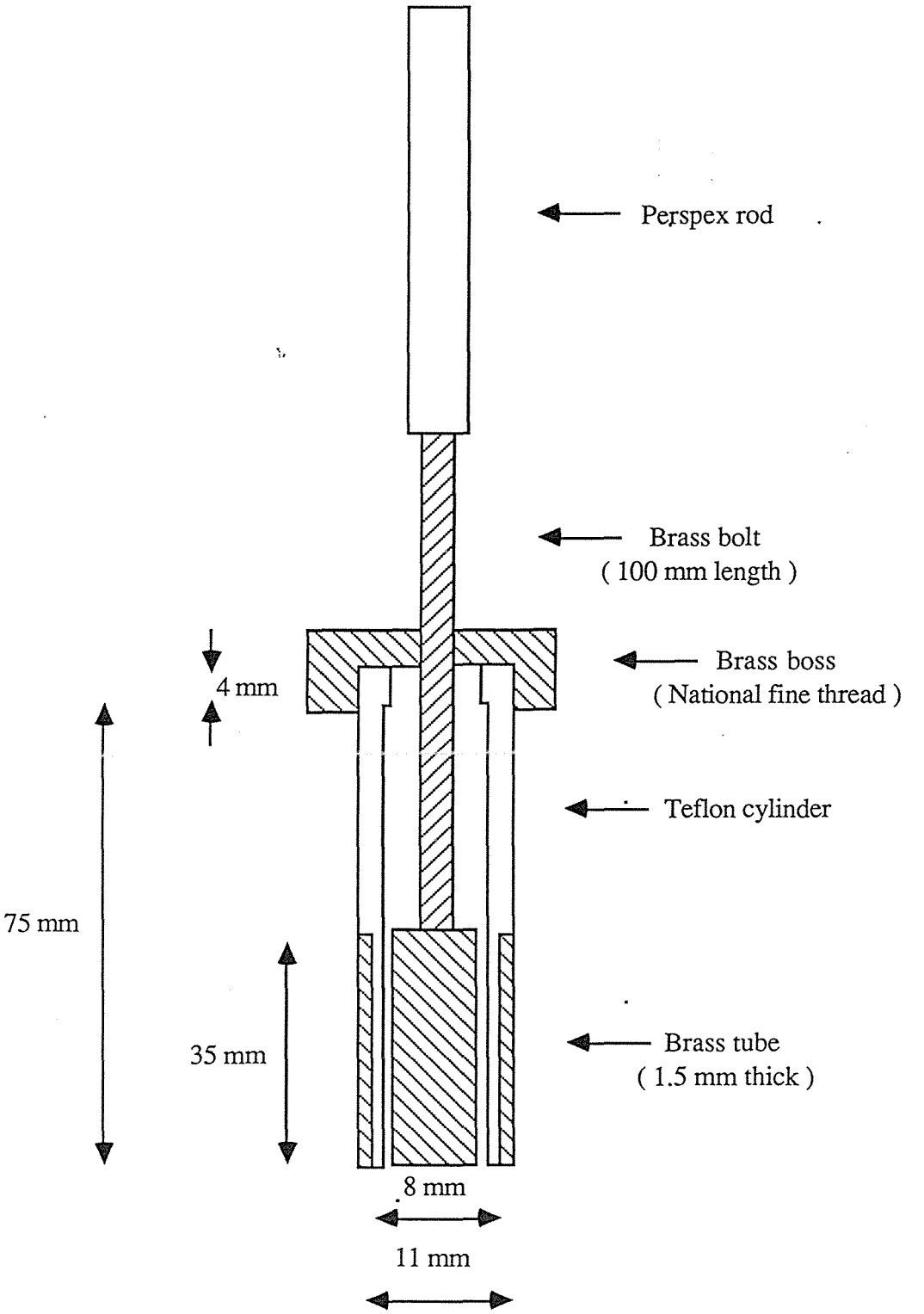

Fig.5-3a

The high voltage capacitor, (not to scale)

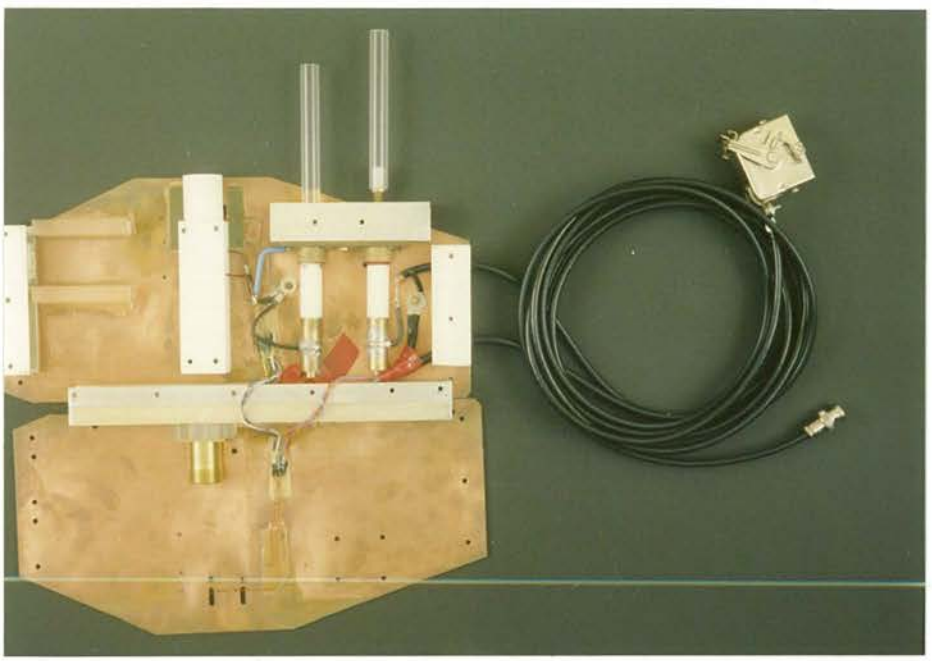

Fig.5-3b

The mounting of the two high voltage capacitors.
The RF coil sits inside the Teflon enclosure (central)
which allows for temperature controlled airflow.

The interconnections between various stages in the $T_{1\rho}$ system are made using 50 ohm coaxial cables and so for maximum power transfer, the impedance of the probe should be 50 ohms.The impedance matching circuit used which achieves this purpose is given in Fig.5-4.

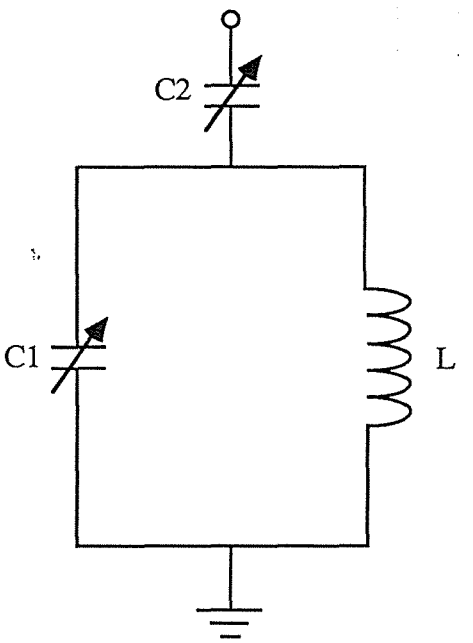

Fig.5-4
Parallel-series RF tank circuit.

Upon resonance, the equivalent parallel resistance is quite high and is given by by the expression $R_{eq} = Q^2 R_{coil}$. As the circuit is detuned below resonance by adjusting C_1 then the resistance R_{eq} is reduced and the circuit begins to look inductive. Capacitor C_2 is then adjusted so as to tune out this inductive component. In this way, then the circuit can be made to look resistive with any value of resistance less than the maximum value of R_{eq}. By using equivalent circuits it has been shown[39] that the values of C_1 and C_2 required are

$$C_1 = (R_{coil} / r'L^2\omega_0^4)^{1/2} \qquad (5.7)$$

$$C_2 = (C_1 / r'Q\omega_0)^{1/2} \qquad (5.8)$$

where r' is the desired matching impedance.An alternative impedance matching circuit is given in Fig.5-5 which works in much the same way.

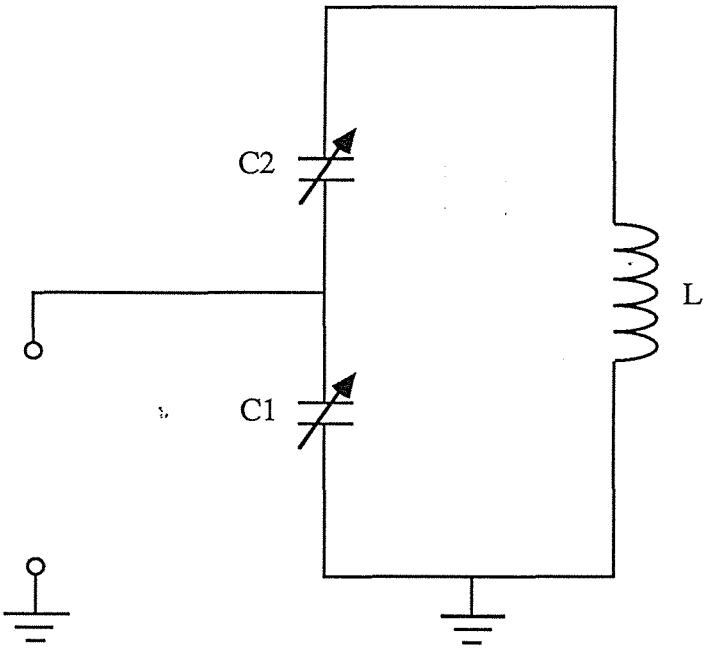

Fig.5-5
Split capacitor RF tank circuit.

This time the circuit is tuned above the resonant frequency by adjusting C_2. This makes the combination of C_2 and L look inductive; C_1 is then adjusted to tune out this inductive component and leave the desired matching resistance. Again by equivalent circuits

$$C_2 \approx 1 / \omega_0^2 L \qquad (5.9)$$

$$C_1 = (QC_2 / \omega_0 R)^{1/2} \qquad (5.10)$$

where $C_1 >> C_2$. This was our first combination which included fixed high voltage capacitors in parallel with the tunable capacitors to give the desired value. However it was found that standard capacitors were not required when the series-parallel circuit shown in Fig.5-4 was used. This was favourable since compact standard capacitors of a high voltage rating were often hard to obtain.The tank circuit was tuned using the RF bridge shown in Fig.5-6.

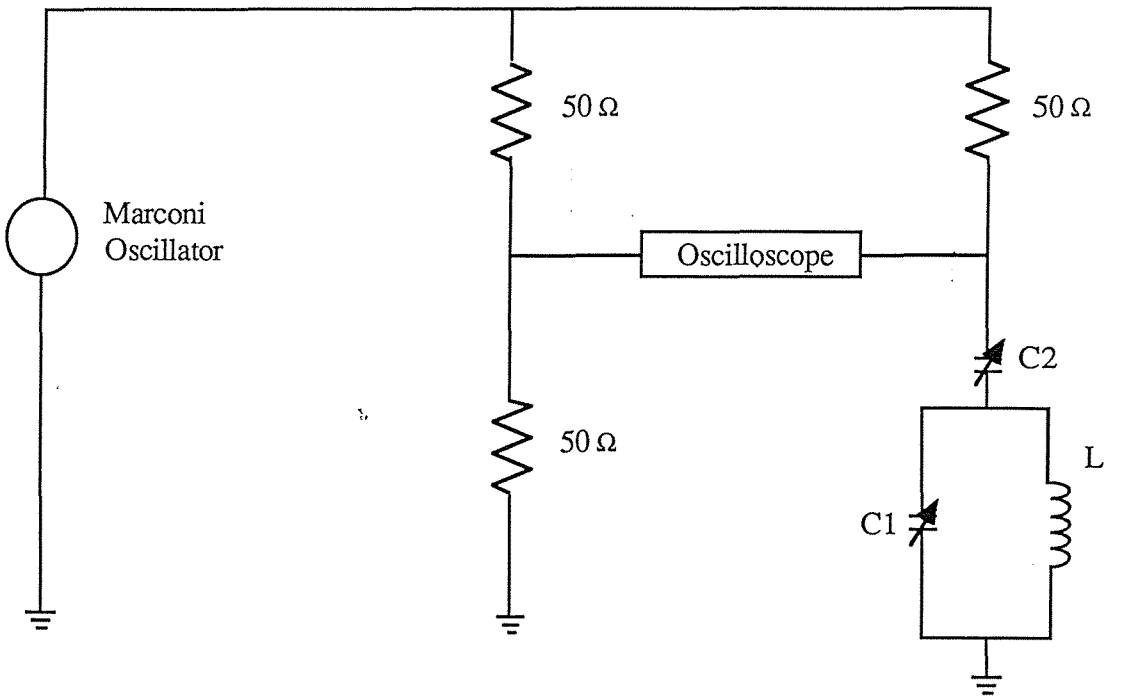

Fig.5-6
The RF tuning circuit.

With the Marconi Oscillator set to 59.95 MHz, capacitors C_1 and C_2 are adjusted until a null is observed on the oscilloscope. By replacing the tank circuit with a 50 Ω load, a comparison can be made. That the probe be 50 Ω was doubly significant since measurements where $T_{1\rho}$ approaches the T_1 end of the scale required the use of a 1kW Henry Radio amplifier. The Henry Radio amplifier could be damaged if it is operated into a load with a standing wave ratio greater than 2:1. The amplifier is discussed in section 5A.4.

5A.2.4 Electrical Current Shims

The electrical shims used consist of simple rectangular current loops with the coil positions and dimensions adjusted to maximise the desired field gradient. The coils are placed symmetrically in two parallel planes straddling the sample. The shims are orthogonal and so the controls are independent of each other. The design of the first-order X,Y & Z gradient coils as given by Anderson[40] is as follows.

Z gradient.

Fig.5-7 shows the dimensions of a Z gradient coil found on one side of the RF probe.An identical coil is placed on the opposite side of the probe.The distance between the two coils is $2Z_0$.

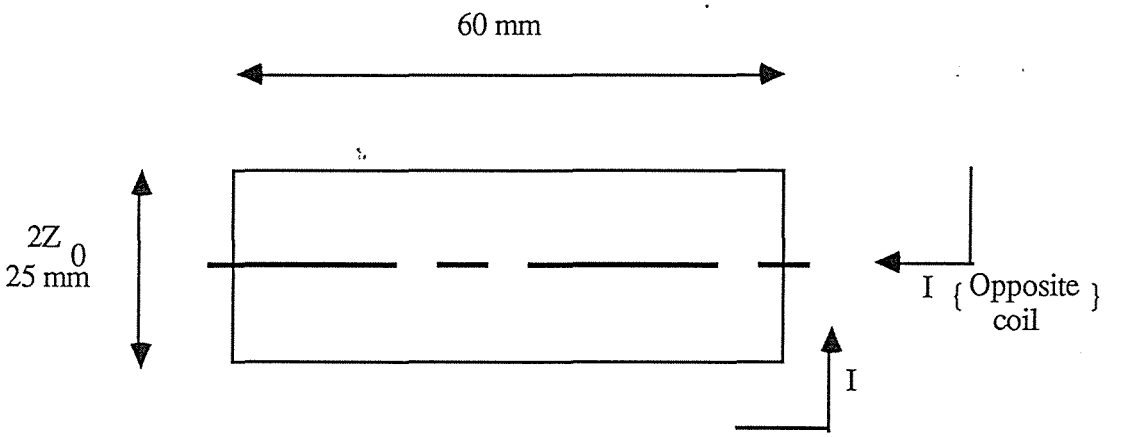

Fig.5-7
The z gradient shim coil. Coils are placed on each side of the RF probe.

The required current was determined for a $\Delta f = 500Hz$ spread in frequency over 1cm. Thus

$$\Delta B = (2\pi / \gamma) \Delta f \qquad (5.11)$$

$$= 1.18 \times 10^{-5} T.$$

$$\Rightarrow \partial B / \partial z = 1.18 \times 10^{-3} Tm^{-1}.$$

According to Anderson

$$\partial B / \partial z = (\mu_0 I_x / 2\pi z_0^2) [-2\eta / (1 + \eta^2)^2] \qquad (5.12)$$

and $\eta = 1$ for B_z proportional to z. I_x was calculated to be about 2A. The $T_{1\rho}$ probe has two loops and the shim current supply can drive up to 1A in each loop.

Y gradient (refer to Fig.5-8)

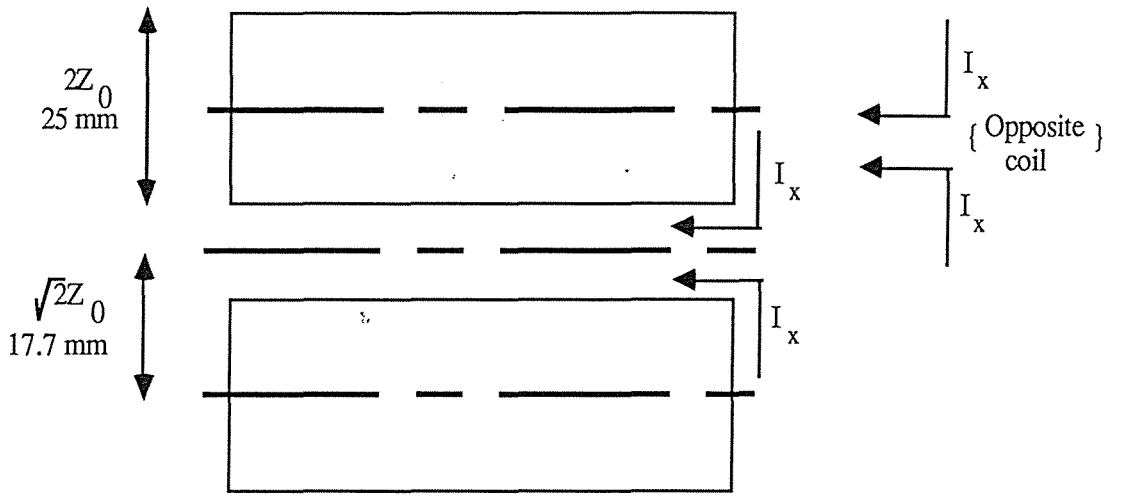

Fig.5-8
The y gradient shim coil. Coils are placed on each side of the RF probe.

For this case

$$\partial B / \partial y = (\mu_0 I_x / 2\pi z_0^2) [1 - \eta^2 / (1 + \eta^2)^2] \qquad (5.13)$$

and $\eta^2 = 0.1716$. Once again for a 500Hz spread over 1cm then I_x can be calculated and the number of turns wound accordingly.

X gradient.

The X gradient shim coils are identical to those for Y (see Fig.5-8) but are rotated by 90° about the z-axis. Fig.5-9a shows the X,Y, and Z gradient coils mounted together while Fig.5-9b shows the location of the coils on the side of the probe.

5A.2.5 Coil Holder

The RF coil is encased within a fixture deemed the coil holder designed so that temperature controlled airflow around the sample tube is possible. The coil holder, made entirely from teflon, is positioned so that the sample will be in the centre of the magnetic field (see Fig.5-3b). The holder is slotted to permit easy removal of the RF coil if required. The slots mean the leads from the coil can be kept short thus reducing stray capacitance.

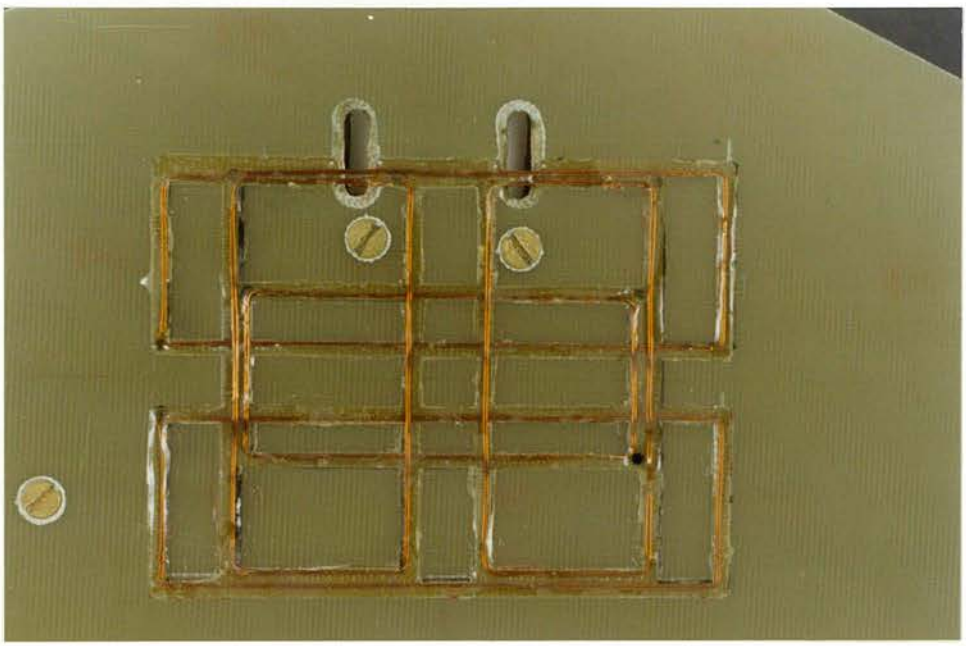

Fig.5-9a

The X, Y, and Z shim coils.

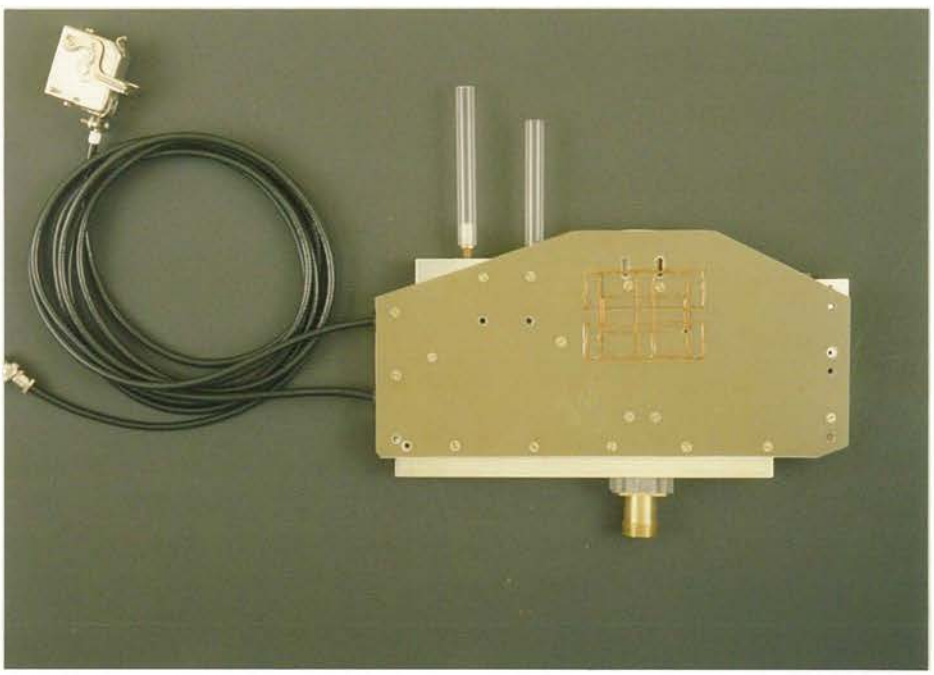

Fig.5-9b

The shim coils are mounted centrally on the side of the probe.

5A.3 Duplexor

Fig.5-10 shows a schematic diagram of a crossed-diode configuration commonly called a duplexor.

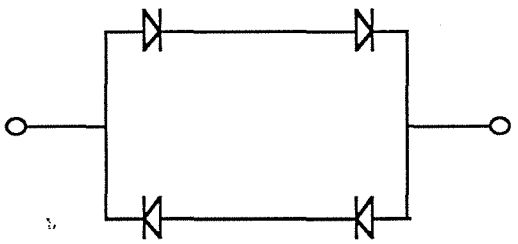

Fig.5-10
A single duplexor.

Provided the potential driving the current exceeds a fairly well defined threshold (0.5 for most Si. diodes) then the above pictured cross-diode configuration has the property that it will pass current in either direction if the voltage is less than -0.5V or greater than 0.5V. Therefore the duplexor acts like a switch which is ON for large signals and OFF for small signals.

A crossed diode circuit placed in parallel with the input of the receiver then acts as a short to protect the input from large signals coming through the matching network while acting as if it were not there at all for the small NMR signal because the short to ground at the receiver acts at the end of a quarter wavelength line. This has the effect of presenting a high impedance to ground in parallel with the probe tank circuit under high voltage conditions. Fig.5-11 shows the practical duplexor set-up.

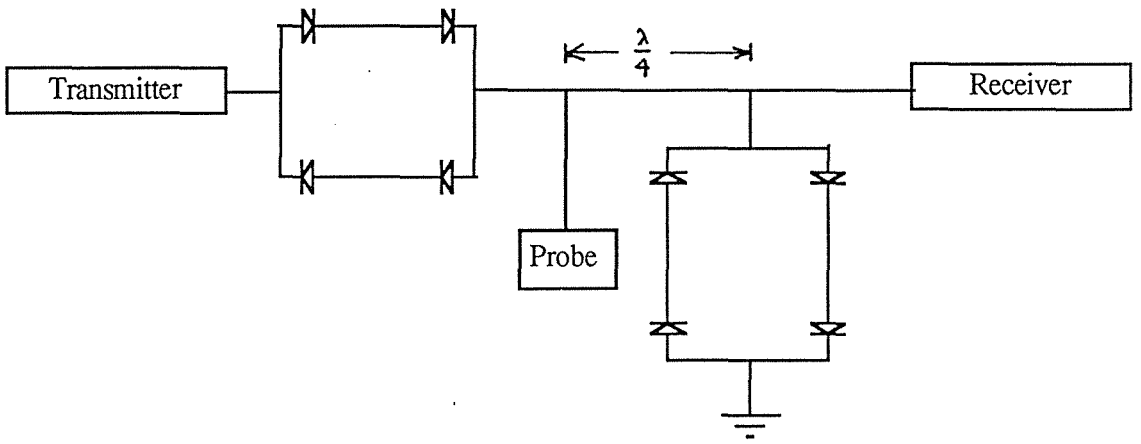

Fig.5-11
The practical duplexor set-up.

A duplexor in series with the transmitter directs the small NMR signal to the receiver. High voltage diodes were used throughout and placed in parallel to share the current as shown in Fig.5-12. Adding diodes in series reduces the capacitance each diode has when non-conducting. The resulting increase in threshold voltage was not found to present any difficulties.

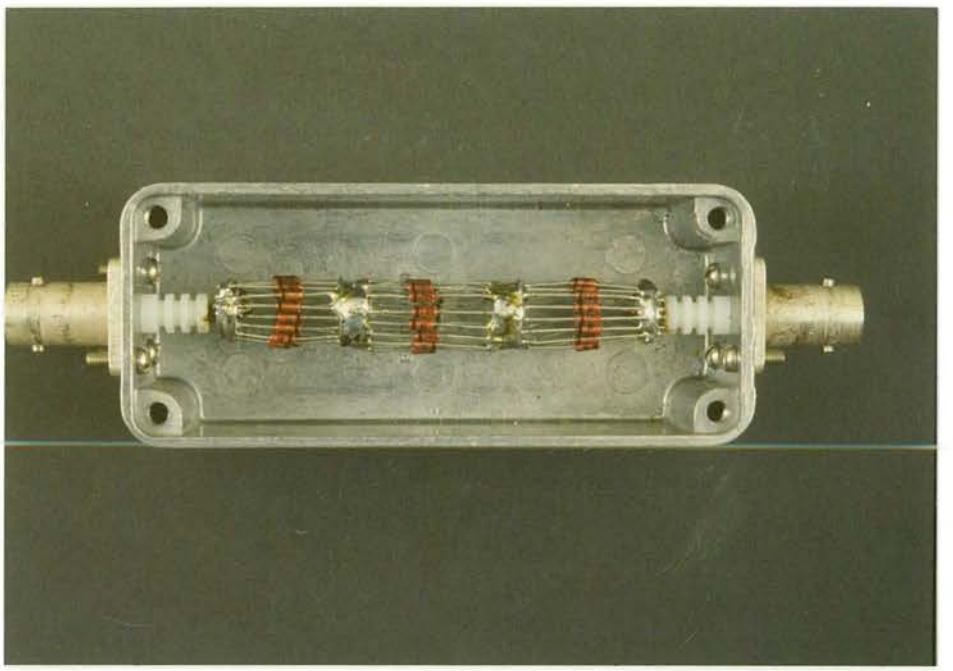

Fig.5-12

The high voltage duplexor; many diodes in parallel.

5A.4 Henry Radio 1kW Linear Amplifier and Driver

The Henry Radio 1kW Linear amplifier and exciter / preamplifier driving unit required to attain large spin-locking fields were factory tested and aligned for 60MHz. Fig.5-13a shows the Henry Radio amplifier and the Driver unit. A description of both follows.

5A.4.1 Exciter / Preamplifier

The solid state Henry Exciter is a low band VHF linear power amplifier. The unit has a drive requirement of 5 to 20W and delivers 65W for 15W input (nominal).

The circuit diagram of the amplifier is shown in Fig.5-13b. The amplifier is made up of three distinct circuits: An RF sensor and relay circuit, a preamplifier stage, and a final power amplifier stage.

In the sensing-relay circuit, RF from the antenna to J3 (RF OUT) goes directly through the relay and J1 (RF IN) into the transceiver during receive. However if the unit is in transmit mode then RF enters through J1 (RF IN) and creates a voltage across D1. The voltage is amplified by Q1 and trips the relay RY1 causing the signal to enter the amplifier stages.

In the preamplifier section (the driver stage), the base of Q4 is matched to 50 ohms by C3, L9 and C15. L9 is a toroidally wound coil on a ferrite core. The preamplifier is decoupled from the DC power line by C16 and L11.

The output from Q4 is matched to and divided between the two final output transistors, Q2 and Q3, by L10, a broad band ferrite matching transformer. C4 matches the impedance between the two stages. The output power from Q2 and Q3 (operating as a push-pull circuit) is delivered to L6 and L7, another broad band ferrite matching transformer and combiner. C14 matches the output impedance to 50 ohms.

C10 through C13 and L1 through L3 form a low pass filter to suppress harmonics generated by the amplifier. D2 is a reverse polarity protection diode.

Fig.5-14a shows a graph of Power Out vs. Power In for the Driver (exciter) while the Gain vs. Power In is shown in Fig.5-14b.

Fig.5-13a

The Henry Radio 1kW Amplifier (above) and the Driver Unit.

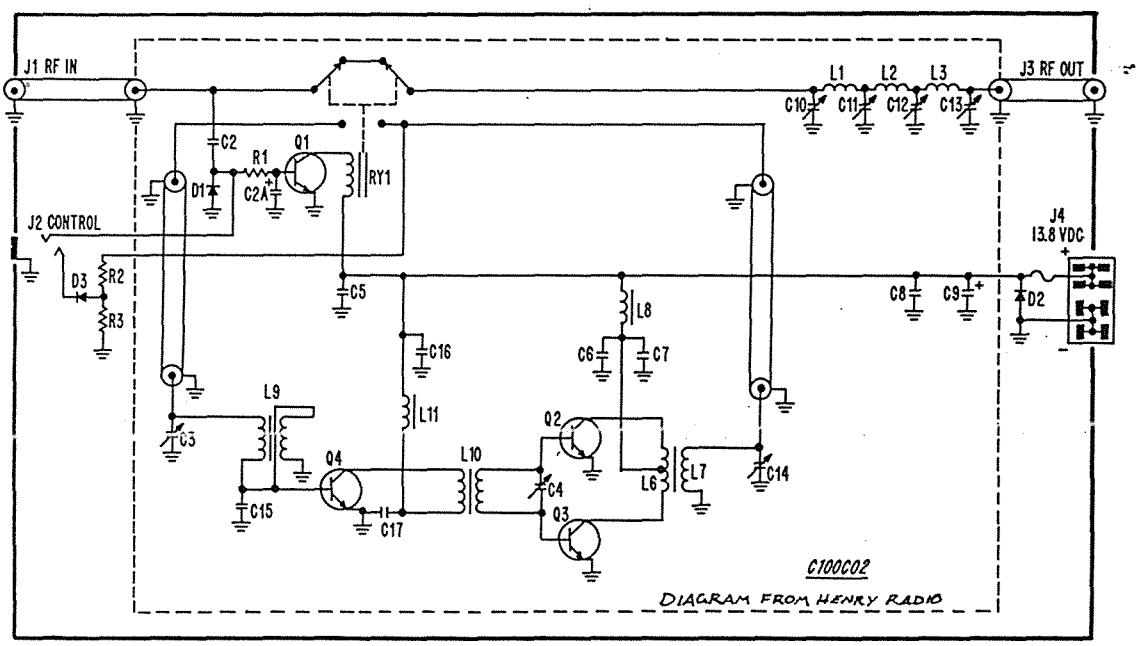

Fig.5-13b

Circuit diagram for the Driver Unit (Exciter / Preamplifier).

Fig.5-14a Driver Characteristics

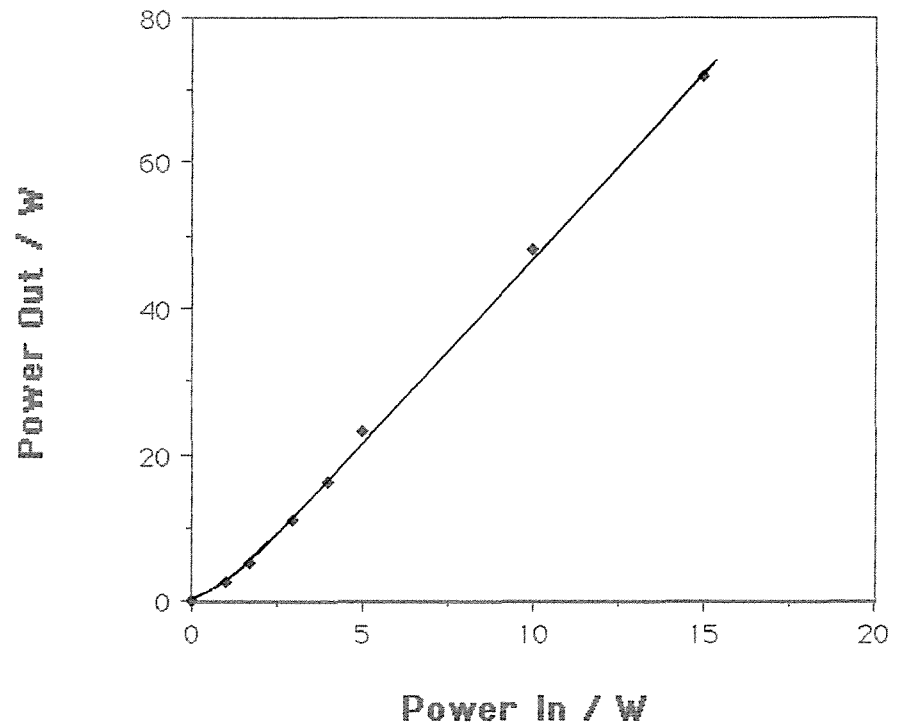

Fig.5-14b Driver Gain vs Power In

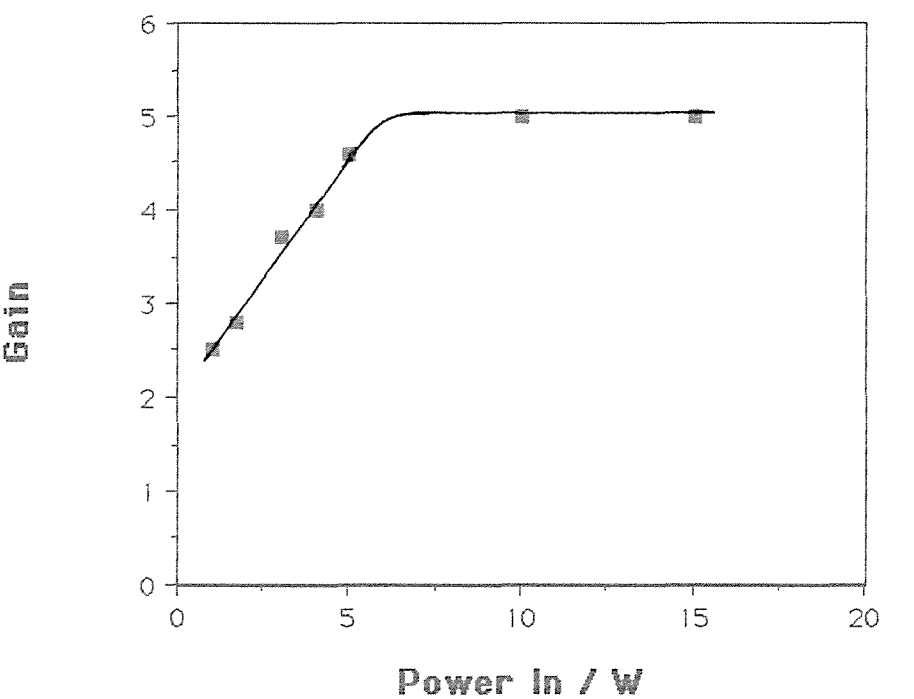

5A.4.2 Henry Radio 1kW Linear Amplifier - Model 2006

The Henry Radio model 2006 shown schematically in Fig.5-15 is a high quality, one-stage linear RF power amplifier which uses a single ceramic high gain triode (Eimac 3CX800A7) in a grounded grid circuit. The amplifier is completely self-contained and employs the use of high quality RF and DC componentry. The output power is specified at 1000W PEP nominal, 500W DC nominal and was measured using a 50 ohm 1kW rated load. These characteristics are shown in Fig.5-16.

The front panel of the unit contains a monitor of the plate current of the 3CX800A7 tube as well as a multimeter which shows either the grid current of the final tube or the high voltage from the power supply. A four position pushbutton switch located just below the meters selects each function, including an enabling or disabling of the amplifier.

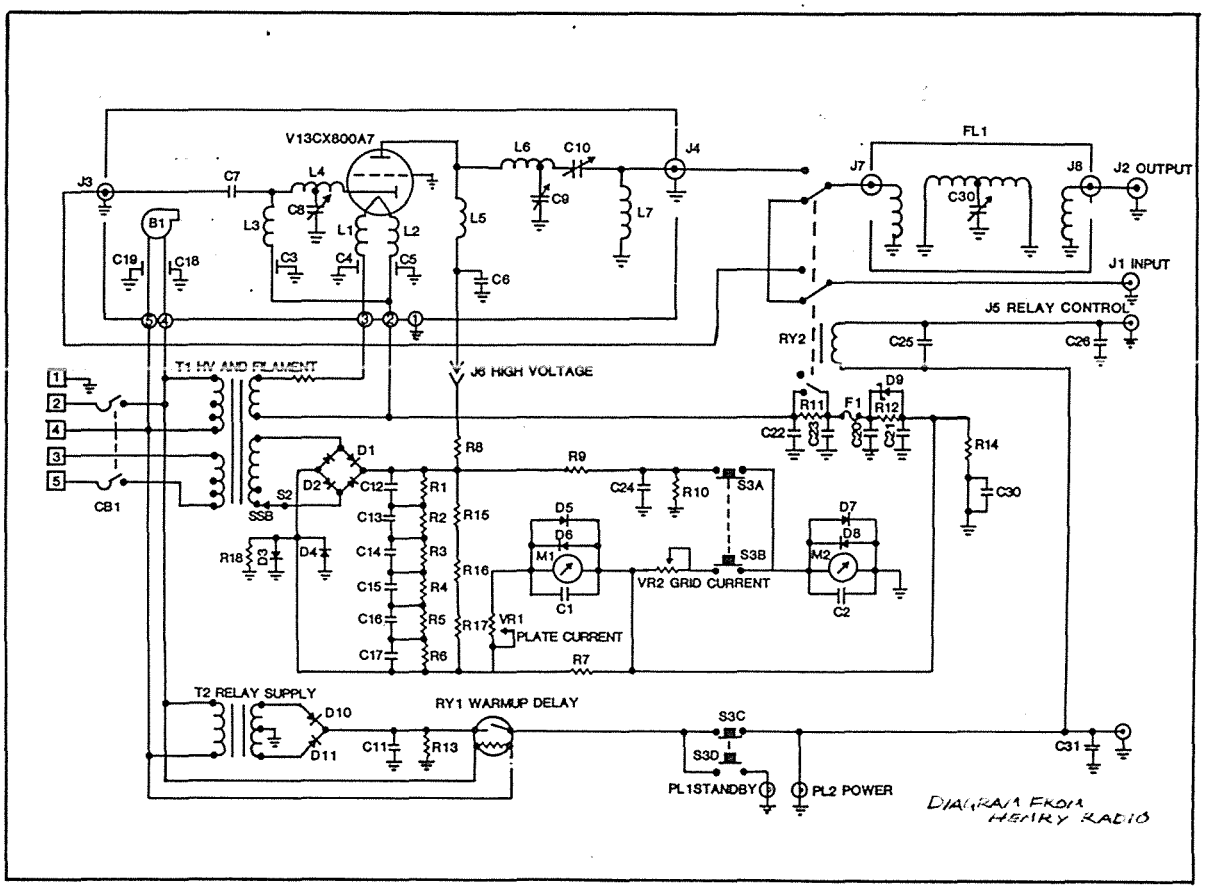

Fig.5-15

Circuit diagram for the Henry Radio 1kW Amplifier.

Fig.5-16 Henry Radio and Driver Characteristics

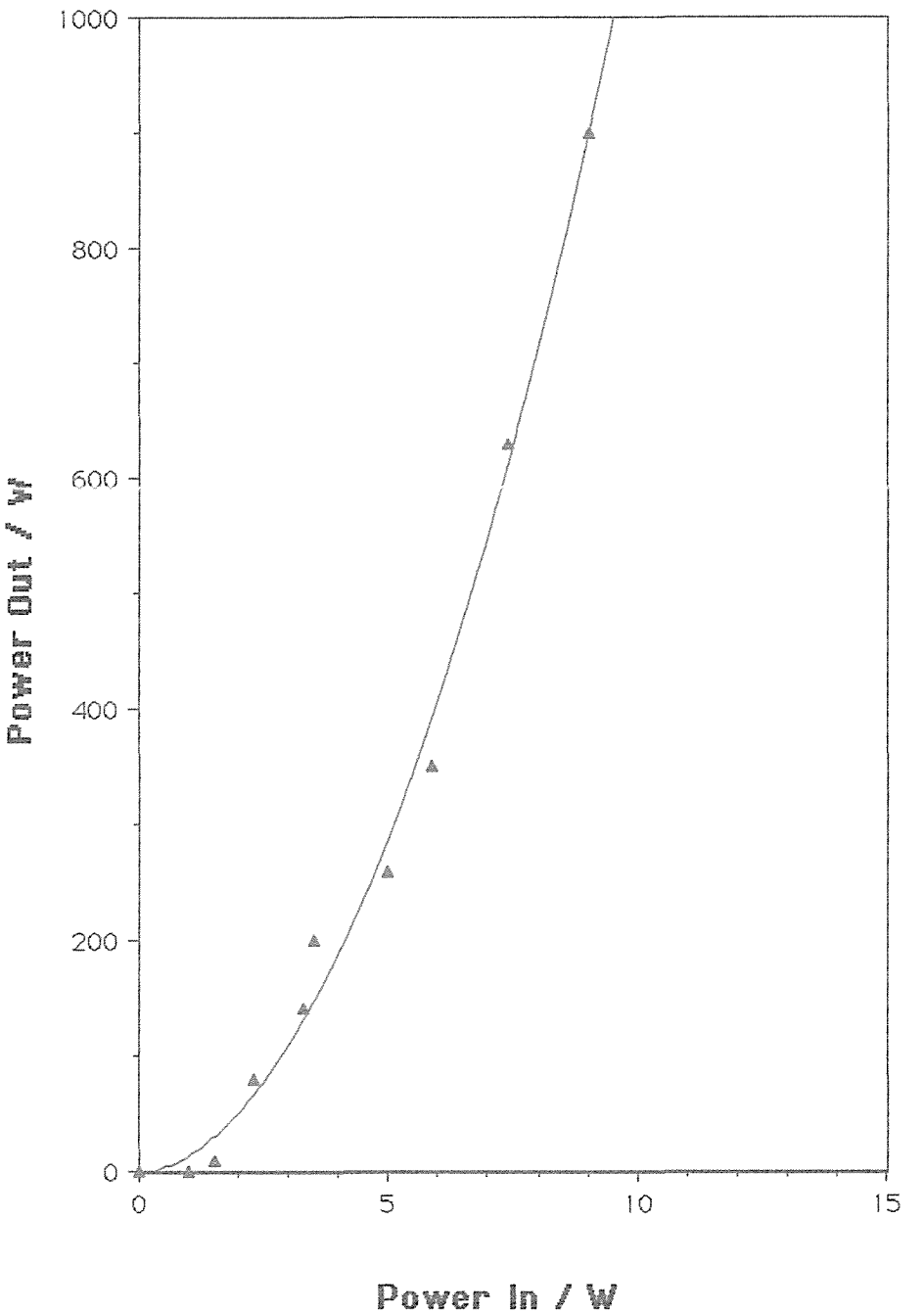

5A.5 60MHz Receiver

The 60MHz receiver which follows the RF preamp. provides further amplification to the NMR signal in the following manner[37]: After passing a single stage 60MHz RF amplifier (see Fig.5-17) , the signal is mixed with a 71MHz signal provided by a local oscillator and an 11MHz IF signal is produced. This IF signal then undergoes two stages of amplification (by two MC 1350 based IF amplifiers) before it passes a second mixer operating as a phase sensitive detector (P.S.D). An audio signal is then produced which is amplified by a single stage variable gain 741 operational amplifier. The signal is next fed to a two stage active bandpass filter having a bandwidth equal to the subsequent digitising stage. The digitised signal is read by a TI-980A computer and stored in memory ready for co-addition and later analysis.

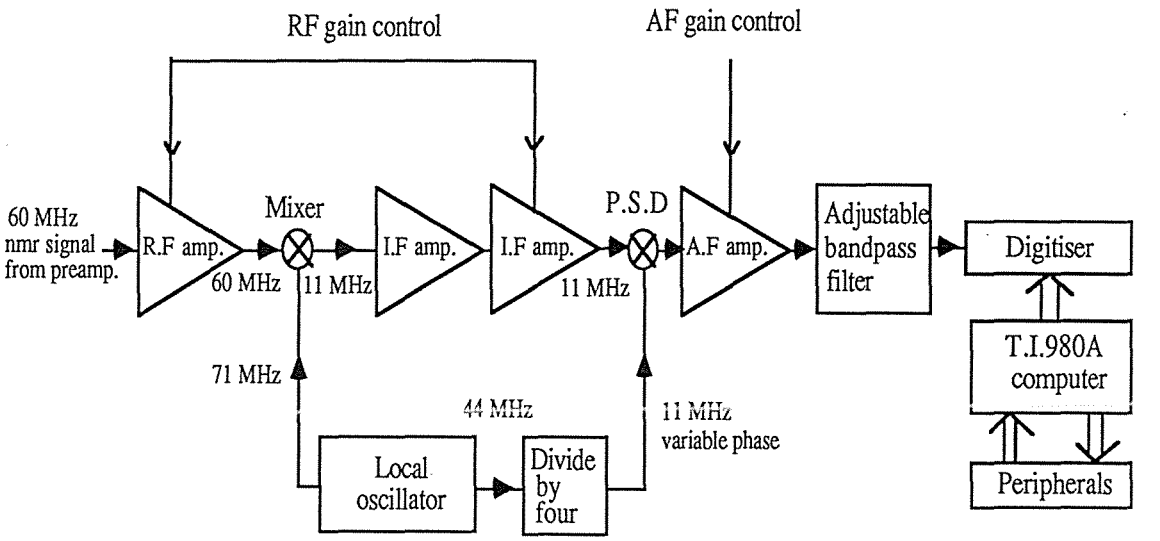

Fig.5-17

Block diagram of the 60MHz receiver.

5A.6 TI-980A Computer

The TI-980A computer is a Texas Instrument progamming machine with 16 bits per instruction and an average execution time of approximately 1μs per instruction. The machine has 32K words of memory and is capable of driving a number of peripherals including an oscilloscope for data display, a plotter for producing a hard copy of the free induction decay or corresponding spectra. Interaction with the software package supplied can be made via a light-pen menu based operating system.

5B Software

5B.1 Software Outline

The $T_{1\rho}$ software, denoted as T1RHO, makes use of the existing Imaging and JEOL FX60 software. Portions of the Imaging software have been modified and additional subroutines written as required. The structure of the T1RHO software is described in the flowcharts given in Fig.5-18a & Fig.5-18b. The corresponding assembly code is given in the program listing of Appendix E. This includes the modified Imaging subroutines together with additional subroutines. The remainder of the Imaging software used by T1RHO can be found in reference 41.

The T1RHO lightpen based menu (see Fig.5-19) can be selected from the main NMR menu via the asterisk in the lower lefthand corner of the FT-NMR menu. This allows control to pass from a normal experiment to an update experiment whereby times governing the length of the B_1 pulse are updated automatically and data is likewise transferred to the Hitachi pc for display.

The basic operations required in a T1RHO experiment may be described as follows:

(1) Select appropriate LEVEL and TIMES. These are parameters of the RF pulse.

(2) Load and start the pulse sequencer.

(3) Accumulate the data.

(4) Transfer the data to the Hitachi pc and update the times.

(5) Repeat steps (2), (3) and (4) until all the runs have been sent to the Hitachi.

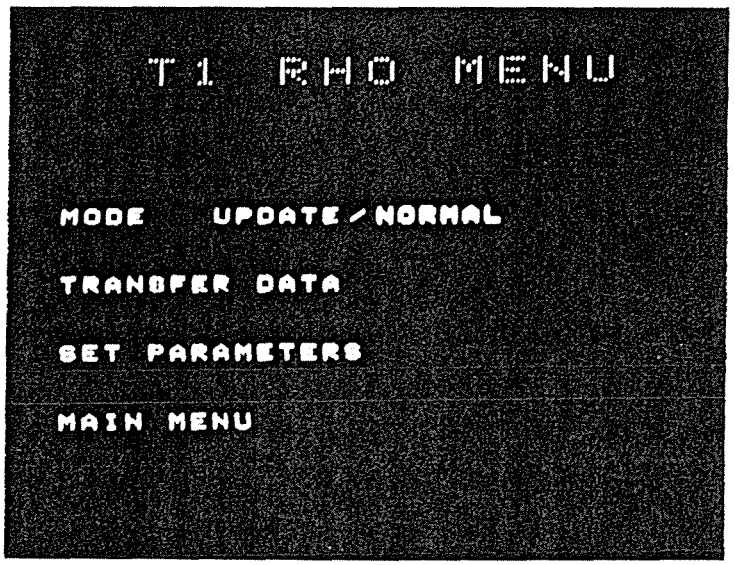

Fig.5-19
T1RHO menu. LEVEL and TIMES of step (i) are selected from ' set parameters '

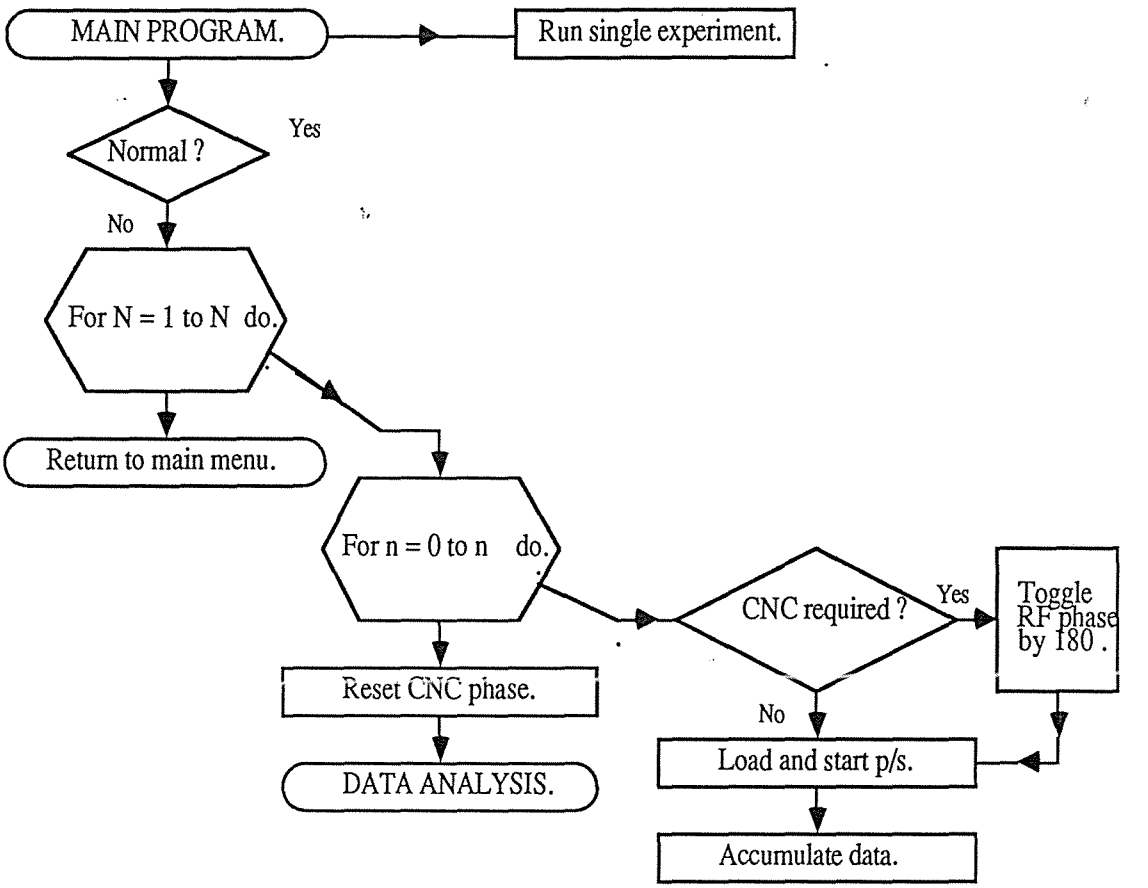

Fig.5-18a

Flowchart for a T1RHO experiment.

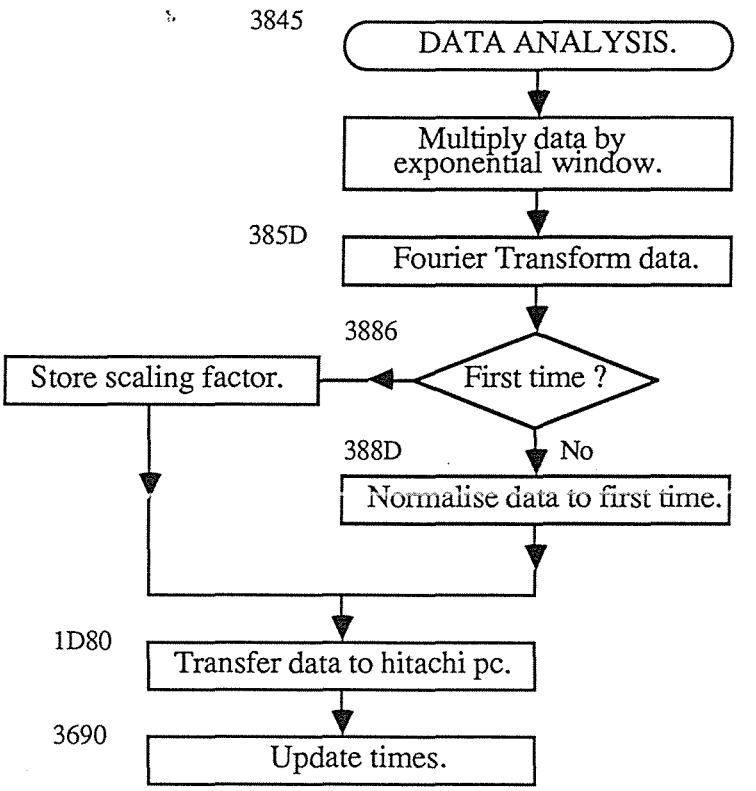

Fig.5-18b

Flowchart for Data analysis.

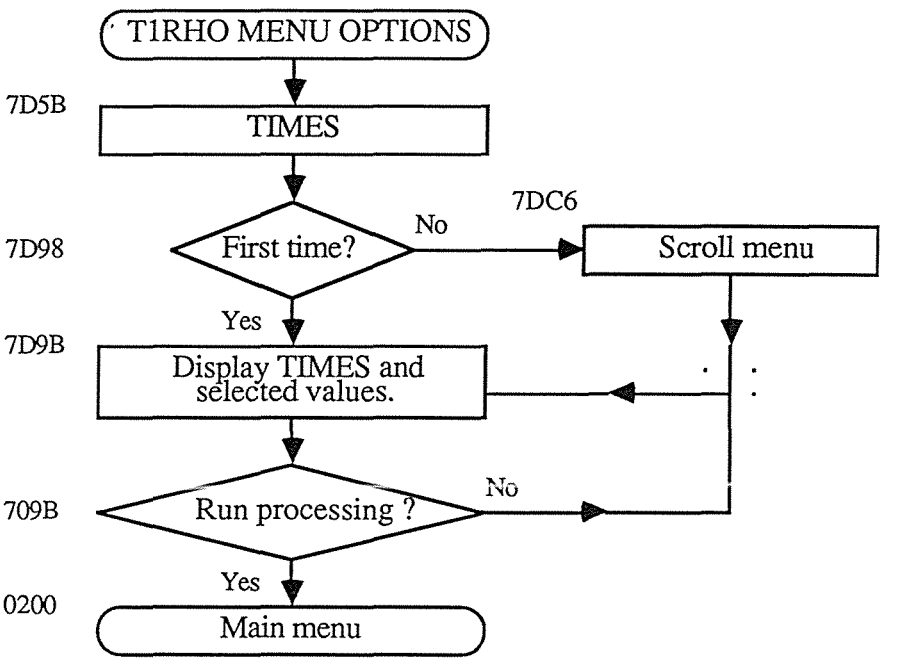

Fig.5-18c

Flowchart for selection of " Times ".

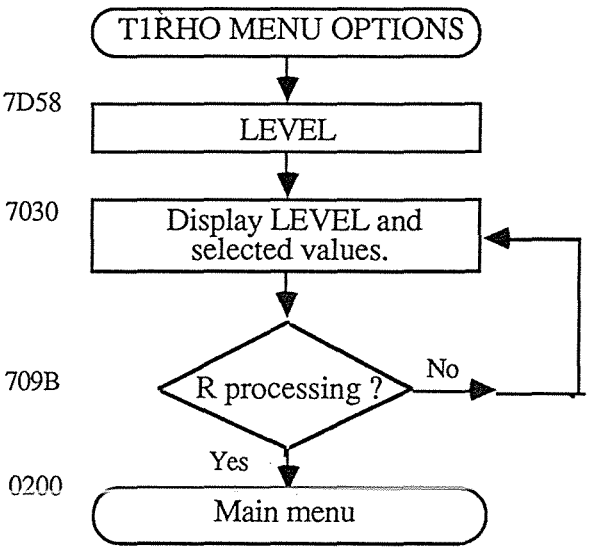

Fig.5-18d
Flowchart for selection of " Level ".

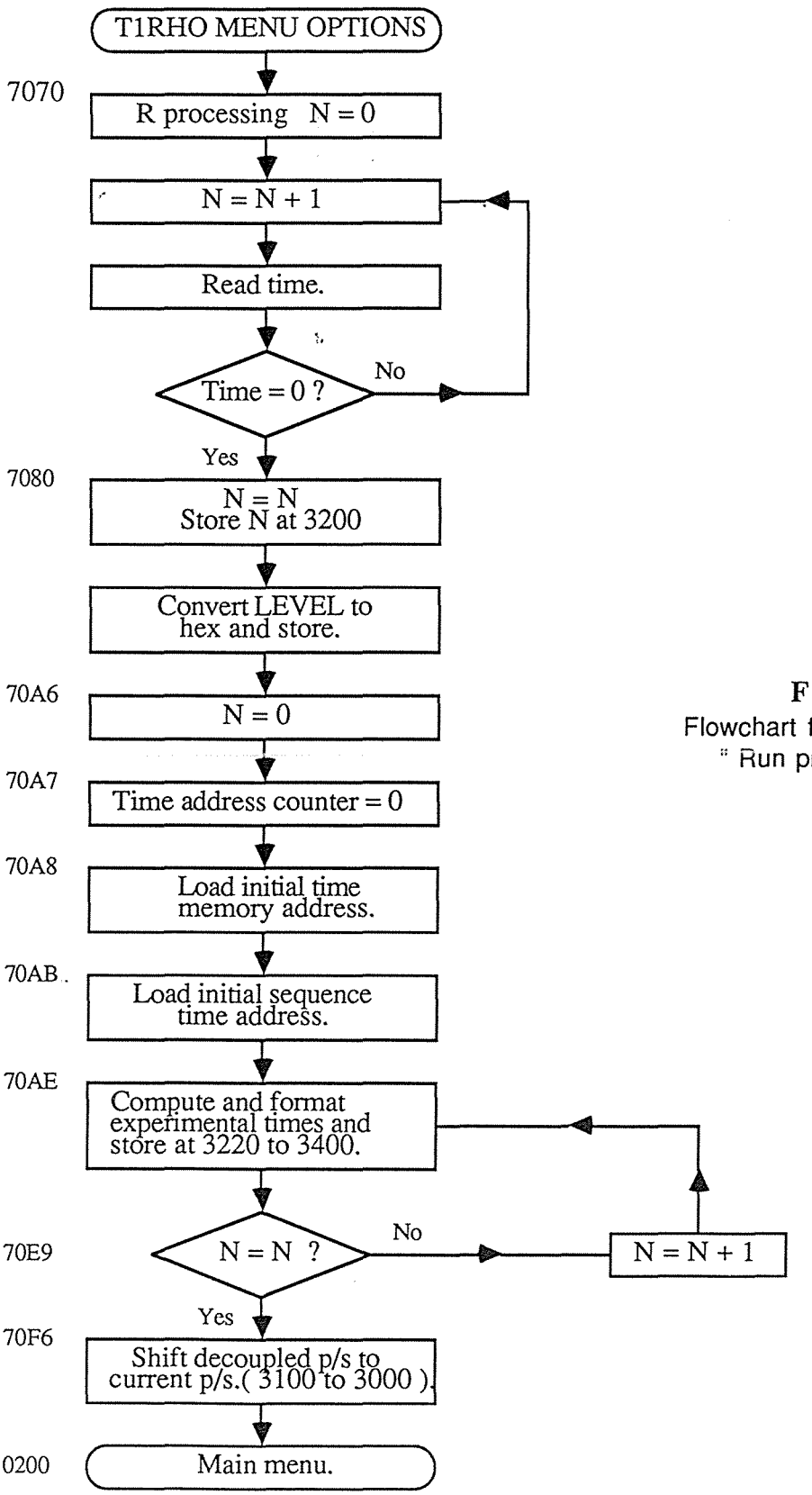

Fig.5-18e
Flowchart for selection of " Run processing ".

5B.2 Set Parameters

There are four modes of operation: 'R', 'L', 'T' and 'M' as shown in Fig.5-20.

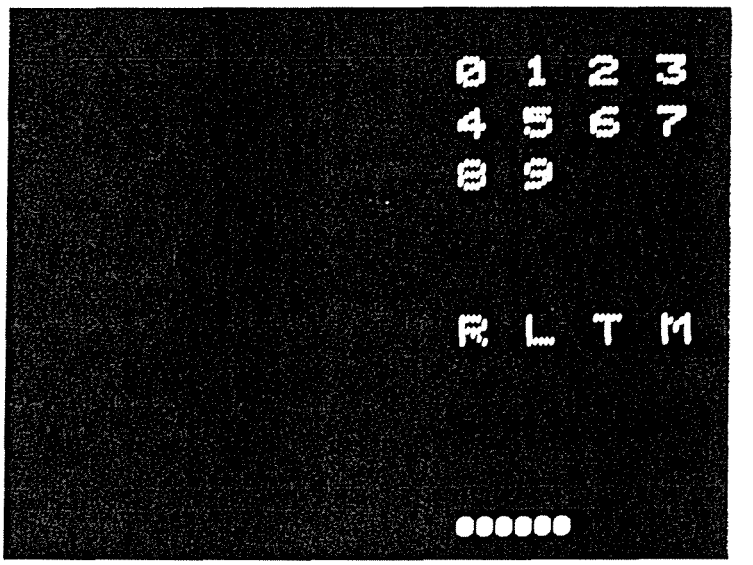

Fig.5-20

The four modes of operation upon selection of ' set parameters '

5B.2.1 Hex Monitor

The hex monitor (see Fig.5-21) forms a convenient means of interacting with the software. The leftmost column of hex digits are the machine addresses while the adjacent column contains the corresponding memory contents. The figures 0 to F shown at the top righthand corner form the 'keypad' while the 16 bit word at the bottom is the 'keypad display buffer'.

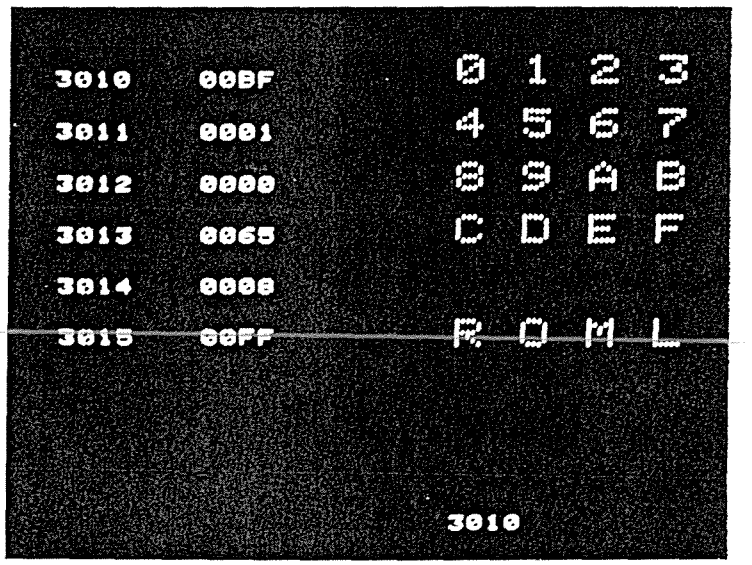

Fig.5-21

Hex. monitor

Program opcodes are entered by selecting the appropriate hexadecimal character from the keypad. The keypad buffer displays each digit as it is selected. The desired word can be entered by pointing the lightpen to either the opcode or address column and pressing the switch. This action modifies the location and changes the current value to that in the keypad buffer. If 'R' is selected in this mode control is passed to the program and the program counter contents are replaced by the keypad buffer.

5B.2.2 'T'- Times

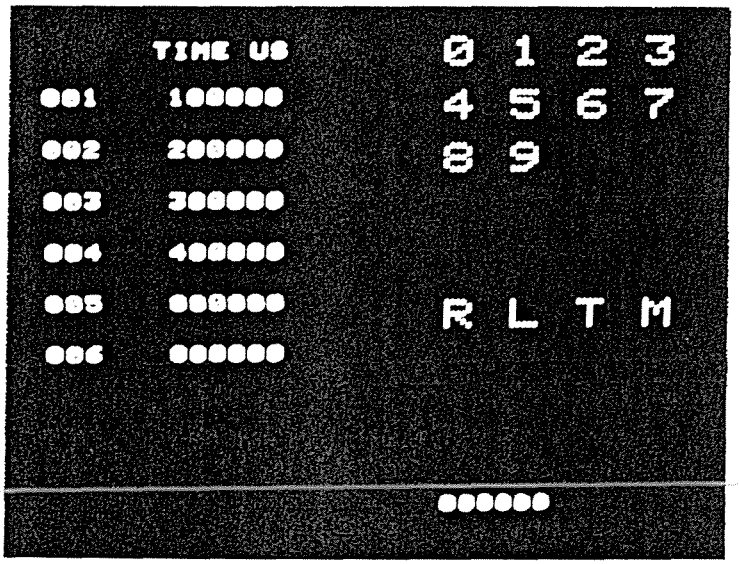

Fig.5-22
Time mode selected

The time in μs is given as a six digit decimal number (see Fig.5-22). Each digit is selected from the keypad and subsequently displayed in the buffer. The lightpen is pointed to the appropriate time, in the TIME μs column, which the new time displayed in the keypad buffer is to replace. Upon pressing the switch the transfer is made. In this way the update times for the entire experiment are stored. Allowance has been made for the storage of 30 time values to be entered in groups of six as shown. The time store memory is scrolled by pressing the lightpen on 'T'. The end of the experiment is indicated by a time value of 000000. The flowchart detailing this process is given in Fig.5-18c.

5B.2.3 'L'- Level

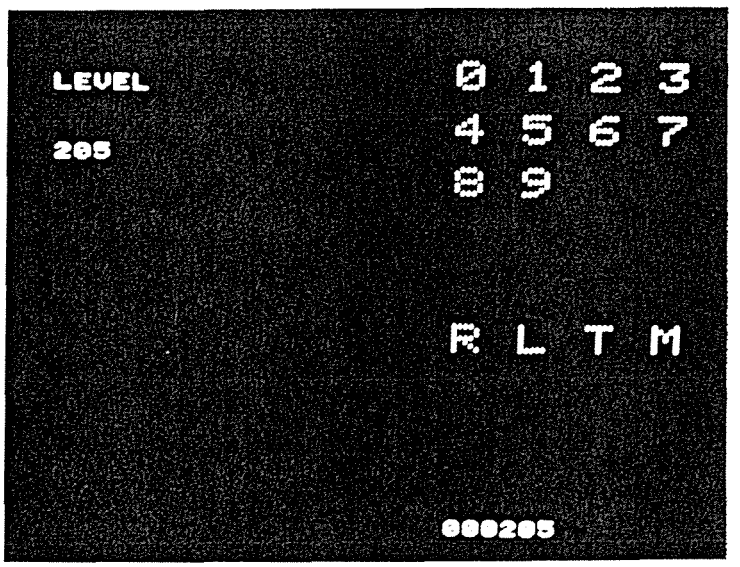

Fig.5-23
RF LEVEL selection

A value for the LEVEL of the RF pulse between 0 and 127_{10} is selected from the keypad and displayed in the buffer (see Fig.5-23). The storage is made in the usual manner by pointing the lightpen at the existing value of LEVEL and pressing the switch. The flowchart detailing this process is given in Fig.5-18d.

5B.2.4 'R'- Run Processing

Selection of 'R' in either LEVEL mode or TIME mode will result in the following. Firstly the LEVEL is converted to hexadecimal and stored at memory address 311A. Secondly time store memory (7DD8 to $7E13_{16}$) is transferred to location 3220 to 3400_{16}. Furthermore, the times are now individually stored as three groups of two bytes each. For example, a time t = 123456 μs would be stored as

Address 1 0012

Address 2 0034

Address 3 0056.

This change in format was to allow a simple method of transferring times to the pulse sequencer.The flowchart detailing this process is given in Fig.5-18e.

5B.3 Running the Experiment

A T1RHO experiment is initiated by selecting 'S' in the ACCUM menu (see Fig.5-24)

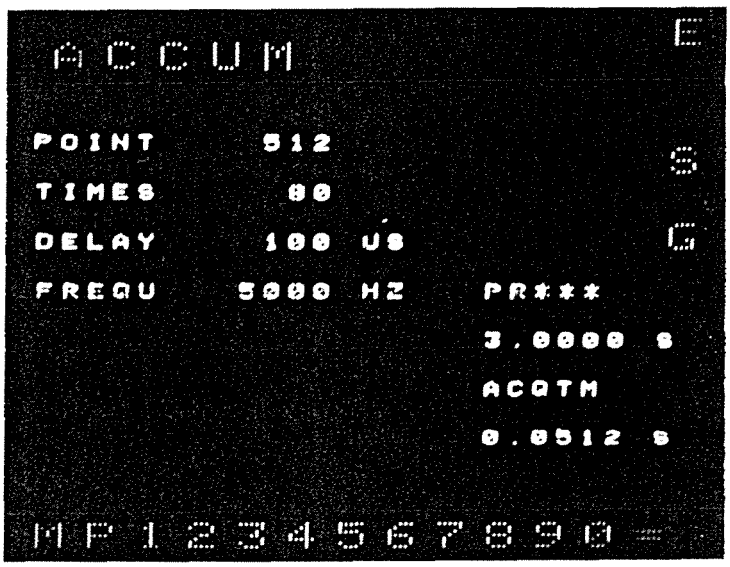

Fig.5-24
The Accumulation (ACCUM) menu

This causes the pulse sequencer data in locations 3000 to $31FF_{16}$ to be transferred to the pulse sequencer. Once the data has been transferred, control is passed to the pulse sequencer which now produces the various RF pulses necessary for the detection of a T1RHO signal.

The T1RHO TEMPLATE pulse sequence is shown in Fig.5-25. This gives the initial pulse sequence and is stored from 3100 to $31FF_{16}$. An experiment is initialised upon switching from NORMAL to UPDATE in the T1RHO menu. This action copies the TEMPLATE from 3100 to 31FF into the new location 3000 to 30FF.

If coherent noise cancellation (CNC) has been selected, alternate experiments will change the initial RF pulse phase by 180°. This will reverse the sign of the detected signal. The accumulation routine is also changed by this phase alteration and data is subtracted rather than added to memory. Thus any coherent signal superimposed on the desired nuclear signal (such as dc offsets or computer interference) is discriminated against by this process. Once the modified phase has been stored in the pulse sequencer, the pulse sequencer is reloaded and the experiment restarted.

After each accumulation the data is transferred to the Hitachi pc. The RF pulse length is then updated and the process is repeated until N_T accumulations have been performed after which the routine will return to the main NMR menu (entry address 0200).

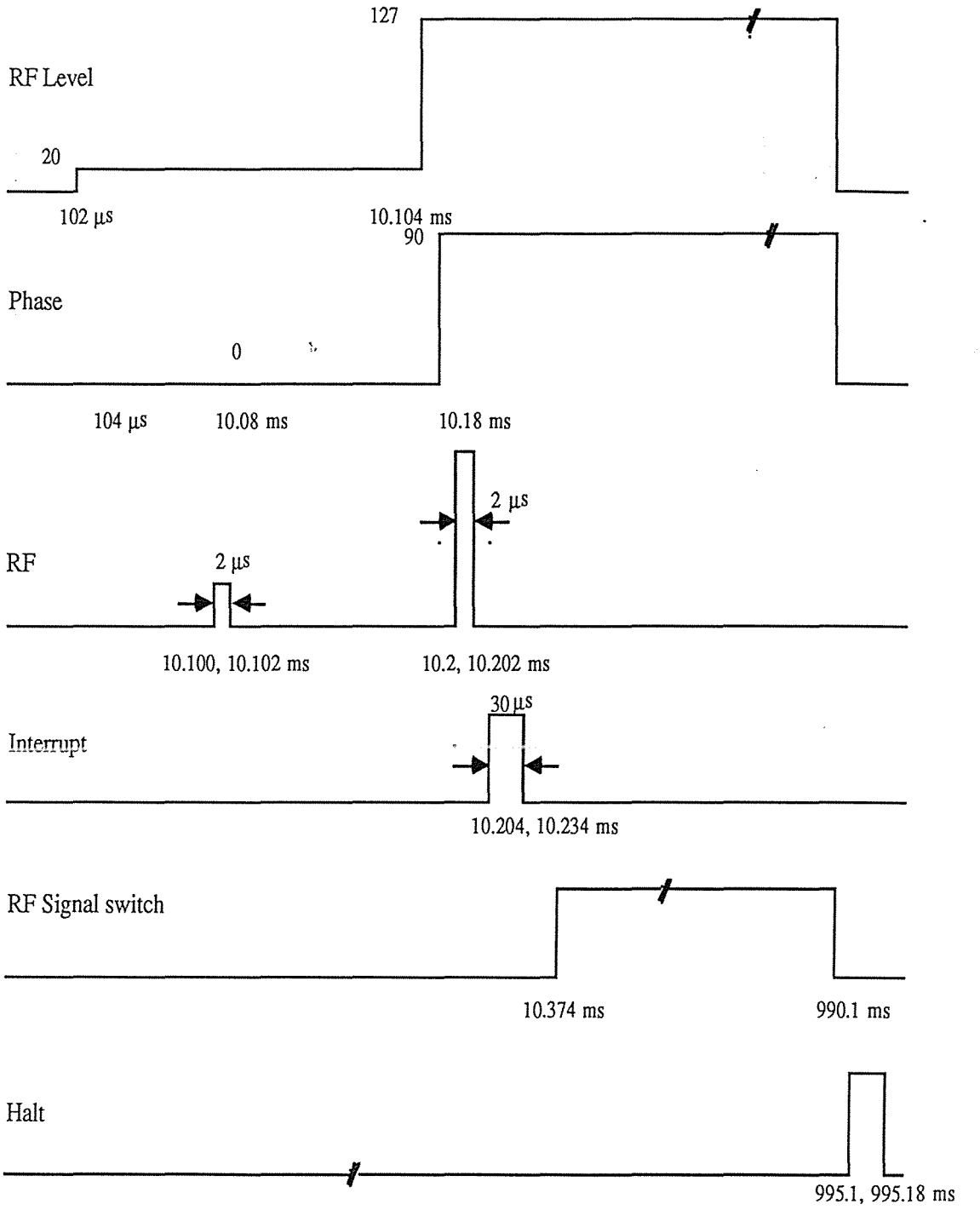

Fig.5-25
Template pulse sequence.

If the NORMAL experimental mode has been selected the routine will return to the main menu after the first N_{acc} accumulations.

5B.4 Memory Organisation

Data is organised as shown by the following memory map:

3000 to 30FF	Pulse sequence data.
3100 to 31FF	Pulse sequence TEMPLATE including LEVEL @ 311A.
3200	Number of update times N_T.
3201 to 320F	Addresses of time data to be updated.
321E	Time (experiment) counter.
321F	Time address counter.
3220 to 3400	Time data required.
3690 to 36C4	Modification : Update " Imaging gradient " to Update " Times".

Upper memory: Modified Imaging software + additional subroutines (See appendix E for program listings).

7000 to 700D	ASCII addresses.
700E to 702E	Display " TIMES μs ".
702F to 7067	Display " LEVEL ".
7068	LEVEL store.
7D00 to 7D1D	Initialise variables.
7D1E to 7D44	Display keypad and test for lightpen hit.
7D45 to 7D52	Display keypad buffer.
7D53 to 7D5F	Select mode.
7D60 to 7D64	Lightpen hit detected.
7D65 to 7D66	Store selected character in keypad buffer.
7D7F to 7D97	Display six nibble hex. digit in A,E register at co-ordinates (S,M).
7D98 to 7DC1	Time mode selected.
7DC2 to 7DC5	Time routine - Lightpen hit on data.
7DC6 to 7DCE	Scroll time display.
7DCF to 7DD7	Reset keypad buffer and mask.
7DD8 to 7E13	Time store memory.
7E14 to 7E43	DATA.
7E44 to 7E4C	Modify mode routine.
7E59 to 7E74	Display three nibble hex. digit in E register at co-ordinates (S,M).
7E80 to 7EC6	Subroutine to add in decimal (A,E) to (M,S). Only the last six hex. digits are added and the first two digits are preserved.
7F01 to 7F17	Display six nibble (hex. digit) in A,E register at co-ordinate (S,M).
7F25 to 7F4C	Modification to store selected character.
7F55 to 7F71	Time mode selected. Hex. to digit conversion.

Chapter 6 Data Analysis

It is a capital mistake to theorise before one has data

... Sherlock Holmes

6.1 Modelling the Observed Behaviour

$T_{1\rho}$ measurements on polydimethylsiloxane (PDMS), polyethylene oxide (PEO) and polyethylene glycol (PEG) were made using the T1RHO system developed. These polymers were chosen because the monomer in each case contains a unique chemical environment for the hydrogen atoms. PEO and PEG have identical monomers but differing end termination. In the present context they are, in effect, identical. In this chapter we will use the acronym PEO to refer to both polyethylene oxide and polyethylene glycol. The atomic arrangement of the polymers is as follows:

PDMS

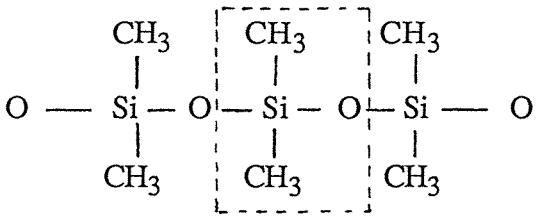

PEO

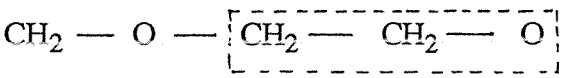

PE

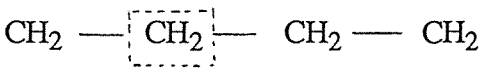

In PEO the protons occur in methylene CH_2 groups so that the (short range) dipolar interaction for each nucleus arises from the other in the pair. In PDMS each methyl group proton interacts with the remaining two.

The PDMS samples were obtained from Polysciences Inc.(Warrington, Pennsylvania) in polydisperse form and subsequently fractionated. They included the following molar masses:

$(M_W M_N)^{1/2}$	(M_W/M_N) After fractionation	M_W	(M_W/M_N) Before fractionation
584702	1.41	537000	1.5
253303	1.37	166000	3.5
169482	1.53	166000	3.5
72596	1.39	77000	2.5
10372	1.45	61000	4.0

The fractionation was performed by progressive non-solvent addition[42 - 44] and the molar mass distribution was measured by gel permeation chromatography.The weight average molar mass, M_W, and the number average molar mass, M_N, are defined as follows:

$$M_W = \frac{\int_0^\infty M^2 P(M)\, dM}{\int_0^\infty M P(M)\, dM}$$

$$M_N = \frac{\int_0^\infty M P(M)\, dM}{\int_0^\infty P(M)\, dM}$$

where P(M) dM is the probability that a molar mass M is located within the range dM. The critical entanglement mass for PDMS is 24500 daltons[45].

Monodisperse PEO samples were obtained from Polymer Laboratories (Church Stretton, Shropshire) and consisted of the following molar masses:

$(M_W M_N)^{1/2}$	(M_W/M_N)
246000 PEO	1.09
105000 PEO	1.06
56000 PEO	1.05
23000 PEO	1.08
23000 PEG	1.08

The critical entanglement mass for PEO is 4400 daltons[45] and for PEG is 3800 daltons[46] so that all of the polymers provide examples above M_c.

The samples were placed in 4mm diameter NMR tubes, flushed with N_2, pumped and sealed *in vacuo*. All experiments in the present work were performed at a temperature of 150°C. The melting points of PEO and PDMS are 137°C and -40°C respectively[46,47]. In the case of PDMS an additional set of data was obtained at 26°C. The apparatus was checked by measuring $T_{1\rho}$ for water at values of f_1 from the minimum frequency of 400Hz to the maximum frequency of 41.7kHz employed in the polymer melt experiments. Approximately 2s was obtained in each case, consistent with the requirement that $T_2 < T_{1\rho} < T_1$.

The results show a double exponential decay as shown in Fig.6-1. At first sight this is surprising since both PDMS and PEO apparently contain " one environment " for the protons and an identical dipolar interaction strength. This suggests that the difference in behaviour arises from a difference in the motion. Assuming that the molten sample is homogeneous, two possibilities arise. First, it may be that the different motion corresponds to protons in different length chains. In the case of PEO this explanation is unlikely since the chains are highly monodisperse. One is therefore led to postulate different physical regions within a given chain. One obvious explanation is that a distinction can be made between the middle of the chain and the chain ends. The molecular segments at the chain ends are freer to rotate rapidly than those confined to the central part of the tube and so could contribute to the long time component in the double exponential decay. The short time component therefore finds its source in the middle of the chain.

Experiments performed on Polyethylene (PE) reported in reference (13) were fitted using a model whereby the chain ends and the middle of the chain form a coupled two-spin system[48]. The division of the spins into two coupled subsystems for PEO will lead

Fig.6-1 Comparison of PEO & PE decays 555Hz

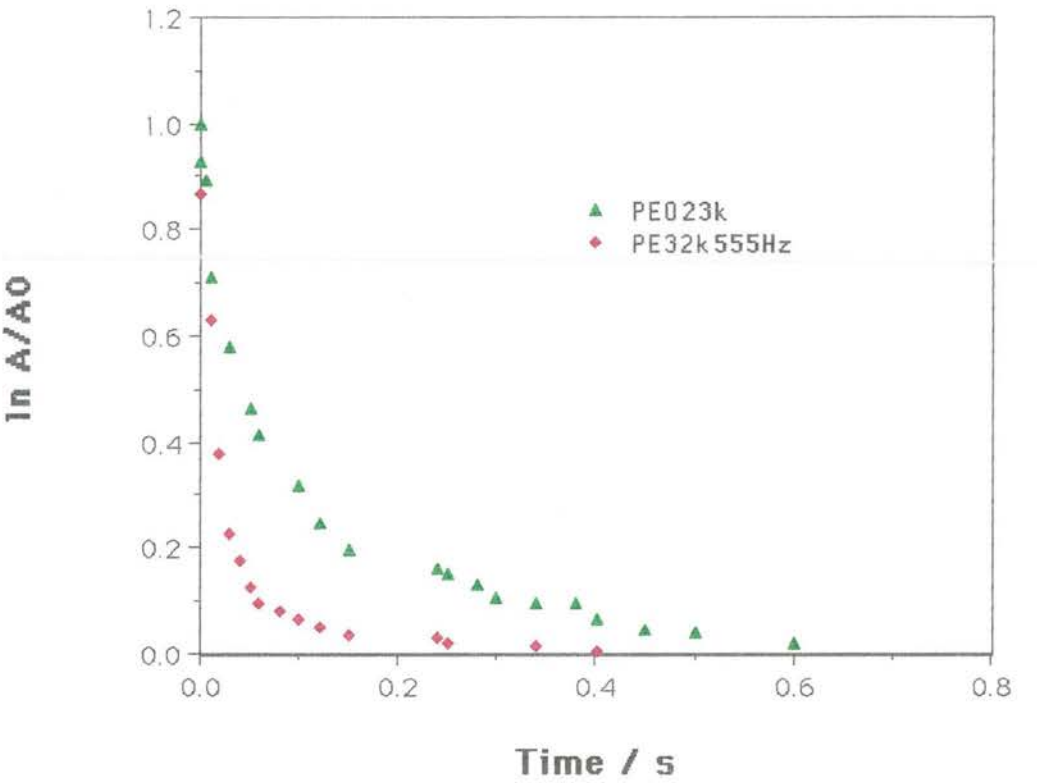

to bi-exponential behaviour provided that each subsystem can be represented by a common spin temperature as for PE. Comparison made with data on PE shows that PEO plots appear to be " stretched out " along the time axis. In other words the rapid $T_{1\rho}$ component for PEO decays at a slower rate than that for PE. This presents a major problem in the data analysis since separation of the fast and slow components is more difficult the closer the time constant. This problem is illustrated in Fig.6-1. The reason for this will be discussed later but the difference in behaviour arises from a difference in a_2, the local segmental anisotropy for rotation.

What we seek is the relaxation time associated with the tight tube. In our model this corresponds to the fast $T_{1\rho}$ component. However it is important to realise that cross-relaxation effects between protons in the chain centre and the chain ends may have the effect of altering the tight tube relaxation rate. Therefore it is important to use the coupled reservoir model to check that such cross-relaxation effects are accounted for.

6.2 The Coupled Two-spin System

The coupled spin system problem was originally solved by Shumacher[48]. For this system, illustrated in Fig.6-2, then,

$$\dot{\theta}_1^{-1} = -R_1 (\theta_1^{-1} - \theta_L^{-1}) - R_{12} (\theta_1^{-1} - \theta_2^{-1}) \qquad (6.3)$$

$$\dot{\theta}_2^{-1} = -R_2 (\theta_2^{-1} - \theta_L^{-1}) - R_{21} (\theta_2^{-1} - \theta_1^{-1}) \qquad (6.4)$$

letting

$$x = \theta_1^{-1} - \theta_L^{-1}$$

$$y = \theta_2^{-1} - \theta_L^{-1}$$

yields

$$\dot{x} = -R_1 x - R_{12} (x-y)$$

$$\dot{y} = -R_2 y + R_{21} (x-y)$$

solving for x then gives

$$x = a_1 \exp (- t / \tau_a) + b_1 \exp (- t / \tau_b) \text{ normalised,} \qquad (6.5)$$

where

$$a_1 = \{ 1 + [(1 / \tau_a) - R_1] / [R_1 - (1 / \tau_b)] \}^{-1} \qquad (6.6)$$

$$b_1 = 1 - a_1 \qquad (6.7)$$

and $$1 / \tau_a = 1/2 \{ (A + C) + [(A + C)^2 - 4 (A - DB)]^{1/2} \} \qquad (6.8)$$

$$1 / \tau_b = 1/2 \{ (A + C) - [(A + C)^2 - 4 (A - DB)]^{1/2} \} \qquad (6.9)$$

where

$$A = R_1 + R_{12}$$

$$B = R_{12}$$

$$C = R_2 + R_{21}$$

$$D = R_{21}$$

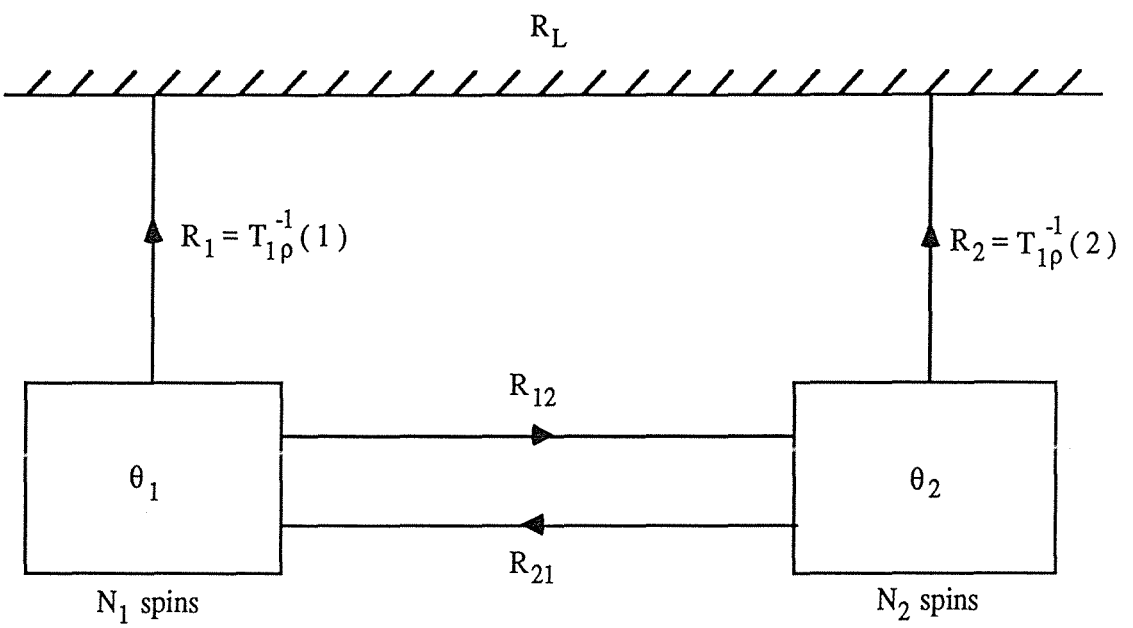

Fig.6-2

The coupled two-spin system used to describe bi-exponential behaviour.

$$y = a_2 \exp(-t/\tau_a) + b_2 \exp(-t/\tau_b) \text{ normalised,} \qquad (6.10)$$

where

$$a_2 = \{ 1 + (b_1/a_1)[A - 1/\tau_b]/[A - 1/\tau_a] \}^{-1} \qquad (6.11)$$

$$b_2 = 1 - a_2. \qquad (6.12)$$

Now $\theta_1^{-1} - \theta_L^{-1}$ is normalised which means that a + b = 1. The resultant signal is given by as $S = N_1x + N_2y$.Therefore,

$$S = (N_1a_1 + N_2a_2)\exp(-t/\tau_a) + (N_1b_1 + N_2b_2)\exp(-t/\tau_b). \qquad (6.13)$$

What we measure in the bi-exponential fit is τ_a^{-1}. What we seek is the tight tube relaxation rate R_1. Unfortunately R_{12} is an adjustable parameter and the values of N_1 and N_2 are subject to assumptions about the size of the chain end fraction. In principle there are four adjustable parameters: R_1, R_2, R_{12}, and (N_1 / N_2) and three experimental parameters (a / b), τ_a, and τ_b. However R_2 is the relaxation rate for a section of the chain in isotropic motion and so may be set equal to T_1^{-1}. Furthermore N_1 / N_2 is fixed for all f_1 values. This should mean that the available data is more than sufficient to fit the theoretical parameters and should therefore provide a test of the model. In practice this proves extremely difficult because of the sensitivity of the fit to experimental errors. Ideally therefore we would prefer that our data exhibited only weak cross-relaxation effects and that R_1 is approximately equal to τ_a^{-1}.This will certainly be the case when N_1 is much greater than N_2 which should apply for large polymers under conditions where the chain ends represent a small fraction of the total chain. It should be noted that significant cross-relaxation effects may be expected for small polymers when R_1 is slow. This problem is exacerbated for PEO and PDMS because of the slower " fast component relaxation rate ", R_1, than that observed in PE. It must be accepted that some of the PEO and PDMS data will not be amenable to reliable interpretation because of these effects.

6.3 Experimental Results

Table 6-I shows the a, b, τ_a (fast component), τ_b (slow component) relaxation times and also the " corrected " $T_{1\rho}(1)$ (tight tube component) relaxation times. These were obtained using a double exponential fit program developed by P. Daivis[49]. In the earlier study on PE, it was seen that $T_{1\rho}$ (1) was much less than $T_{1\rho}(2)$ and cross-relaxation effects on $T_{1\rho}(1)$ were minimal. In the case where f_1 was very small N_2 / N_1 could be fitted independently of cross-relaxation effects and corresponded to chain ends each of length M_c. This seems entirely reasonable. In making the necessary correction for cross-relaxation in PEO and PDMS the value of N_2 / N_1 is therefore set to $2M_c / (M - 2M_c)$, $T_{1\rho}(2)$ is set to T_1 and R_{12} and $T_{1\rho}(1)$ are adjusted to provide the best consistency with a, b, τ_a and τ_b.

The data is shown graphically through Fig.6-3 to Fig.6-6 for PEO and PDMS. Note that the ordinate axis plots $\ln J_0(2\omega_1)$ since the J_1 and J_2 components of $T_{1\rho}^{-1}$ are given by $0.7T_1^{-1}$ at high frequencies and under extreme narrowing (see appendix D).This correction is negligible at low frequencies but must be used at high frequencies.

	23k PEG N_1= 0.62 N_2= 0.38 $T_{1\rho}(2)$ = 1s			23k PEO N_1= 0.62 N_2= 0.38 $T_{1\rho}(2)$ = 1s			56k PEO N_1 = 0.86 N_2= 0.14 $T_{1\rho}(2)$ = 1s		
f_1 / Hz	[a] [b]	τ_a τ_b	$T_{1\rho}$ (1) T_{12}	[a] [b]	τ_a τ_b	$T_{1\rho}$ (1) T_{12}	[a] [b]	τ_a τ_b	$T_{1\rho}$ (1) T_{12}
555	0.56 0.44	0.124s 0.66s	**0.13s** 3s	0.57 0.43	0.100s 0.66s	**0.112s** 3s	0.81 0.11	0.038s 0.232s	**0.042s** 1.8s
833				0.56 0.44	0.100s 0.66s	**0.112s** 3s	0.75 0.25	0.039s 0.147s	**0.042s** 1s
1250	0.52 048	0.120s 0.57s	**0.13s** 2s				0.79 0.21	0.042s 0.234s	**0.055s** 1.8s
2500	0.51 0.49	0.120s 0.55s	**0.13s** 1.8s	0.39 0.61	0.120s 0.37s	**0.12s** 0.8s	0.62 0.38	0.069s 0.168s	**0.077s** 1.1s
4000	0.50 0.50	0.124s 0.55s	**0.14s** 1.8s	0.30 0.70	0.124s 0.37s	**0.15s** 0.7s	0.51 0.49	0.082s 0.169s	**0.09s** 1s
6760	0.38 0.62	0.129s 0.43s	**0.153s** 1.8s	0.39 0.61	0.129s 0.45s	**0.16s** 1.1s	0.64 0.36	0.135s 0.295s	**0.137s** 1s
8000									**0.16s** 1s
10000									**0.19s** 1s
12500									
20000									**0.27s** 1s
31250									**0.32s** 1s
41700									**0.39s** 1s

Table 6-I
The data from the two-spin coupled bath model

	105k PEO $N_1 = 0.92$ $N_2 = 0.08$ $T_{1\rho}(2) = 1s$			246k PEO $N_1 = 0.96$ $N_2 = 0.04$ $T_{1\rho}(2) = 1s$		
f_1 / Hz	[a] [b]	τ_a τ_b	$T_{1\rho}$ (1) T_{12}	[a] [b]	τ_a τ_b	$T_{1\rho}$ (1) T_{12}
400	0.86 0.14	0.025s 0.09s	**0.023s** 1.1s			
555	0.88 0.12	0.029s 0.124s	**0.027s** 1.6s	0.64 0.36	0.027s 0.04s	**0.025s** 0.8s
833	0.72 0.28	0.029s 0.54s	**0.027s** 1.6s	0.64 0.36	0.030s 0.04s	**0.028s** 0.9s
1250	0.51 0.49	0.043s 0.063s	**0.041s** 1.6s			**0.048s** 0.6s
2500	0.53 0.47	0.069s 0.10s	**0.066s** 1.1s			**0.08s** 0.6s
4000			**0.105s** 1.1s			**0.110s** 0.6s
6760			**0.135s** 1.1s			**0.137s** 0.6s
12500			**0.29s** 1.1s			**0.29s** 0.6s
20000			**0.34s** 1.1s			**0.37s** 0.6s
31250			**0.37s** 1.1s			**0.39s** 0.6s
41700			**0.40s** 1.1s			

Table 6-I cont'd

The data from the two-spin coupled bath model

Fig.6-3 PEO(PEG) Raw data

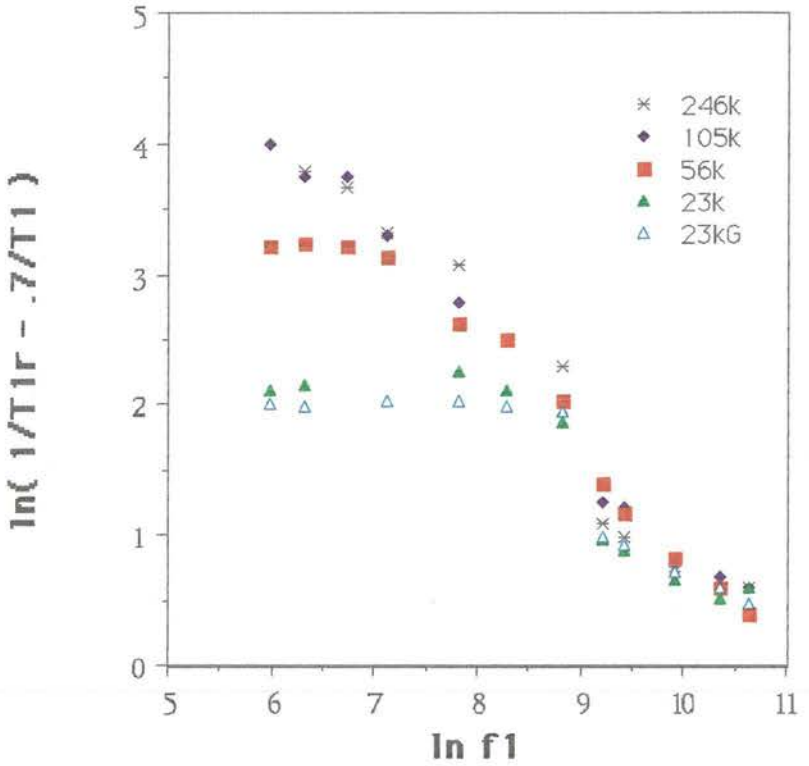

Fig.6-4 PEO(PEG) Coupled two-spin model

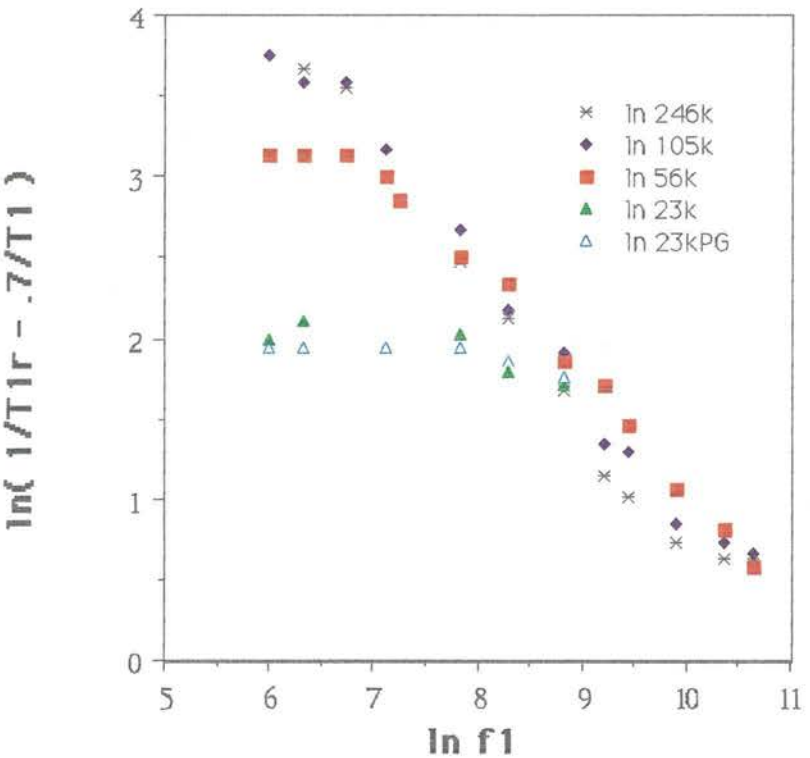

Fig.6-5 PDMS Room Temperature RT = 26C

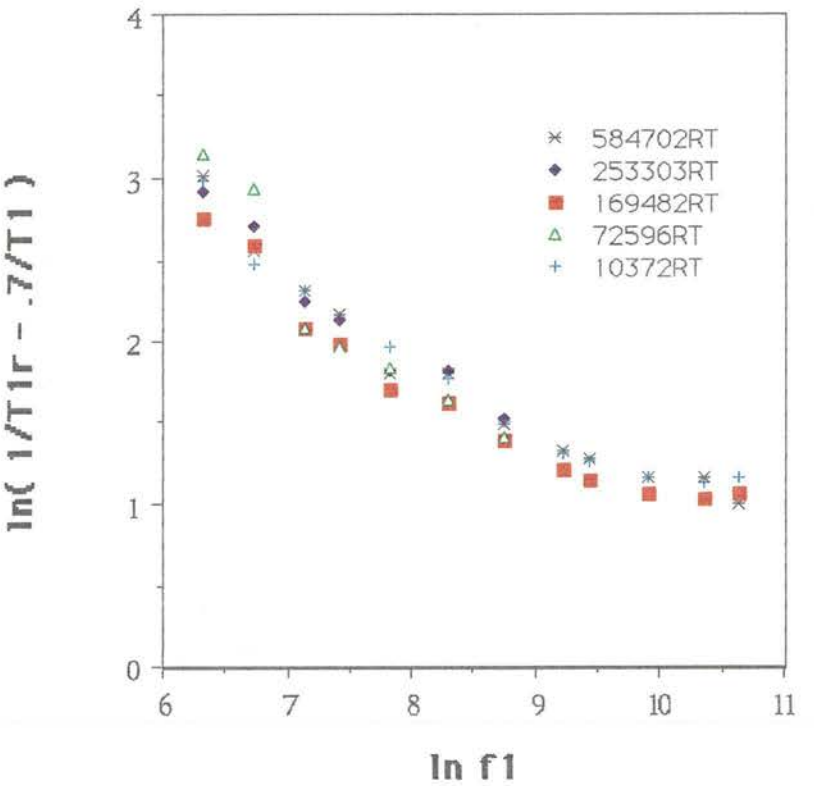

Fig.6-6 PDMS T = 150C

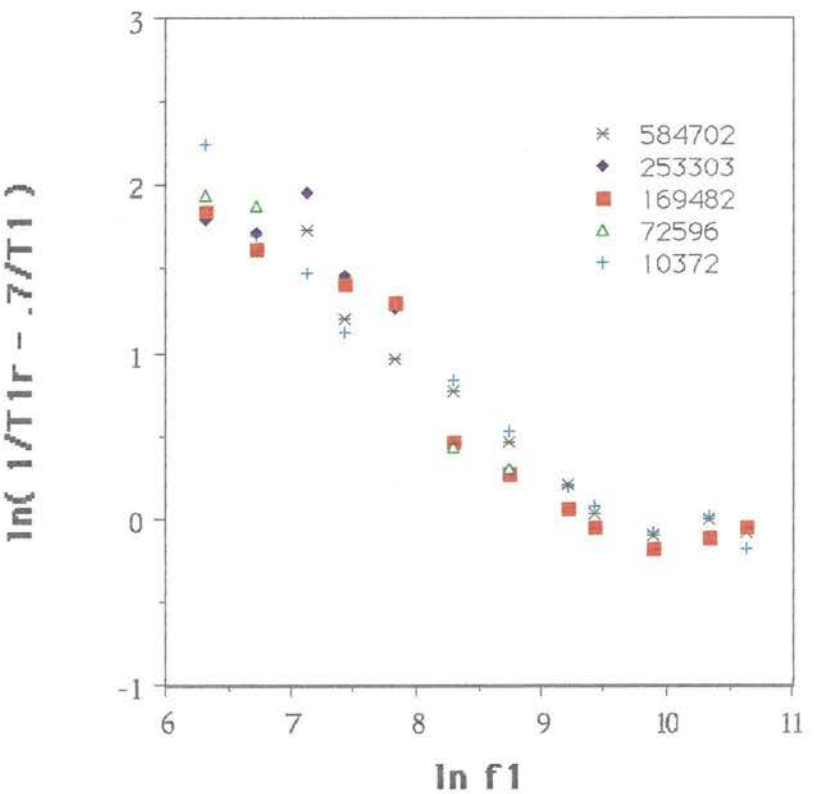

The effect of the coupled bath model on the raw data is to " pull up " the higher frequency data. The model causes large corrections at lower masses and the corrections made to the molar masses PEO 23000 and PEG 23000 diverged with small changes in the model parameters and so could not be plotted with confidence. This behaviour contrasts with the earlier study of $T_{1\rho}$ in PE where the effects of cross-relaxation were insignificant.

Despite the difficulties experienced in interpreting the high frequency data for low molar masses PEO above 20kHz, the data shown in Fig.6-4 corresponds to frequencies and molar masses where the effects of cross-relaxation are not severe.

The experimental error is difficult to establish a priori but it is indicated by the scatter.A good indication of the experimental error is given by the deviation between the two 23000 dalton masses corresponding to PEO and PEG samples respectively.

The most dramatic feature of the PEO $J_0(\omega)$ data is the separation of the molar masses PEO 23k(PEG 23k), PEO 56k, and PEO 105k data as f_1 is lowered. The 105k mass does not exhibit a plateau down to 400Hz, the lowest frequency used experimentally.

In contrast with PEO and the earlier PE study, the PDMS exhibits no dependence of $T_{1\rho}$ on molar mass over the frequency range covered. The general shape of the data is seen to remain the same at both room temperature and high temperature. A levelling of the graph at frequencies greater than 20kHz is seen at both temperatures.

6.4 Comparison with Theory (Discussion and Interpretation)

6.4.1 PEO Data

The theoretical model of Kimmich involves the adjustable parameters τ_R, τ_l, τ_s and a_2. By appropriate choice of these parameters it is possible to obtain fair agreement with the main features of the data as shown in Fig.6-7 for PEO. The PE data of reference (13) is reproduced in Fig.6-8 to provide a comparison with the PEO data. Table 6-II lists the resulting correlation times applicable to the three-step model of Kimmich and the rotation anisotropy constants, a_2, for each is also given.

According to de Gennes the time taken for complete disengagement from an initial tube, $\tau_R{}^r$, varies with molar mass as $\tau_R \propto M_W{}^3$. This dependence is seen to be broadly in agreement with the crossover frequencies shown by the data for PEO and is a major new observation. The results for PE and PEO clearly indicate the capacity of $T_{1\rho}$ experiments to provide a direct measure of polymer reptation times. Because the observed τ_R arises from a clearly defined spectral feature, namely the position of crossover to the low frequency plateau, its measurement is unambiguous. By contrast the value of the anisotropy constant a_2 is sensitive to the choice of τ_l. In broad terms τ_l is determined from the high frequency slope of log $J_0(\omega)$ vs log f_1 while a_2 is determined by the height of the plateau below $\tau_R{}^{-1}$. The degree of interdependence of a_2 and τ_l is indicated for PE in Fig.6-12.

Fig.6-7 Comparison with theory. PEO(PE6) 2-spin model

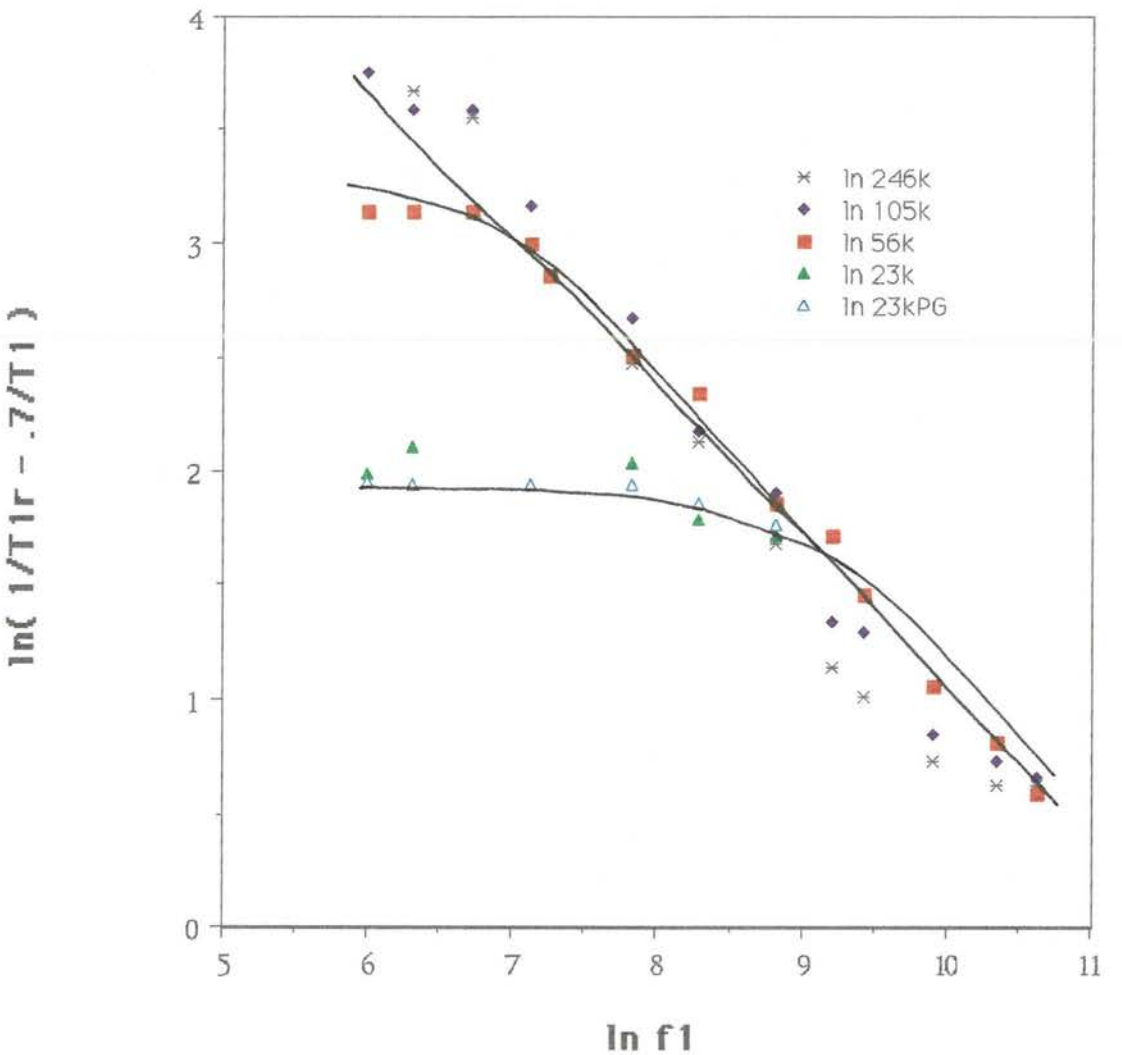

Fig.6-8 Polyethylene data 1987. Reference (13)

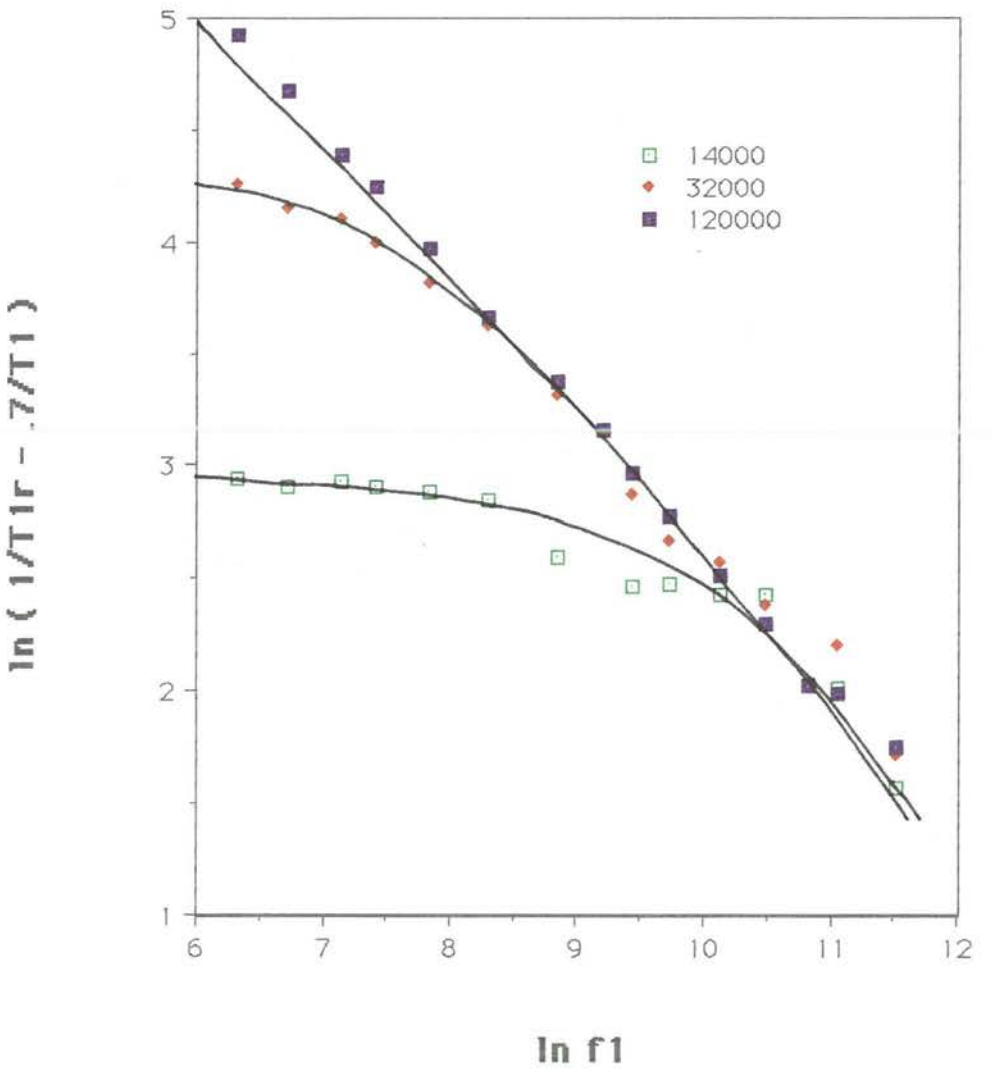

	PDMS (26°C)	PDMS (150°C)	PEO (150°C)	PE (150°C)
a_2	0.01%	0.005%	0.09% 0.7%	0.45% 3.2%
τ_s	4.0×10^{-10} s	1.2×10^{-10} s	4.0×10^{-11} s 3.0×10^{-10} s	5×10^{-11} s 4×10^{-10} s
τ_1	2.0×10^{-5} M^0 s	2.0×10^{-5} M^0 s	2.0×10^{-7} M^0 s	1.0×10^{-7} M^0 s
τ_R	$\gtrsim 5.0 \times 10^{-16}$ M^3 s	$\gtrsim 5.0 \times 10^{-16}$ M^3 s	4.0×10^{-19} M^3 s	1.0×10^{-18} M^3 s

Table 6-II

Correlation times and anisotropy constants for PDMS and PEO melts
The upper values for a_2 and τ_s correspond to direct calculations from T_1 while the lower values relate to τ_s values from reference (51)

We would expect a_2 to be a function of the monomer structure but not the molar mass. Immediately we notice that τ_1 is apparently independent of molar mass since the dispersions for all molar masses are coincident in the intermediate frequency regime

$$J_0(\omega) \approx 2a_2 (2\omega_1)^{-1/2} \tau_1^{1/2} \qquad (6.14)$$

The role of τ_1 and a_2 is indicated in the schematic diagram for $J_0(\omega)$, Fig.4-4. At τ_1^{-1} the slope of the dispersion changes from -1/2 to -3/2. In Fig.6-12 it is apparent that where τ_1^{-1} is in the vicinity of the low frequency plateau the choice of τ_1 influences the "vertical separation" of the plateau for different molar masses. This provides a useful aid in fitting for τ_1. However where τ_1^{-1} is much greater than τ_R^{-1}, its influence on the plateau separation is minimal. It was apparent in fitting both the PE and PEO dispersions that the magnitude of the plateau separation between the two lowest molar masses was consistent with this limit. In particular, $\tau_1 \leq 2 \times 10^{-7}$ s. However, it was also apparent in both the PE and PEO experiments that the slope of the $J_0(2\omega_1)$ dispersions, at the highest frequencies employed, was significantly steeper than -1/2, indicating that the crossover at τ_1^{-1} had been reached. This placed a lower limit on τ_1. The best fit to the PE and PEO data yielded $\tau_1 \approx 1 \times 10^{-7}$ s and 2×10^{-7} s respectively.

Having determined τ_R and τ_1, it is then possible to obtain a value for a_2. In PE and PEO the high frequency crossover at $2\omega_1 \approx (a_2 \tau_1^{-1} \tau_s^{-2})^{1/3}$ is not visible but the low frequency plateau at $J_0(\omega) \approx 2a_2 (2\tau_1\tau_R)^{-1/2}$ is clearly apparent for the lowest molar mass of 14000 and 23000 respectively. To fit this however requires an absolute relationship between the term $J_0(2\omega_1)$ and $\ln [T_{1\rho}(1)^{-1} - 0.7T_1^{-1}]$. This is established by equating the high frequency plateau $(a_2\tau_1^{-1}\tau_s^{-2})^{1/3} \leq 2\omega_1 \leq \tau_s^{-1}$ to $0.3T_1^{-1}$.

The magnitude of the high frequency plateau depends on τ_s, the correlation time for segmental rotation about the bond. This can be directly obtained from T_1 measurements since

$$T_1^{-1} = (3/2) \gamma^4 \hbar^2 I(I+1) [J_1(\omega_0) + J_2(2\omega_0)] \qquad (6.15a)$$

T_1 is sensitive to high frequency motion arising from the isotropic $(1 - a_2)$ fraction of the motion. Since $(1 - a_2)$ is approximately equal to unity the expression for T_1^{-1} is given by the isotropic high frequency limit

$$T_1^{-1} = (\gamma^4 \hbar^2 / r^6) I(I+1) (\mu_0 / 4\pi)^2 (2\tau_s) \qquad (6.15b)$$

where the factors of $(\mu_0 / 4\pi)^2$ and the internuclear vector, r, raised to the sixth power have been included to provide the absolute fit. The value of r is 1.8 Angstroms[50]. The isotropic high frequency limit assumption gives 5×10^{-11} s and 4×10^{-11} s respectively for PE and PEO. This disagrees with more direct high frequency spectral density

measurements by Kimmich and Schmauder[51] where τ_s is found to be 4 x 10^{-10} s and 3 x 10^{-10} s for PE and PEO at 150°C. Table 6-II shows a_2 values calculated using both approaches.

Referring to Table 6-II we see that the segmental reorientation time, τ_s, and the tube renewal time, τ_R, of the PEO melt are both shorter than those of the PE melt. However the time scale for reptation around tube bends, τ_l, appears to be larger for PEO than PE. Thus the smallest distance scale molecular motion, namely the rotation of the bonds occurs more rapidly in PEO than in PE and the largest distance scale molecular motion also occurs more rapidly in PEO. In other words a new chain configuration is achieved in PEO faster than in PE. The observation of more rapid segmental orientation and tube renewal motion in PEO is also consistent with the observation of smaller anisotropy. In essence, the tube is " looser " in the melt of PEO than in the more compact PE structure.

The difference in the τ_l values is an apparent contradiction. Furthermore it is noteworthy that in both the PE and PEO experiments, τ_l is apparently molar mass independent. If τ_l arose from reptational diffusion of the whole chain then it should vary as M^1 within a particular polymer type and should also reflect differences in overall curvilinear diffusion rates between different polymers. The molar mass independence suggests that diffusion around tube bends is governed by the motion of semi-local sections of the chain independent from the whole. This would arise from " stored length " effects illustrated in Fig.6-9. In this case the different τ_l values in PE and PEO may reflect different stored length fractions.

6.4.2 PDMS Data

In contrast with both PE and PEO, the PDMS melts at both 26°C and 150°C show no evidence of a $J_0(2\omega_1)$ plateau, thus clearly demonstrating that τ_R is much larger in this polymer (refer to Fig.6-10 and Fig.6-11). In PDMS and over this frequency regime τ_R is therefore unmeasurable. We may say however that its value must be greater than about 5 x 10^{-16} M^3 s since separation of the lowest molar mass occurs at frequencies lower than 500Hz for all molar masses down to 10372 daltons.

In PDMS a high frequency plateau is clearly visible. τ_s can be found from the height of the plateau and by allowing that $a_1 \approx 1$. By contrast with PE and PEO, and consistent with the notion that the frequency scale is laterally displaced for PDMS, the high frequency crossover at $(a_2\tau_l^{-1}\tau_s^{-2})^{1/3}$ is observed.

The slope of the graph at frequencies below the plateau region is somewhat dependent on a_2, the anisotropy constant, but mostly depends on τ_l. The degree of interdependence is indicated for PE in Fig.6-12. In practice both the position of crossover to the plateau and the slope below the plateau may be used to separately indicate τ_l and a_2. These values are shown in Table 6-II. Reference to Fig.6-5 and Fig.6-6 shows the slope of the graph to be approximately the same at both temperatures of T = 26°C and T = 150°C, the value of a_2 decreasing as the graph shifts downwards along the ordinate axis. In broad terms, as the polymer melt is heated the chain becomes less restrictive and motion is freer.

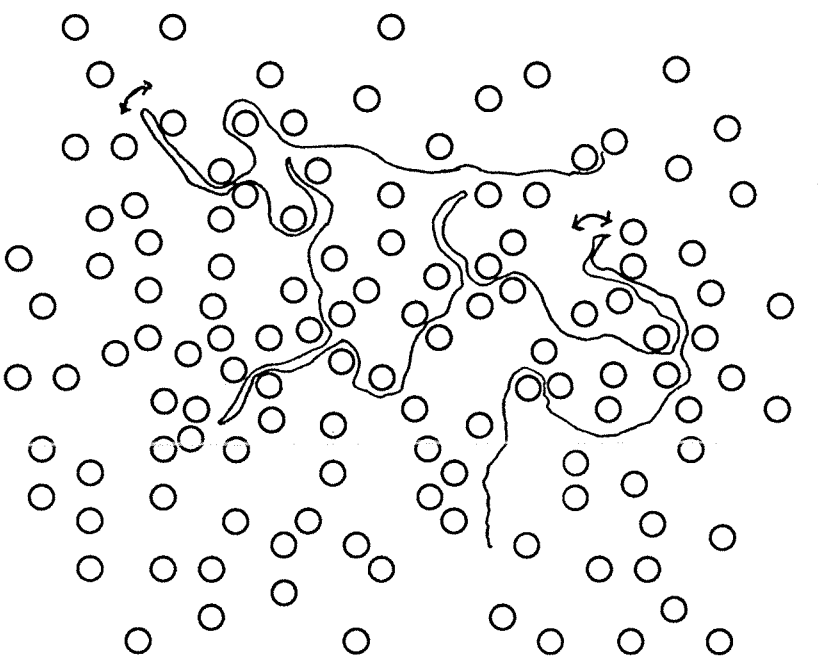

Fig.6-9

Schematic of chain showing " stored lengths "

Fig.6-10 Comparison with theory. PDMS RT = 26C

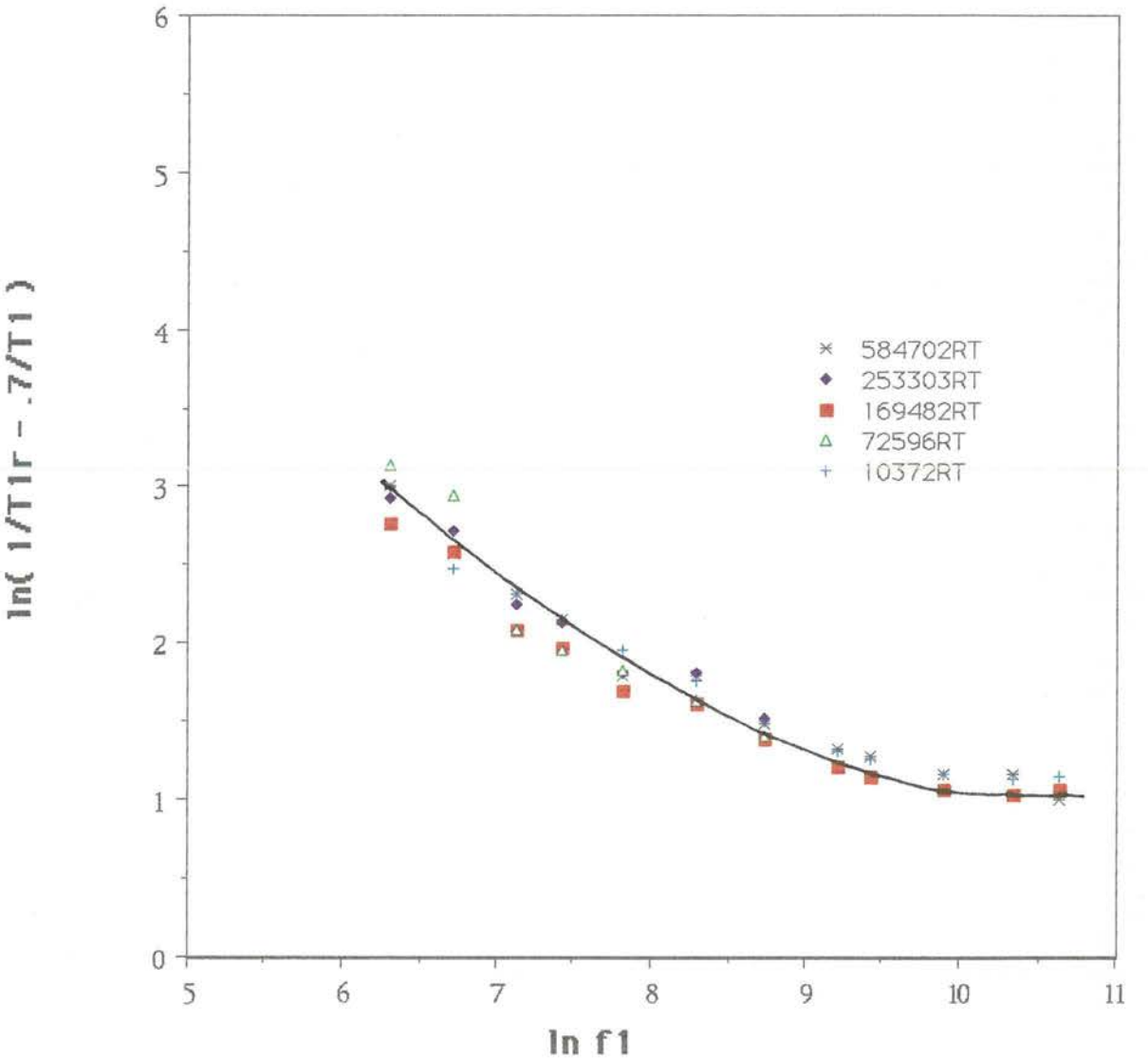

Fig.6-11 Comparison with theory. PDMS T = 150C

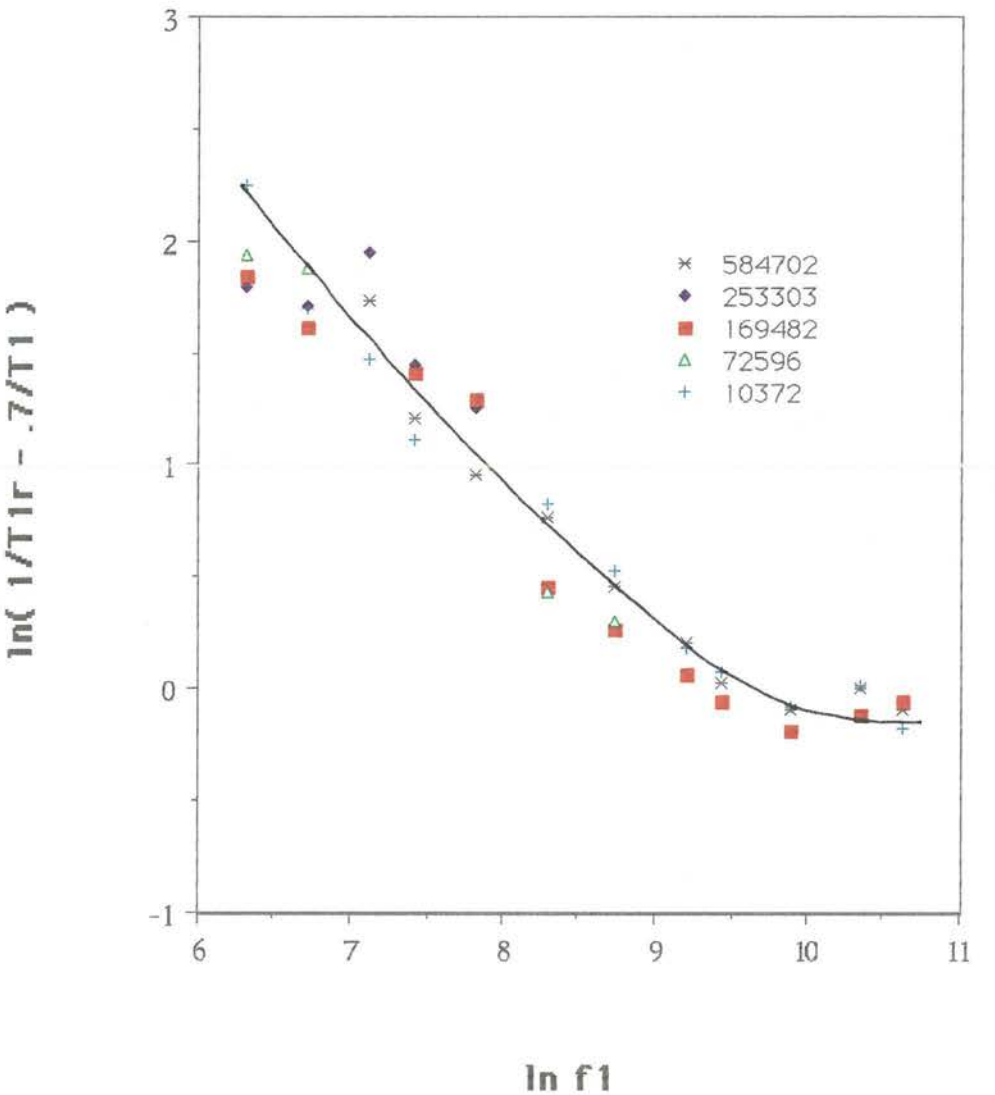

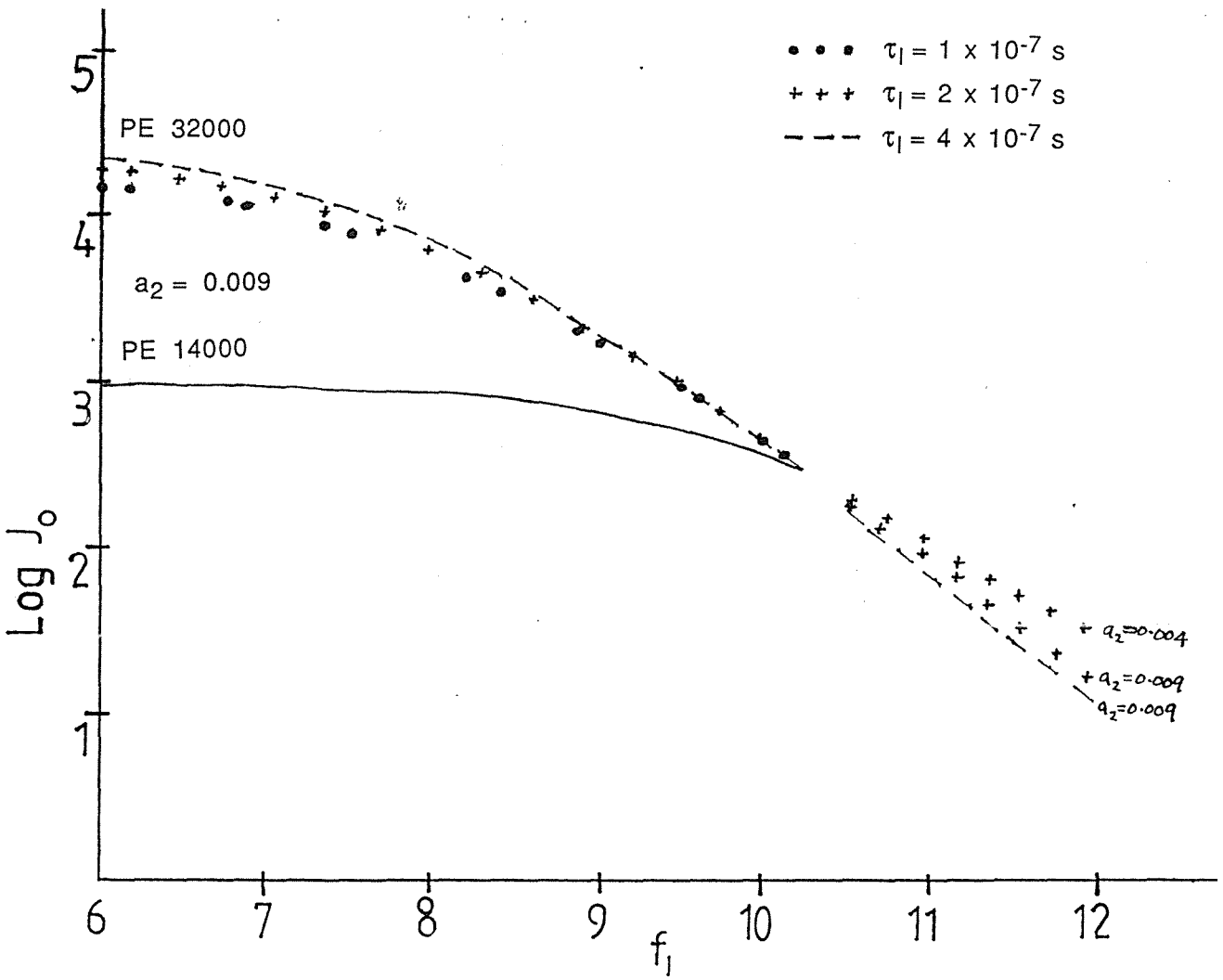

Fig.6-12

Low frequencies: The spacing between PE 32000 and PE 14000 is affected by the value of τ_l as shown for an anisotropy constant of a_2 = 0.009. For a_2 = 0.004 the spacing remains the same.

High frequencies: In contrast with low frequencies, the a_2 value is now seen to affect the slope as shown for a_2 = 0.009 and a_2 = 0.004 with τ_l = 2 x 10^{-7} s. The τ_l value also affects the slope at high frequencies as seen for τ_l = 4 x 10^{-7} s, a_2 = 0.009.

Chapter 7 Conclusion

This mystery has been revealed so that you
may know the interpretation and that you may
understand ... The Book of Daniel 2:30

This thesis has described a study of molecular motion in polymer melts by using NMR relaxation time measurements to probe the spectral densities of fluctuating dipolar interactions between nuclear spins. The theory of polymer melt dynamics was introduced in chapter one together with the relationship between NMR relaxation times and spectral densities.

A major component of this work was the development of new apparatus and software and the extension of the theory of methyl group relaxation to account for the spectral density $J_0(\omega_1)$ which dominates $T_{1\rho}$ dispersions.

$T_{1\rho}$ measurements have been obtained for the two polymer systems polydimethylsiloxane (PDMS) and polyethylene oxide (PEO) and compared with work on polyethylene (PE). The essential conclusion of this work rests with the comparitive time constants shown in Table 6-II.

While the Kimmich model does not give an exact quantitative fit to the data, the broad features of the model are clearly represented. The remaining discrepancies could arise from some of the assumptions in the model. For example, the exponential distance-distribution of the nearest tube bends for the microstructure of the chain is assumed. Also the validity of curvilinear diffusion within a stationary tube is assumed. (That the tube is stationary is problematic as it contradicts the growth and shrinkage of folds).

While a_2, τ_s, and τ_l arise from fits to " indirect features " of the spectral densities, τ_R arises from a " directly " observed spectral feature namely the observation of the crossover frequency, τ_R^{-1}. In both the PE and PEO study the low frequency behaviour is consistent with the de Gennes reptative mechanism for tube renewal since the associated spectral features follow the molar mass scaling law $\tau_R \propto M^3$. This is the first time that the reptation time has ever been measured directly and microscopically in polymer melts. In PDMS the reptational motion is too slow to be observed even at the lowest molar mass employed.

The second significant observation arising from the present study is the independence of τ_l on molar mass in all polymer melts. This is a major new conclusion not previously predicted, but in fact consistent with semi-local motion being governed by stored length effects rather than whole chain motion. In the de Gennes model, chain reptation arises from the propagation of defects in rotational conformations. The " engine " for such motion is the chain segment rotation. Table 6-II shows however that the " chain friction " may differ considerably between polymers as is apparent in the vastly different τ_R but similar τ_s values for PDMS and PEO. A clue to these effects is given by the rotational anisotropy parameter a_2. This varies dramatically between the polymers. First, compare PEO and PE. In PEO a_2 is a factor of five smaller and τ_s is about 20% shorter. It is reasonable to assume that the alternating oxygen atom in PEO permits free rotation by separating CH_2 groups in the same chain. This freer motion may then lead to a more

disordered structure consistent with the lower a_2 value. PEO tube renewal occurs twice as rapidly as in PE. However it is apparent in PDMS, despite segmental anisotropy some two orders of magnitude smaller than in PE, that the reptation is much slower than in either of the other two polymers. We might possibly conclude that the methyl side groups in PDMS cause a much greater friction for lateral motion. This conclusion needs to be verified by some independent study. A suitable method would be the direct measurement of translational diffusion in PE, PEO and PDMS melts via pulsed gradient spin echo (PGSE) NMR.

Appendix A

Spin-1 analysis of Spin-echo using cartesian tensors, the result being:

Spin-echo $90|_x - \tau - 180|_y$: $\mathcal{H} = -\Delta\omega J_z$ refocuses all of Zeeman.

Spin-echo

Consider what happens to J_z under $90|_x$ pulse.

$J_z \rightarrow J_y$. Likewise $J_y \rightarrow J_x$ Hence a basis set consists of I, J_x & J_y.

$$\rho = I + a_x J_x + a_y J_y$$

Now $\dot{\rho} = -i\Delta\omega[\rho, J_z]$

$$\therefore \dot{a}_x = \Delta\omega a_y$$

$$\dot{a}_y = -\Delta\omega a_x$$

$$\therefore a_y(t) = \cos\Delta\omega t.J_y + \sin\Delta\omega t.J_x$$

$$a_x(t) = \cos\Delta\omega t.J_x - \sin\Delta\omega t.J_y$$

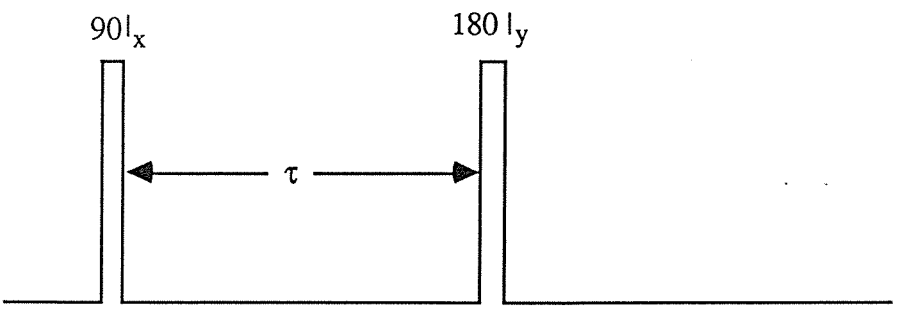

$J_z \rightarrow J_y \rightarrow \cos\Delta\omega t.J_y + \sin\Delta\omega t.J_x$

Fig.A-1

After $180|_y$: $J_x \rightarrow -J_x$
$J_y \rightarrow J_y$

This means that $\cos\Delta\omega t\, J_y + \sin\Delta\omega t\, J_x$ becomes, following $180|_y$

$$\cos\Delta\omega t\,[\,\cos\Delta\omega t\, J_y + \sin\Delta\omega t\, J_x\,] +$$
$$-\ \sin\Delta\omega t\,[\,\cos\Delta\omega t\, J_x - \sin\Delta\omega t\, J_y\,]$$

Taking the average over the inhomogeneous broadening $\Delta\omega$ after a time τ yields

$$\overline{\cos^2\Delta\omega\tau}.J_y + \overline{\sin^2\Delta\omega\tau}.J_y$$
$$= J_y$$

i.e Refocuses all of Zeeman ($\Delta\omega$) at time 2τ from $90|_x$.
Similar analysis applied to a solid-echo results in the following :

Solid-echo $90|_x - \tau - 90|_y$: $\mathcal{H} = \Delta P T_{zz} - \Delta\omega J_z$

refocuses half of Zeeman but all of quadrupole.

$90|_x - \tau - 90|_x$: $\mathcal{H} = \Delta P T_{zz} - \Delta\omega J_z$

refocuses half of Zeeman and none of quadrupole.

Appendix B

This appendix shows in detail the derivation of $J_1(\omega)$ and $J_2(\omega)$ following the procedure given in chapter four.

$$F_1(t) = \frac{e^{i\gamma}}{4r^3}\left[\sin\alpha\,\sin 2\beta + \sqrt{3}\sin\alpha\cos 2\beta - (i/2)\sin 2\alpha\cos 2\beta + \frac{i\sqrt{3}}{2}\sin 2\alpha\sin 2\beta + 2i\sin 2\alpha\right]$$

$$= \phi_1^1(t).1 + \phi_1^2(t).\sin 2\beta + \phi_1^3(t).\cos 2\beta$$

where

$$\phi_1^1(t) = \frac{e^{i\gamma}}{4r^3}(2i\sin 2\alpha) = -\frac{i}{3r^3}\sqrt{\frac{24\pi}{5}}\,Y_2^1(\alpha,\gamma)$$

$$\phi_1^2(t) = \frac{e^{i\gamma}}{4r^3}\left(\sin\alpha + \frac{i\sqrt{3}}{2}\sin 2\alpha\right)$$

$$= -\frac{1}{4r^3}\sqrt{\frac{8\pi}{3}}\,Y_1^1(\alpha,\gamma) - \frac{i}{4r^3}\sqrt{\frac{8\pi}{5}}\,Y_2^1(\alpha,\gamma)$$

$$\phi_1^3(t) = \frac{e^{i\gamma}}{4r^3}\left(\sqrt{3}\sin\alpha - (i/2)\sin 2\alpha\right)$$

$$= -\frac{1}{r^3}\sqrt{\frac{\pi}{2}}\,Y_1^1(\alpha,\gamma) + \frac{i}{12r^3}\sqrt{\frac{24\pi}{5}}\,Y_2^1(\alpha,\gamma)$$

Hence

$$\langle \phi_1^{1*}(t+\tau).\phi_1^1(t)\rangle = -\frac{i}{3r^3}\sqrt{\frac{24\pi}{5}} \times \frac{i}{3r^3}\sqrt{\frac{24\pi}{5}} \times \frac{1}{4\pi} \times e^{-t/\tau_2}$$

$$= \frac{2}{15r^6}e^{-t/\tau_2}$$

$$\langle \phi_1^{2*}(t+\tau).\phi_1^2(t)\rangle = \frac{1}{16r^6}\,\frac{8\pi}{3}\,\frac{e^{-t/\tau_1}}{4\pi} + \frac{1}{16r^6}\,\frac{8\pi}{5}\,\frac{e^{-t/\tau_2}}{4\pi}$$

$$= \frac{1}{24r^6} e^{-t/\tau_1} + \frac{1}{40r^6} e^{-t/\tau_2}$$

Similarly

$$\langle \phi_1^{3*}(t+\tau)\, \phi_1^3(t) \rangle = \frac{1}{8r^6} e^{-t/\tau_1} + \frac{1}{120r^6} e^{-t/\tau_2}$$

Therefore

$$\langle F_1(t).F_1^*(t+\tau) \rangle = \frac{2}{15r^6} e^{-t/\tau_2} + \frac{1}{48r^6} e^{-t/\tau_1'} + \frac{1}{80r^6} e^{-t/\tau_2'}$$

$$+ \frac{1}{16r^6} e^{-t/\tau_1'} + \frac{1}{240r^6} e^{-t/\tau_2'}$$

$$= \frac{1}{60r^6} (8e^{-t/\tau_2} + 5e^{-t/\tau_1'} + e^{-t/\tau_2'})$$

where $\tau_1'^{-1} = \tau_1^{-1} + \tau_c'^{-1}$

This gives the result

$$J_1(\omega) = \frac{1}{30r^6} \left\{ \frac{8\tau_2}{1+\omega^2\tau_2^2} + \frac{5\tau_1'}{1+\omega^2\tau_1'^2} + \frac{\tau_2'}{1+\omega^2\tau_2'^2} \right\} \text{ Q.E.D}$$

In the same way

$$F_2(t) = \frac{e^{2i\gamma}}{2r^3} [i\cos\alpha \sin 2\beta + i\sqrt{3}\cos\alpha\cos 2\beta$$

$$- 1/2(1+\cos^2\alpha)\cos 2\beta - \frac{\sqrt{3}}{2}(1+\cos^2\alpha)\sin 2\beta + 2\sin^2\alpha$$

$$= \phi_2^1(t).1 + \phi_2^2(t).\sin 2\beta + \phi_2^3(t).\cos 2\beta$$

where

$$\phi_2^1(t) = \frac{e^{2i\gamma}}{2r^3}\,(2\sin^2\alpha) = \frac{1}{3r^3}\sqrt{\frac{96\pi}{5}}\,Y_2^2$$

$$\phi_2^2(t) = \frac{i}{2r^3}\sqrt{\frac{14\pi}{15}}\,Y_3^2 + \frac{i}{2r^3}\sqrt{\frac{22\pi}{105}}\,Y_5^2$$

$$-\frac{\sqrt{3}}{4r^3}\sqrt{\frac{24\pi}{5}}\,Y_2^2 - \frac{\sqrt{3}}{4r^3}\sqrt{\frac{8\pi}{5}}\,Y_4^2$$

$$\phi_3^2(t) = \frac{i\sqrt{3}}{2r^3}\sqrt{\frac{14\pi}{15}}\,Y_3^2 + \frac{i\sqrt{3}}{2r^3}\sqrt{\frac{22\pi}{105}}\,Y_5^2$$

$$-\frac{1}{4r^3}\sqrt{\frac{24\pi}{5}}\,Y_2^2 - \frac{1}{4r^3}\sqrt{\frac{8\pi}{5}}\,Y_4^2$$

yielding

$$J_2(\omega) = \frac{1}{30r^6}\left\{\frac{32\tau_2}{1+\omega^2\tau_2^2} + \frac{9\tau'_2}{1+\omega^2\tau'^2_2} + \frac{7\tau'_3}{1+\omega^2\tau'^2_3}\right.$$

$$\left. + \frac{3\tau'_4}{1+\omega^2\tau'^2_4} + \frac{11}{7}\,\frac{\tau'_5}{1+\omega^2\tau'^2_5}\right\}$$

Appendix C

The exact expression arising from Eq.(4.52) is given below from Kimmich[4].

$$J_0(2\omega_1) = \sum_{j=o}^{1} 2A^{0,j} \frac{\delta_j + 2a\, b_{0,j} \cos\phi_{0,j}}{b_{0,j}^4 + 4a^2 b_{0,j}^2 + 4a\, b_{0,j} (\delta_j \cos\phi_{0,j} + 2\omega_1 \sin\phi_{0,j})}$$

$$J_1(\omega_0) = \sum_{j=o}^{1} 2A^{1,j} \frac{\delta_j + 2a\, b_{1,j} \cos\phi_{1,j}}{b_{1,j}^4 + 4a^2 b_{1,j}^2 + 4a\, b_{1,j} (\delta_j \cos\phi_{1,j} + \omega_0 \sin\phi_{1,j})}$$

$$J_2(2\omega_0) = \sum_{j=o}^{1} 2A^{2,j} \frac{\delta_j + 2a\, b_{2,j} \cos\phi_{2,j}}{b_{2,j}^4 + 4a^2 b_{2,j}^2 + 4a\, b_{2,j} (\delta_j \cos\phi_{2,j} + 2\omega_0 \sin\phi_{2,j})}$$

$J_1(\omega_0)$ and $J_2(2\omega_0)$ are both negligible at frequencies of ω_1.

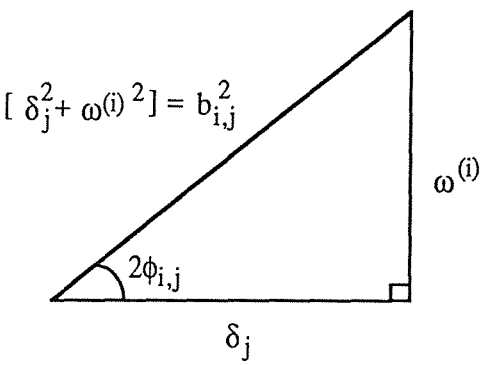

Fig.C-1

From Fig.C-1 it can be seen that

$$\cos\phi_{i,j} = \frac{1}{\sqrt{2}} \left(1 + \cos 2\phi_{i,j} \right)^{1/2}$$

$$\sin\phi_{i,j} = \frac{1}{\sqrt{2}} \left(1 - \cos 2\phi_{i,j} \right)^{1/2}$$

hence

$$\cos\phi_{i,j} = \frac{1}{\sqrt{2}} \left[1 + \left(1 + \omega(i)^2 \tau_j^2 \right)^{-1/2} \right]^{1/2}$$

$$\sin\phi_{i,j} = \frac{1}{\sqrt{2}} \left[1 - \left(1 + \omega(i)^2 \tau_j^2 \right)^{-1/2} \right]^{1/2}$$

For example,

$$\cos\phi_{0,0} = \frac{1}{\sqrt{2}} \left[1 + \left(1 + 4\omega_1^2 \tau_r^2 \right)^{-1/2} \right]^{1/2}$$

$$\sin\phi_{0,0} = \frac{1}{\sqrt{2}} \left[1 - \left(1 + 4\omega_1^2 \tau_r^2 \right)^{-1/2} \right]^{1/2}$$

$$\cos\phi_{0,1} = \frac{1}{\sqrt{2}} \left[1 + \left(1 + 4\omega_1^2 \tau_s^2 \right)^{-1/2} \right]^{1/2}$$

$$\sin\phi_{0,1} = \frac{1}{\sqrt{2}} \left[1 - \left(1 + 4\omega_1^2 \tau_s^2 \right)^{-1/2} \right]^{1/2}$$

Also

$$\delta_0 = \tau_r^{-1}$$

$$\delta_1 = \tau_s^{-1}$$

$$2a = \left(2\tau_1 \right)^{-1/2}$$

$$b_{0,0} = \tau_r^{-1/2} \left(1 + 4\omega_1^2 \tau_r^2 \right)^{1/4}$$

$$b_{0,1} = \tau_s^{-1/2} \left(1 + 4\omega_1^2 \tau_s^2 \right)^{1/4}$$

Similarly for $J_1(\omega_0)$ and $J_2(2\omega_0)$.

Inserting the above expressions into the Kimmich equation for $J_0(2\omega_1)$ yields the various limiting cases. For example,

(1) $j = 1,\ \omega_1\tau_r >> 1,\ \omega_1\tau_s << 1$

$$J_0(2\omega_1) \approx 2A^{0,1}\,\frac{\tau_s^{-1} + (2\tau_1)^{-1/2}\tau_s^{-1/2}}{\tau_s^{-2} + (2\tau_1)^{-1}\tau_s^{-1} + 2(2\tau_1)^{-1/2}\tau_s^{-1/2}\,\tau_s^{-1}}$$

$$= 2A^{0,1}\,\tau_s \quad \text{since } \tau_1 >> \tau_s$$

This term is minor provided the frequency is sufficiently low. In this manner the limiting cases of section 4.5 are produced.

Appendix D

The spectral densities of Eq.(3.55) reduce to a particularly simple form for isotropic rotational diffusion[26], namely,

$$J_0(\omega) = r^{-6}(24/15)\tau_c/(1+\omega^2\tau_c^2)$$

$$J_1(\omega) = r^{-6}(4/15)\tau_c/(1+\omega^2\tau_c^2)$$

$$J_2(\omega) = r^{-6}(16/15)\tau_c/(1+\omega^2\tau_c^2)$$

where τ_c is the rotational correlation time. Under extreme narrowing $\omega << \tau_c^{-1}$ and the high frequency, the J_1 and J_2 components of $T_{1\rho}^{-1}$ (Eq.3.55) become

$$(5/2)J_1 + (1/4)J_2 = r^{-6}(5/2)(4/15)\tau_c + r^{-6}(1/4)(16/15)\tau_c$$

$$= r^{-6}(14/15)\tau_c$$

The J_1 and J_2 component of T_1^{-1} is given by

$$J_1 + J_2 = r^{-6}(4/3)\tau_c$$

Thus the J_1 and J_2 component of $T_{1\rho}^{-1}$ is given by $0.7T_1^{-1}$ under extreme narrowing conditions and high frequencies. This relationship is useful when extracting the $J_0(2\omega_1)$ spectral density function from $T_{1\rho}$ measurements.

Appendix E

This appendix gives the program listings for the additional software and modifications made to existing Imaging software[41] in order to measure $T_{1\rho}$.

ASCII addresses

```
7000  004C  LDA   ( 704D )      ;L
7001  0045  LDA   ( 7047 )      ;E
7002  0056  LDA   ( 7059 )      ;V
7003  0045  LDA   ( 7049 )      ;E
7004  004C  LDA   ( 7051 )      ;L
7005  0020  LDA   ( 7026 )      ;" "
7006  0020  LDA   ( 7027 )      ;" "
7007  0054  LDA   ( 705C )      ;T
7008  0049  LDA   ( 7052 )      ;I
7009  004D  LDA   ( 7057 )      ;M
700A  0045  LDA   ( 7050 )      ;E
700B  0020  LDA   ( 702C )      ;" "
700C  0055  LDA   ( 7062 )      ;u
700D  0053  LDA   ( 7061 )      ;s
```

Display " TIME us "

```
700E  0000  LDA   ( 700F )
700F  B8OO  DATA
7010  C504  RMO   A,S           ;x coordinate = -7000
7011  1800  LDM   ( 7012 )
7012  6500  DATA                ;y coordinate = 6000
7013  1700  LDX   0             ;Initialise list counter ( Characters to be displayed )
7014  9129  STX   ( (B) + 29 )
7015  02F1  LDA   ( 7007 + (X) )
7016  DA26  WDS   206
7017  0004  DATA  S             ;Set x coordinate
7018  DA27  WDS   207
7019  0003  DATA  M             ;Set y coordinate
701A  0F02  LDE   2
701B  892A  STE   ( (B) + 2A )  ;Set number of times to be displayed
701C  DC39  WDS   419           ;Display character
701E  78FD  BRU   701C
701F  1000  LDX   ( 7020 )
7020  FFA0  DATA
7021  40FF  BIX   7021          ;Wait while character is being displayed
7022  492A  DMT   ( (B) + 2A )  ;Have we displayed the character twice?
7023  78F8  BRU   701C          ;If not then redisplay
7024  0000  LDA   ( 7025 )
7025  0700  DATA
7026  C084  RAD   A,S           ;Increment the x coordinate by 1800
7027  1129  LDX   ( (B) + 29)   ;Restore list counter
7028  C322  RIN   X,X           ;Increment list counter
7029  C520  RMO   X,A           ;Have all the characters been displayed?
702B  CD20  SEQ
702C  78E7  BRU   7014
702D  7C00  BRU   ( 702E )
702E  7DC0  DATA
```

Display " LEVEL "

```
7030  0000  LDA   ( 7031 )
7031  9000  DATA
7032  C504  RMO   A,S          ;x coordinate
7033  1800  LDM   ( 7034 )
7034  6000  DATA               ;y coordinate
7035  0701  LDA   1
7036  8126  STA   ( (B) + 26 ) ;MCF = 1
7037  1700  LDX   0            ;( Characters to be displayed )
7038  9129  STX   ( (B) + 29 )
7039  02C6  LDA   ( 7000 + (X) )
703A  DA26  WDS   206
703B  0004  DATA  S            ;Set x position
703C  DA27  WDS   207
703D  0003  DATA  M            ;Set y position
703E  0F02  LDE   2            " Display counter " = 4
703F  892A  STE   ( (B) + 2A ) ;Number of times character is to be displayed
7040  DC39  WDS   419
7041  0080  DATA  A            ;Display character
7042  78FD  BRU   7040
7043  1000  LDX   ( 7044 )
7044  FFA0  DATA
7045  40FF  BIX   7045         ;Wait for 80µs to allow for display
7046  492A  DMT   ( (B) + 2A ) ;Have we displayed the character twice?
7047  78F8  BRU   7040         ;If not then redisplay
7048  0000  LDA   ( 7049 )
7049  0700  DATA
704A  CO84  RAD   A,S
704B  1129  LDX   ( (B) + 29 ) ;Reset display counter
704C  C322  RIN   X,X          ;Increment character pointer
704D  C520  RMO   X,A
704E  6707  CPL   7            ;Have all characters been displayed?
704F  CD20  SEQ
7050  78E7  BRU   7038
7051  1800  LDM   ( 7052 )
7052  4000  DATA               ;y = 4000
7053  0000  LDA   ( 7054 )
7054  9000  DATA
7055  C504  RMO   A,S          ;x = -7000
7056  0811  LDE   ( 7068 )     ;Memory ( Level )
7057  7400  BRL   ( 7058 )     ;Branch to three digit display
7058  7E59  DATA
7059  DC18  RDS   418
705A  0000  DATA  A
705B  DB0F  TABZ  F            ;Test for lightpen hit
705C  7801  BRU   705E         ;Branch to 705E if test positive
705D  7807  BRU   7066
705E  0122  LDA   ( (B) + 22 )
705F  C8C4  LLA   4
7060  C844  LRA   4
7061  0800  LDE   ( 7062 )
7062  0255  DATA               ;Maximum allowed
7063  C401  RCA   A,E
7064  CD40  SGT
7065  8002  STA   ( 7068 )
7066  7C00  BRU   ( 7067 )
7067  7DCC  DATA
7068  0205  LDA   ( 706E + (X) ) ;Level store
```

Run processing

1. Calculate N_T first
2. Get Level; convert to hex. and store

```
7070  7E14    BRU  (7085)+(X)
7071  C560    RMO  B,A
7072  80FD    STA  (7070)
7073  1700    LDX  0
7074  0000    LDA  (7075)
7075  7DD8    DATA
7076  C506    RMO  A,B
7077  B300    DLD  ((B)+(X)+0)
7078  C322    RIN  X,X
7079  C322    RIN  X,X
707A  C490    ROR  E,A
707B  CC80    SNZ
707C  7801    BRU  707E
707D  78F9    BRU  7077
707E  C520    RMO  X,A
707F  C841    LRA  1
7080  8400    STA  ((7081))
7081  3200    DATA
7082  00ED    LDA  (7070)
7083  C506    RMO  A,B
7084  0400    LDA  ((7085))
7085  7068    DATA
7086  C848    LRA  8
7087  9800    MPY  (7088)
7088  0064    DATA
7089  C512    RMO  E,X
708A  0400    LDA  ((708B))
708B  7068    DATA
708C  C8C8    LLA  8
708D  C84C    LRA  C
708E  9F0A    MPY  A
708F  C092    RAD  E,X
7090  0400    LDA  ((7091))
7091  7068    DATA
7092  C8CC    LLA  C
7093  C84C    LRA  C
7094  C082    RAD  A,X
7095  C520    RMO  X,A
7096  2000    ADD  (7097)
7097  0000    DATA
7098  8400    STA  ((7099))
7099  311A    DATA
709A  7809    BRU  70A4
```

Initialise variables

```
7D00  0700    LDA  0
7D01  C508    RMO  A,ST          ;Clear status register
7D02  0000    LDA  (7D03)
7D03  7E14    DATA
7D04  C506    RMO  A,B           ;Set base register to point to data list
7D05  0F00    LDE  0
7D06  C512    RMO  E,X
7D07  8B1B    STE  ((B)+(X)+1B)
7D08  C322    RIN  X,X
7D09  C520    RMO  X,A
7D0A  6F14    CPA  14
7D0B  CD20    SEQ
7D0C  78FA    BRU  7D07          ;Clear variable space 7E2F to 7E42
7D0D  7C00    BRU  (7D0E)
7D0E  7F25    DATA               ;Branch to 7F25: Set " Mask " and " Keypad buffer pointer
7D0F  0000    LDA  (7D10)
7D10  7DD8    DATA
7D11  8123    STA  ((B)+23)      ;Starting address of time store ( " Address memory 1 " )
7D12  1800    LDM  (7D13)
7D13  6000    DATA               ;( M ) = " y coordinate " = 6000
7D14  0000    LDA  (7D15)
7D15  1800    DATA
7D16  C505    RMO  A,L           ;( L ) = " Delta " = 1800 ( Offset between characters in same row )
7D17  1700    LDX  0             ;Set character pointer to zero
7D18  077F    LDA  7F
7D19  DC38    WDS  418
7D1A  0000    DATA A             ;Reset display characters
7D1B  0786    LDA  86
7D1C  DC38    WDS  418
7D1D  0000    DATA A             ;Set parameters to display large not bright characters
```

Display keypad and test for lightpen hit

```
7D1E  0000    LDA  (7D1F)
7D1F  2000    DATA
7D20  C504    RMO  A,S           ;( S ) = " x coordinate " = 2000
7D21  0704    LDA  4
7D22  8128    STA  ((B)+28)      ;" Horizontal loop counter " = 4   ( Number of columns on the keypad )
7D23  9129    STX  ((B)+29)      ;Save the character pointer
7D24  DA26    WDS  206
7D25  0004    DATA S             ;Set x position
7D26  DA27    WDS  207
7D27  0003    DATA M             ;Set y position
7D28  0704    LDA  4
7D29  812A    STA  ((B)+2A)      ;" Display counter " = 4   ( Number of times character is to be displayed )
7D2A  0300    LDA  ((B)+(X)+0    ;Load character to be displayed
7D2B  DC39    WDS  419
7D2C  0080    DATA A             ;Display character
7D2D  78FD    BRU  7D2B
7D2E  1000    LDX  (7D2F)
7D2F  FFC0    DATA
7D30  40FF    BIX  7D30          ;Wait for 80µs to allow for display
7D31  492A    DMT  ((B)+2A)      ;Have we displayed the character twice?
7D32  78F8    BRU  7D2B          ;If not the redisplay
7D33  1129    LDX  ((B)+29)      ;Reset display counter
7D34  DC18    RDS  418
7D35  0004    DATA A
7D36  DB0F    TABZ  F            ;Test for lightpen hit
7D37  7828    BRU  7D60          ;Lightpen hit positive so branch to lightpen routine
7D38  C0D4    RAD  L,S           ;Increment character x coordinate by delta
```

```
7D39  C322      RIN   X,X          ;Increment character pointer
7D3A  4928      DMT   ((B)+28)     ;Decrement horizontal loop counter and test for zero
7D3B  78E7      BRU   7D23         ;If not zero branch to 7D23 and display next row
7D3C  C520      RMO   X,A          ;What stage have we reached in the display procedure?
7D3D  6F14      CPA   14           ;Ready to display keypad buffer?
7D3E  CDA0      SNE                ;No, so branch to 7D40
7D3F  7805      BRU   7D45         ;Branch to 7D45 and display keypad buffer
7D40  6F10      CPA   10           ;Ready to display command line?
7D41  CDA0      SNE                ;No, so branch to 7D43
7D42  C053      RSU   L,M          ;Move down two lines at end of keypad
7D43  C053      RSU   L,M          ;Move down one line at end of row
7D44  78D9      BRU   7D1E         ;Branch to start of display routine
```

Display keypad buffer

```
7D45  077F      LDA   7F
7D46  DC38      WDS   418
7D47  0000      DATA  A            ;Reset display
7D48  0785      LDA   85
7D49  DC38      WDS   418          ;Set parameters to display small not bright characters
7D4A  0000      DATA  A
7D4B  0000      LDA   (7D4C)
7D4C  2000      DATA               ;" x coordinate " = 2000
7D4D  C504      RMO   A,S
7D4E  1800      LDM   (7D4F)
7D4F  9000      DATA               ;" y coordinate = -7000
7D50  B121      DLD   ((B)+21)
7D51  702D      BRL   7D7F         ;Display keypad buffer
7D52  0125      LDA   ((B)+25)     ;Load accumulator with monitor mode
```

```
7D53  6F10      CPA   10           ;Test mode
7D54  CDA0      SNE
7D55  7966      BRU   (B)+66       ;Run mode ( " R " ) selected. ( Branch to 7E7A )
7D56  6F11      CPA   11
7D57  CDA0      SNE
7D58  7810      BRU   7D69         ;Level mode ( " L " ) selected
7D59  6F12      CPA   12
7D5A  CDA0      SNE
7D5B  783C      BRU   7D98         ;Time mode ( " T " ). Branch to 7D98
7D5C  6F13      CPA   13
7D5D  CDA0      SNE
7D5E  7943      BRU   (B)+43
7D5F  78B2      BRU   7D12         ;Return to monitor ( " M " )
```

Lightpen hit detected

```
7D60  912E      STX   ((B)+2E)     ;Character pointer to selected digit
7D61  C520      RMO   X,A
7D62  6F0F      CPA   F            ;Is the character selected a hex. digit?
7D63  CD80      SGE                ;Yes, so skip next instruction
7D64  7815      BRU   7D7A         ;No, so branch to ' Modify mode ' routine
```

Store selected character in keypad buffer

```
7D65  012B    LDA   ((B)+2B)  ;Keypad buffer pointer to
7D66  812C    STA   ((B)+2C)  ;      keypad buffer counter
7D67  7C00    BRU   (7D68)
7D68  7F30    DATA            ;Branch to selected character routine at 7F30
7D69  7C00    BRU   (7D6A)
7D6A  7030    DATA            ;To Level display

7D7A  7930    BRU   (B)+30    ;To modify mode routine from 7D64

7D7D  7894    BRU   7D12      ;From 7DCE
```

Display six nibble hex. digit in A,E register at coordinates (S,M)

```
7D7F  7C00    BRU   (7D80)
7D80  7F01    DATA            ;Branch to 7F01
7D81  7C00    BRU   (7D82)
7D82  7F08    DATA
7D84  DA26    WDS   206
7D85  0004    DATA  S         ;Set x coordinate of character
7D86  DA27    WDS   207
7D87  0003    DATA  M         ;Set y coordinate of character
7D88  0702    LDA   2
7D89  812A    STA   ((B)+2A)  ;Set number of times displayed to two
7D8A  0300    LDA   ((B)+(X)+0) ;Obtain ASCII code for character to be displayed
7D8B  DC39    WDS   419
7D8C  0080    DATA  A
7D8D  78FD    BRU   7D8B      ;Display character
7D8E  1000    LDX   (7D8F)
7D8F  FFA0    DATA
7D90  40FF    BIX   7D90      ;NOP for 120µs. Time to display character
7D91  492A    DMT   ((B)+2A)  ;Have we displayed the character twice?
7D92  78F8    BRU   7D8B      ;If not then redisplay
7D93  00F4    LDA   (7D88)    ;Increment x coordinate by 0700
7D94  C084    RAD   A,S
7D95  4928    DMT   ((B)+28)  ;Decrement digit counter
7D96  78EA    BRU   7D81      ;Display next digit if not finished
7D97  C557    RMO   L,PC      ;Return to calling program
```

Time mode selected

```
7D98  0126    LDA   ((B)+26)  ;Load ' mode change flag '
7D99  CC00    SZE             ;Skip if zero
7D9A  782B    BRU   7DC6      ;Branch to zero if mode has already been changed
7D9B  0000    LDA   (7D9C)
7D9C  9000    DATA
7D9D  C504    RMO   A,S       ;x coordinate = -7000
7D9E  1800    LDM   (7D9F)
7D9F  5000    DATA            ;y coordinate = 500
7DA0  0701    LDA   1
7DA1  8126    STA   ((B)+26)  ;Mode change flag = 1
7DA2  0706    LDA   6         ;Initialise ' time ' counter to six
7DA3  8129    STA   ((B)+29)  ;  ( Number of time locations to be displayed )
7DA4  0123    LDA   ((B)+23)  ;Load memory address to be displayed
7DA5  2702    ADD   2
7DA6  C501    RMO   A,E
7DA7  7C00    BRU   (7DA8)      branch to 7F55 ( Hex. to Decimal conversion )
7DA8  7F55    DATA
```

```
7DA9   702D     BRL   7DD7          ;Branch and link into three digit routine
7DAA   00F3     LDA   (7D9E)
7DAB   C084     RAD   A,S           ;X coordinate of data = 1800
7DAC   B523     DLD   (((B)+23))    ;Load contents of memory address
7DAD   70D1     BRL   7D7F          ;into A,E register and display
7DAE   DC18     RDS   418
7DAF   0000     DATA  A
7DB0   DB0F     TABZ  F             ;Test for lightpen hit
7DB1   7810     BRU   7DC2          ;Branch to 7DC2 if test positive
7DB2   00EB     LDA   (7D9E)
7DB3   C003     RSU   A,M           ;Decrement y coordinate by 1800 ( next time down )
7DB4   0000     LDA   (7DB5)
7DB5   9000     DATA
7DB6   C504     RMO   A,S           ;X coordinate = -7000 ( restore x coordinate of address )
7DB7   5123     IMO   ((B)+23)
7DB8   5123     IMO   ((B)+23)      ;Increment memory address one by two
7DB9   4929     DMT   ((B)+29)      ;Decrement list counter and test for zero
7DBA   78E9     BRU   7DA4          ;If not finished branch to 7DA4
7DBB   0123     LDA   ((B)+23)
7DBC   2F0C     SUB   C
7DBD   8123     STA   ((B)+23)      ;Restore memory address one
7DBE   7C00     BRU   (7DBF)        ;Display time ( µs ) then branch to 7DCC
7DBF   700E     DATA
7DC0   780B     BRU   7DCC
7DC1   78E8     BRU   7DAA
```

Time routine - Lightpen hit on data

```
7DC2   B121     DLD   ((B)+21)      ;Transfer contents of keypad buffer
7DC3   A523     DST   (((B)+23))    ;to address pointed to by ' memory address one '
7DC4   700A     BRL   7DCF          ;Reset mask and buffer pointer
7DC5   78EC     BRU   7DB2          ;Branch back to program
```

Scroll time display

```
7DC6   0127     LDA   ((B)+27)      ;Load mode flag
7DC7   CC80     SNZ
7DC8   78D2     BRU   7D9B          ;If this is the first pass branch to 7D9B
7DC9   0123     LDA   ((B)+23)
7DCA   270C     ADD   C             ;Increment memory address one by C
7DCB   8123     STA   ((B)+23)
7DCC   0700     LDA   0
7DCD   8127     STA   ((B)+27)      ;Reset current mode flag
7DCE   78AE     BRU   7D7D          ;Branch to start of program
```

Reset keypad buffer and mask

```
7DCF   0706     LDA   6
7DD0   812B     STA   ((B)+2B)      ;Set buffer pointer = 6
7DD1   0000     LDA   (7DD2)
7DD2   FF0F     DATA
7DD3   0800     LDE   (7DD4)        ;Set mask = FF0F FFFF
7DD4   FFFF     DATA
7DD5   A11F     DST   ((B)+1F)
7DD6   C557     RMO   L,PC          ;Return to calling program
7DD7   7945     BRU   (B)+45        ;From 7DA9
```

Modify mode routine

```
7E44  6925    CPA  ((B)+25)  ;Compare selected mode with current mode
7E45  CDA0    SNE             ;Skip instruction if a different mode is required
7E46  7802    BRU  7E49       ;Mode is the same
7E47  0700    LDA  0
7E48  8126    STA  ((B)+26)   ;Mode change flag = 0
7E49  0701    LDA  1
7E4A  8127    STA  ((B)+27)   ;This mode is now current
7E4B  9125    STX  ((B)+25)   ;Save monitor mode
7E4C  7881    BRU  7DCE       ;Branch to start of program


7E57  7C00    BRU  (7E58)     ;Return to monitor
7E58  3E00    DATA
```

Display three nibble hex. digit in E register at coordinates (S,M)

```
7E59  C510    RMO  E,A
7E5A  C8C4    LLA  4
7E5B  C501    RMO  A,E
7E5C  0703    LDA  3
7E5D  8128    STA  ((B)+28)   ;Initialise digit counter to three
7E5E  0700    LDA  0          ;Set ( A ) = 0 and shift ( A,E ) left one byte
7E5F  C8E4    LLD  4          ;Byte to be displayed ends up in A register
7E60  C502    RMO  A,X        ;Store byte to be displayed in X register
7E61  DA26    WDS  206
7E62  0004    DATA S          ;Set x coordinate
7E63  DA27    WDS  207
7E64  0003    DATA M          ;Set y coordinate
7E65  0702    LDA  2
7E66  812A    STA  ((B)+2A)   ;Set number of times displayed to two
7E67  0300    LDA  ((B)+(X)+0) ;Obtain ASCII code for character to be displayed
7E68  DC39    WDS  419
7E69  0080    DATA A
7E6A  78FD    BRU  7E68       ;Display character
7E6B  1000    LDX  (7E6C)
7E6C  FFA0    DATA
7E6D  40FF    BIX  7E6D       ;NOP for 120µs. Time for character to be drawn
7E6E  492A    DMT  ((B)+2A)   ;Have we displayed the character twice?
7E6F  78F8    BRU  7E68       ;If not then redisplay
7E70  00ED    LDA  (7E5E)
7E71  C084    RAD  A,S        ;Increment x coordinate by 0700
7E72  4928    DMT  ((B)+28)   ;Decrement digit counter
7E73  78EA    BRU  7E5E       ;Display next digit if not finished
7E74  C557    RMO  L,PC       ;Return to calling program


7E78  7400    BRL  (7E79)
7E79  3E7F    DATA
7E7A  7C00    BRU  (7E7B)     ;Go to ' Run processing '
7E7B  7071    DATA
7E7C  0000    LDA  (7E7D)
7E7D  DB0F    DATA
7E7E  797B    BRU  (B)+7B
7E7F  C322    RIN  X,X
```

Subroutine to add in decimal (A,E) to (M,S)
Only the last six hex. digits are added
and the first two digits are preserved

```
7E80  0000    LDA   (7E81)        ;DATA   A     Buffer 1
7E81  0000    DATA                ;DATA   E     Buffer 2
7E82  0013    LDA   (7E96)        ;DATA   X
7E83  0049    LDA   (7ECD)        ;DATA   M     Buffer 3
7E84  0100    LDA   ((B)+0)       ;DATA   S     Buffer 4
7E85  70CB    BRL   7E51          ;DATA   L     Link
7E86  7DFE    BRU   ((B)+FE)      ;DATA   B
7E87  0049    LDA   (7ED1)        ;DATA         Buffer 5
7E88  0100    LDA   ((B)+0)       ;DATA         Buffer 6
7E89  0000    LDA   (7E8A)        ;DATA         Digit counter
7E8A  D8E0    DATA                ;SRF at 7E80
7E8B  7E80    BRU   (7E0C)+(X)    ;Initialise
7E8C  0800    LDE   (7E8D)
7E8D  FF00    DATA  ~             ;Mask
7E8E  C690    RAN   E,A
7E8F  0F00    LDE   0
7E90  A0F6    DST   (7E87)        ;Buffer 5,6 = ( A1A200,0000 )
7E91  0706    LDA   6
7E92  80F6    STA   (7E89)        ;Digit counter = 6
7E93  1700    LDX   0                                   digit conversion
7E94  B0EB    DLD   (7E80)        ;Buffer 1,2
7E95  C8FC    LLD   1C
7E96  C87C    LRD   1C
7E97  C513    RMO   E,M           ;( M ) = 000X1
7E98  B0EA    DLD   (7E83)        ;Buffer 3,4
7E99  C8FC    LLD   1C
7E9A  C87C    LRD   1C
7E9B  701E    BRL   7EBA          ;To addition
7E9C  0700    LDA   0             ;( A,E ) = ( 0000,000( X1 + X2 )10 )
7E9D  C8E0    LLD   0             ;Place digit in correct location
7E9E  C503    RMO   A,M
7E9F  C514    RMO   E,S
7EA0  B0E6    DLD   (7E87)        ;Buffer 5,6
7EA1  C0B0    RAD   M,A
7EA2  C0C1    RAD   S,E
7EA3  A0E3    DST   (7E87)        ;Buffer 5,6
7EA4  48E4    DMT   (7E89)        ;Digit counter
7EA5  7801    BRU   7EA7          ;Branch to finish
7EA6  7808    BRU   7EAF                    Other digit conversion
7EA7  00ED    LDA   (7E95)
7EA8  2F04    SUB   4             ;Change instruction
7EA9  80EB    STA   (7E95)
7EAA  80EE    STA   (7E99)
7EAB  00F1    LDA   (7E9D)
7EAC  2704    ADD   4
7EAD  80EF    STA   (7E9D)        ;To digit conversion
7EAE  78E5    BRU   7E94
7EAF  0000    LDA   (7EB0)                          Finish
7EB0  C8FC    DATA                ;A = " LLD 28 "
7EB1  80E3    STA   (7E95)
7EB2  80E6    STA   (7E99)        ;Restored to LLD 28
7EB3  0000    LDA   (7EB4)
7EB4  C8E0    DATA                ; LLD 0 "
7EB5  80E7    STA   (7E9D)
7EB6  D8A0    LRF   (7EB7)
7EB7  7E80    DATA
7EB8  B0CE    DLD   (7E87)        ;Buffer 5,6
7EB9  C557    RMO   L,PC
```

Data storage

Addition routine

```
7EBA  C0B1    RAD   M,E
7EBB  C0A1    RAD   X,E
7EBC  C510    RMO   E,A
7EBD  6F0A    CPA   A
7EBE  CDC0    SLE                ;Skip if 10 LTE ( A )
7EBF  7804    BRU   7EC4
7EC0  1701    LDX   1            ;If sum GTE 10 then carry 1
7EC1  2F0A    SUB   A            ;and subtract 10
7EC2  C501    RMO   A,E          ;Return with digit in LSB of E register
7EC3  C557    RMO   L,PC
7EC4  1700    LDX   0
7EC5  C501    RMO   A,E
7EC6  C557    RMO   L,PC         ;Return with digit in LSB of E register
```

Display six nibble hex. digit in A,E register at coordinates (S,M)

```
7F01  C8E8    LLD   8    ;00A1A2 / E1E2E3E4 to A1A2E1E2 / E3E400
7F02  8400    STA   ((7F03))
7F03  7FFE    DATA             ;( 7FF0 ) = A1A2E1E2
7F04  8C00    STE   ((7F05))
7F05  7FFF    DATA             ;( 7FF1 ) = E3E400
7F06  0706    LDA   6
7F07  8128    STA   ((B)+28)   ;Initialise digit counter to six
7F08  0700    LDA   0
7F09  0C00    LDE   ((7F0A))   ;( A,E ) = 0000, A1A2E1E2
7F0A  7FFE    DATA
7F0B  C8E4    LLD   4          ;( A,E ) = 000A1, A2E1E20
7F0C  C502    RMO   A,X        ;( X ) = 000A1
7F0D  C510    RMO   E,A        ;( A ) = A2E1E20
7F0E  C844    LRA   4          ;( A ) = 0A2E1E2
7F0F  0C00    LDE   ((7F10))
7F10  7FFF    DATA             ;( A,E ) = 0A2E1E2, E3E400
7F11  C8E4    LLD   4          ;( A,E ) = A2E1E2E3, E4000
7F12  8400    STA   ((7F13))
7F13  7FFE    DATA             ;( 7FF0 ) = A2E1E2E3
7F14  8C00    STE   ((7F15))
7F15  7FFF    DATA             ;( 7FF1 ) = E4000
7F16  7C00    BRU   (7F17)
7F17  7D84    DATA             ;Back to write character
```

Modification to store selected character

1. Change mask

```
7F25  B000    DLD   (7F26)  ;DLD Mask
7F26  FF0F    DATA
7F27  FFFF    CLC           ;" Mask " = FF0F FFFF
7F28  A11F    DST   ((B)+1F)
7F29  0706    LDA   6
7F2A  812B    STA   ((B)+2B)  " Keypad buffer pointer " = 6
7F2B  7C00    BRU   (7F2C)
7F2C  7D0F    DATA            ;Return to program
```

2. Selected character routine

```
7F30  0700    LDA  0
7F31  C521    RMO  X,E
7F32  492C    DMT  ((B)+2C)  ;Shift character left until in current cursor position
7F33  7817    BRU  7F4B
7F34  C502    RMO  A,X       ;Save shifted character in the X register
7F35  0121    LDA  ((B)+21)  ;Load contents of keypad buffer into A
7F36  391F    AND  ((B)+1F)
7F37  C4A0    ROR  X,A       ;[ Buffer AND Mask ] OR Character ( First mask )
7F38  8121    STA  ((B)+21)  ;( Add character to keypad buffer )
7F39  C512    RMO  E,X
7F3A  0122    LDA  ((B)+22)
7F3B  3920    AND  ((B)+20)
7F3C  C4A0    ROR  X,A       ;Second mask
7F3D  8122    STA  ((B)+22)
7F3E  B11F    DLD  ((B)+1F)  ;Mask into ( A,E )
7F3F  CBC4    CRD  4         ;Rotate mask right 1 byte
7F40  A11F    DST  ((B)+1F)  ;Save rotated mask
7F41  492B    DMT  ((B)+2B)  ;Have all digits been displayed in the buffer?
7F42  7805    BRU  7F48      ;No, so branch to 7F48 and display the next
7F43  0706    LDA  6
7F44  812B    STA  ((B)+2B)  ;Reset buffer counter to six
7F45  B11F    DLD  ((B)+1F)
7F46  CBC8    CRD  8         ;Reset mask
7F47  A11F    DST  ((B)+1F)
7F48  112E    LDX  ((B)+2E)  ;Monitor mode into ( X )
7F49  7C00    BRU  (7F4A)    ;Branch to 7D38 and display next
7F4A  7D38    DATA           ;character in keypad
7F4B  C8E4    LLD  4         ;Shift character to left one place
7F4C  79E5    BRU  7F32      ;  and return to 7F32
```

Time mode selected

Hex. to Decimal

```
7F55  0000    LDA  (7F56)
7F56  7DD8    DATA
7F57  C001    RSU  A,E       ;E=((B)+23)-A
7F58  C510    RMO  E,A
7F59  C841    LRA  1         ;Divides by two
7F5A  6F1E    CPA  1E        ;See if address is too high
7F5B  CD80    SGE            ;If GTE skip next instruction
7F5C  7813    BRU  7F70
7F5D  C501    RMO  A,E
7F5E  7002    BRL  7F61
7F5F  7C00    BRU  (7F60)
7F60  7DA9    DATA
7F61  900D    STX  (7F6F)    ;Store X register
7F62  0700    LDA  0         ;A = 0
7F63  1700    LDX  0         ;X = 0
7F64  5F64    DIV  64
7F65  C8C8    LLA  8         ;Place as third digit in X register
7F66  C082    RAD  A,X
7F67  0700    LDA  0
7F68  5F0A    DIV  A
7F69  C8C4    LLA  4
7F6A  C082    RAD  A,X       ;Place as second digit in X register
7F6B  C092    RAD  E,X
7F6C  C521    RMO  X,E       ;Remainder as first digit
7F6D  1002    LDX  (7F70)
7F6E  C557    RMO  L,PC
7F6F  0000    LDA  (7F70)
7F70  7C00    DATA
7F71  7D0F    BRU  ((B)+F)   ;Return
```

```
709B  0049    LDA   (70E5)
709C  0100    LDA   ((B)+0)
709D  0049    LDA   (70E7)
709E  0001    LDA   (70A0)
709F  0000    LDA   (70A0)
70A0  7DD8    DATA
70A1  0005    LDA   (70A7)
70A2  3206    LOR   (70A9+(X))
70A3  7E14    BRU   (70B8)+(X)
70A4  C560    RMO   B,A
70A5  80FD    STA   (70A3)
70A6  1700    LDX   0
70A7  90F9    STX   (70A1)
70A8  0000    LDA   (70A9)
70A9  7DD8    DATA
70AA  80F5    STA   (70A0)
70AB  0000    LDA   (70AC)
70AC  3201    DATA
70AD  80F4    STA   (70A2)
70AE  04F3    LDA   ((70A2))
70AF  2000    ADD   (70B0)
70B0  0100    DATA
70B1  C506    RMO   A,B
70B2  0100    LDA   ((B)+0)
70B3  80E7    STA   (709B)
70B4  04ED    LDA   ((70A2))
70B5  2000    ADD   (70B6)
70B6  0102    DATA
70B7  C506    RMO   A,B
70B8  0900    LDE   ((B)+0)
70B9  04E8    LDA   ((70A2))
70BA  2000    ADD   (70BB)
70BB  0101    DATA
70BC  C506    RMO   A,B
70BD  0100    LDA   ((B)+0)
70BE  C8C8    LLA   8
70BF  C490    ROR   E,A
70C0  80DB    STA   (709C)
70C1  80D9    DLD   (709B)
70C2  C503    RMO   A,M
70C3  C514    RMO   E,S
70C4  00DB    LDA   (70A0)
70C5  C0A0    RAD   X,A
70C6  C0A0    RAD   X,A
70C7  C506    RMO   A,B
70C8  B100    DLD   ((B)+0)
70C9  7400    BRL   (70CA)
70CA  7E8A    DATA
70CB  A0CF    DST   (709B)
70CC  00CF    LDA   (709C)
70CD  C8C8    LLA   8
70CE  C848    LRA   8
70CF  80CF    STA   (709F)
70D0  00CB    LDA   (709C)
70D1  C848    LRA   8
70D2  80CB    STA   (709E)
70D3  0CC7    LDA   (709B)
70D4  80C9    STA   (709D)
```

```
70D5  0400    LDA  ((70D6))
70D6  3200    DATA
70D7  98C9    MPY  (70A1)
70D8  C510    RMD  E,A
70D9  9F03    MPY  3
70DA  C510    RMD  E,A
70DB  2000    ADD  (70DC)
70DC  3220    DATA
70DD  C0A0    RAD  X,A
70DE  C0A0    RAD  X,A
70DF  C0A0    RAD  X,A
70E0  C506    RMD  A,B
70E1  00BB    LDA  (709D)
70E2  8100    STA  ((B)+0)
70E3  00BA    LDA  (709E)
70E4  8101    STA  ((B)+1)
70E5  00B9    LDA  (709F)
70E6  8102    STA  ((B)+2)
70E7  C322    RIN  X,X
70E8  C520    RMD  X,A
70E9  6400    CPL  ((70EA))
70EA  3200    DATA
70EB  CD20    SEQ
70EC  78C1    BRU  70AE
70ED  50B3    IMD  (70A1)
70EE  50B3    IMD  (70A2)
70EF  00B1    LDA  (70A1)
70F0  6F05    CPA  5
70F1  CD20    SEQ
70F2  7801    BRU  70F4
70F3  7802    BRU  70F6
70F4  1700    LDX  0
70F5  78B8    BRU  70AE
```

Template shift

```
70F6  1700    LDX  0
70F7  0000    LDA  (70F8)
70F8  3000    DATA
70F9  C504    RMD  A,S
70FA  0000    LDA  (70FB)
70FB  3100    DATA
70FC  C506    RMD  A,B
70FD  0300    LDA  ((B)+(X)+0)
70FE  C546    RMD  S,B
70FF  8300    STA  ((B)+(X)+0)
7100  C322    RIN  X,X
7101  C520    RMD  X,A
7102  6800    CPA  (7103)
7103  00FF    DATA
7104  CDC0    SLE
7105  78F4    BRU  70FA
7106  7D00    BRU  (7107)
7107  0200    DATA
```

```
3690  0700    LDA  0
3691  8400    STA  ((3692))   ;Reset time address counter ( tac )
3692  321F    DATA
3693  0400    LDA  ((3694))
3694  3200    DATA            ;( A ) = N_T
3695  9C00    MPY  ((3696))
3696  321F    DATA
3697  C510    RMO  E,A
3698  9F03    MPY  3
3699  C510    RMO  E,A        ;( A ) = 3.N_T.tac
369A  2000    ADD  (369B)
369B  3220    DATA            ;( A ) = 3220 + 3.N_T.tac
369C  0C00    LDE  ((369D))
369D  321E    DATA
369E  C090    RAD  E,A
369F  C090    RAD  E,A
36A0  C090    RAD  E,A        ;... + 3.Time counter ( tc )
36A1  C506    RMO  A,B        ;( B ) = 3220 + 3.N_T.tac + 3.tc
36A2  0400    LDA  ((36A3))
36A3  321F    DATA
36A4  2000    ADD  (36A5)
36A5  3201    DATA
36A6  801D    STA  (36C4)
36A7  1C1C    LDM  ((36C4))
36A8  B100    DLD  ((B)+0)
36A9  1102    LDX  ((B)+2)
36AA  C536    RMO  M,B
36AB  A100    DST  ((B)+0)
36AC  9102    STX  ((B)+2)
36AD  5400    IMO  ((36AE))
36AE  321F    DATA            ;Increment tac
36AF  0400    LDA  ((36B0))
36B0  321F    DATA
36B1  6705    CPL  5          ;Have all time address values been considered?
36B2  CD20    SEQ
36B3  78DF    BRU  3693       ;If not, back to 3693
36B4  5400    IMO  ((36B5))
36B5  321E    DATA            ;Increment tc
36B6  0400    LDA  ((36B7))
36B7  321E    DATA
36B8  6400    CPL  ((36B9))
36B9  3200    DATA            ;Is ( A ) = N_T
36BA  CDC0    SLE             ;If it is then skip the next instruction
36BB  7802    BRU  36BE
36BC  7C00    BRU  (36BD)
36BD  0200    DATA            ;Back to MMR main menu
36BE  0000    LDA  (36BF)
36BF  0200    DATA
36C0  C506    RMO  A,B
36C1  7C00    BRU  (36C2)
36C2  070E    DATA
```

Bibliography

1 Rahalker, R.R. et al *Proc. R. Soc. Lond. A* 1984, **394**, 207

2 Rouse, P.E. *J. Chem. Phys.* 1953, **21**, 1272

3 Kimmich, R. *Polymer* 1984, **25**, 187

4 Kimmich, R. *Polymer* 1977, **18**, 233

5 Kimmich, R. *Naturforsch* 1976, **31a**, 693

6 Doi, M. and Edwards, S.F. *J. Chem. Soc. Faraday Trans.* 1978, **II 74**, 1789

7 de Gennes, P.G. *J. Chem. Phys.* 1971, **55**, 572

8 Bloembergen, N., Purcell, E.M., Pound, R.V. *Phys. Rev.* 1948, **73**, 679

9 Voigt, G. and Kimmich, R. *Polymer* 1980, **21**, 1001

10 Koch, H., Bachus, R. and Kimmich, R. *Polymer* 1980, **21**, 1009

11 Kimmich, R. *Colloid and Polymer Science* 1974, **252**, 786

12 Kimmich, R. *Polymer* 1975, **16**, 851

13 Callaghan, P.T. *Polymer* 1988, **29**, 1951

14 Pauli, W. *Naturwissenscaften* 1924, **12**, 741

15 Stern, O. *Zeitschrift fur Physik* 1921, **7**, 249

16 Gerlach, W. and Stern, O. *Annalen der Physik Leipzig* 1924, **74**, 673

17 Purcell, E.M., Torrey, H.C., Pound, R.V. *Phys. Res.*, 1946, **69**, 37

18 Bloch, F., Hansen, W.W. and Packard, M. *Phys. Res.*, 1946, **69**, 127

19 Bloch, F., Hansen, W.W. and Packard, M. *Phys. Res.*, 1946, **70**, 474

20 Torrey, H.C. *Phys. Rev.* 1949, **76**, 1059

21 Hahn, E.L. *Phys. Rev.* 1951, **80**, 580

22 Ernst, R.R. and Anderson, W.A. *Res. Sci. Instrum.*, 1966, **37**, 93

23 Abragam, A. " *The Principles of Nuclear Magnetism* " Oxford, 1961, p.139

24 Redfield, A.G. *Phys. Rev.* 1955, **98**, 1787

25 Look, D.C. and Lowe, I.J. *J. Chem. Phys.* 1966, **44 / 8**, 2995

26 Abragam, A. " *The Principles of Nuclear Magnetism* " Oxford, 1961, p.264

27 Hebel, L.C. and Slichter, C.P. *Phys. Rev.* 1959, **113**, 1504

28 Abragam, A. " *The Principles of Nuclear Magnetism* " Oxford, 1961, p.103

29 Abragam, A. " *The Principles of Nuclear Magnetism* " Oxford, 1961, p.104

30 Abragam, A. " *The Principles of Nuclear Magnetism* " Oxford, 1961, pp.272

31 Abragam, A. " *The Principles of Nuclear Magnetism* " Oxford, 1961, p.291

32 Abragam, A. " *The Principles of Nuclear Magnetism* " Oxford, 1961, p.555

33 Stejskal, E.O. and Gutowsky, H.S. *J. Chem. Phys.* 1958, **28 / 3**, 388

34 Abragam, A. " *The Principles of Nuclear Magnetism* " Oxford, 1961, pp.298

35 Edwards, S.F. *Polymer* 1985, **26**, 163

36 Chandrasekhar, S. *Rev. Mod. Phys.* 1943, **15**, 1

37 Eccles, C.D. " *Microscopic NMR Imaging Vol. I* " Ph.D Thesis, Massey University, 1987

38 Fukushima, E. and Roeder, S.B.W. " *Experimental Pulse NMR* " Addison - Wesley, Publishing Company, Inc. Reading, Massachusetts, 1981

39 Hoult, D.I. *Progress in NMR spectroscopy* 1978, **12**, 41

40 Anderson, W.A. *Rev. of Sci. Instr.* 1961, **32 / 3**, 241

41 Eccles, C.D. " *Microscopic NMR Imaging Vol. II* " Ph.D Thesis, Massey University, 1987

42 Brandrup, J. and Immergut, E.H. "*Polymer Handbook* " Wiley Second Edition, New York

43 Allen, P.W. " *Techniques of Polymer Characterization* " London, 1959

44 Guzman, G.M. " *Fractionation of High Polymers* "

45 Ferry, J.D. " *Viscoelastic Properties of Polymers* " Wiley Third Edition, 1980

46 Young, R.J. " *Introduction to Polymers* " Chapman and Hall, London, 1981

47 Mandelkern, L. " *Introduction to Macromolecules* " Springer-Verlag, Berlin, 1983

48 Schumacher, R.T. *Phys. Rev.* 1958, **112 / 3**, 837

49 P. Daivis, private communication

50 Aylward, G.H. and Findlay, T.J.V. " *S.I. chemical data* " Wiley Second Edition, 1974

51 Kimmich, R. and Schmauder, Kh. *Polymer* 1977, **18**, 239